Development of Highly Efficient Organic and Perovskite Solar Cells

Li Xianqiang

Supervisor: Associate Professor Wang Hong

Co-supervisor: Associate Professor Tang Xiaohong

School of Electrical and Electronic Engineering

A thesis submitted to the Nanyang Technological University in partial fulfillment of the requirement for the degree of Doctor of Philosophy

August 2017

Acknowledgements

First, I would like to express my gratitude and respect to my supervisor Assoc Prof. Wang Hong and my co-supervisor Assoc Prof. Tang Xiaohong for supporting me to pursue my PhD degree. They have provided valuable advice and guidance to help me achieve the goals of my research project even when they have busy schedules. They are always there to offer me support when I have problems and difficulties in my PhD research period. Their motivation and encouragement are very important for me to insist on pursuing my PhD degree. Besides, I would like to express my gratitude to them for supporting me to attend local and overseas conferences to present and discuss my work with researchers worldwide.

Second, I would like to thank the School of Electrical and Electronic Engineering (EEE), Nanyang Technological University (NTU), for providing my the NTU Research Scholarship, the financial support for my PhD study, and also the various opportunities for overseas and local academic conferences. I would like to thank Institute of Materials Research and Engineering (IMRE) for providing the opportunity of PhD student attachment program. I would thank Dr. Li Jun and Dr. Wang Xizu, my co-supervisors from IMRE, for their patient guidance in the area of organic and perovskite solar cells. They provided necessary sources for me to conduct my experiments in IMRE. Their immense knowledge and rich research experience are valuable for me. I would also thank Asst Prof. Leong Wei Lin from NTU for her constructive suggestions and instructions for starting my research in the first year of my PhD study.

Furthermore, I am thankful for the help and support provided by the staffs in IMRE and Photonics Labs in NTU, specifically, Dr. Guo Shifeng, Dr. Vijila Chellappan, Dr. Wang Fei, Mr. Ye Tao, Dr. Goh Wei Peng, Dr. Ong Kok Haw, Dr. Ooi Zi-En, Ms. Ivy Wong Hoi Ka, Ms. Tjiu Weng Weei, Ms. Yee Yang Boey, Ms. Leng-Low Poh Chee, Mr. Tsay Chi Huang, Mr. Lim Teng Keng and Mr. Yong Kim Lam. I would like to thank Prof. Liu Bin and Dr. Liu Jie from NUS for providing materials and instructions for my research in organic solar cells. I would also thank my group mates, Mrs. Wu Dan, Mr. Lingeswaran Arunagiri, for their kind support and suggestions.

Last but not least, I feel extremely grateful to my family and friends for their love, understanding and constant encouragement in my PhD research period. I would like to thank my girlfriend, Ms. Yang Yijie, for helping me go through the difficult time during my PhD study. She encouraged me to overcome the difficulties and challenges in both study and life.

Abstract

With rapid industrial development and global population growth in 21st century, the search for renewable energy source becomes more important. Among various renewable energy sources, solar energy is the most plentiful one. Great efforts have been made to develop highly efficient and low-cost photovoltaic (PV) technologies. So far, the dominant PV technology is based on inorganic semiconductor materials, such as Silicon (Si) and Gallium arsenide (GaAs). Despite the high power conversion efficiency, these PV technologies require strict manufacturing processes and have very high materials and fabrication costs, thus preventing them from being widely accepted. To reduce the PV technology price, researchers have been searching for new generations of PV technologies based on cheaper materials and low-cost manufacturing processes. In recent years, organic solar cells and perovskite solar cells using organic or organic-inorganic hybrid materials in photoactive layers have attracted lots of attentions as a new generation of PV technologies. They are attractive because of their low-cost fabrication processes, mechanical flexibility, solution processability, etc. Flexible organic solar cells and perovskite solar cells can be fabricated by a simply printing process like newspapers and have potential to be applied on various substrates, such as curved roofs, uneven roads and clothes. The objective of this work is to develop low temperature processed interfacial organic materials and novel fabrication techniques to improve the performance and reduce fabrication costs of organic solar cells and perovskite solar cells.

First, a newly synthesized n-type conjugated polyelectrolyte, poly [9,9-bis((60-N,N,N-trimethylamino)hexyl)-fluorene-alt-cobenzoxadia zole dibr-omide] (PFBD), was applied into organic solar cells with an inverted structure

as electron transporting layer (ETL) to improve the organic solar cells' performance. The organic solar cells using PFBD as the ETL exhibited a highest power conversion efficiency (PCE) of 7.21% and improved stability compared with the commonly used another ETL, PFN. The improved stability should come from the neutral nature of the PFBD solution because the good solubility of PFBD in methanol without the requirement of acetic acid. Besides the good photovoltaic performance of PFBD, we observed a light-soaking effect that the organic solar cells' performance kept improving with increasing the sun light illumination time during the measurement of organic solar cells with PFBD ETL. To solve this problem, we proposed a UV pre-treatment method and demonstrated that the UV pre-treatment could successfully eliminate the light-soaking effect. Through Kelvin Probe measurement and impedance analysis, we found that the change of work function of ITO electrodes modified by PFBD plays an important role in influencing the organic solar cells' performance. UV-vis absorption measurement results revealed that UV light had a great influence on benzoxadiazole (BD) unites on polymer backbone of PFBD, thus leading to the light-soaking effect. Our results demonstrate that PFBD is a promising material for highly efficient and stable organic solar cells.

Second, we developed and applied a series of newly synthesized p-type polymers into perovskite solar cells as hole transporting layers (HTLs). The perovskite solar cells based on these polymer HTLs exhibited good stability and PCE. Besides, these polymer HTLs can achieve a good photovoltaic performance without requiring a complex doping process which is often needed in other commonly used small molecular or polymer HTLs in perovskite solar cells. Without the requirement for doping process, the manufacturing costs of perovskite solar cells based on our polymer HTLs can be further reduced and

the devices' stability was improved. Besides we also studied the factors that influence the performance of the polymer HTLs. Through molecular design, these polymer HTLs have almost the same band energy levels but different crystallinity, thus demonstrating different performance when applied into perovskite solar cells. So except for band alignment between HTLs and photoactive layers, crystallinity of the HTLs is also very important. The polymer HTL with the highest crystallinity has the best performance when used in perovskite solar cells with a highest PCE of 14.02%. The best perovskite solar cells exhibited excellent stability that the PCE of the device still retained 80% of the original value after storing in a nitrogen filled glove box for 113 days.

Last, we designed and fabricated organic solar cells and perovskite solar cells by using a transfer printing technique to deposit the top Au electrodes. The top Au electrodes are normally deposited by vacuum deposition methods, such as thermal evaporator and E-beam evaporator. The vacuum deposition methods increase the fabrication costs of organic solar cells and perovskite solar cells and are not compatible with roll-to-roll manufacturing process. To reduce the manufacturing costs, we used a PDMS stamp coated with Au film to transfer print the Au onto the top of organic solar cells and perovskite solar cells as top electrodes. Compared with the vacuum deposition methods, our transfer printing method improved the performance and stability of organic solar cells and perovskite solar cells. The perovskite solar cells with transfer printed Au electrodes have a highest PCE of 13.72%, which is higher than the highest PCE of the control devices with the thermally evaporated Au electrodes. The organic solar cells with transfer printed and thermally evaporated Au electrodes have comparable PCE. Both perovskite solar cells and organic solar cells with

transfer printed top electrodes have good stability. The good stability of the solar cells with transfer printed electrodes was demonstrated to come from less diffused Au atoms into the organic interfacial layers as indicated by the SCLC analysis and XPS measurement results.

Table of Contents

List of Tables

List of Tables

Chapter 1 Introduction

1.1 Motivation

With rapid industrial development and global population growth in 21st century, we are inevitably facing severe energy crisis and climate change as a result of our high dependence of fossil fuels. As reported by International Energy Agency (IEA) in 2015, fossil fuels, petroleum, coal and natural gas, which contain high percentages of carbon account for 80.1% of primary energy consumption in the world [1]. Burning fossil fuels to generate electricity accompany by producing and emitting large amounts of carbon dioxide, which is well known as one of the primary greenhouse gases into environment. Since the beginning of Industrial Revolution in the year 1750, the atmospheric carbon dioxide concentration has increased 40% from 280 ppm in 1750 to 400 ppm in 2016 due to human activities as a result of fast increasing annual global anthropogenic carbon dioxide (CO_2) emissions as shown in Figure 1.1 [2]. As shown in Figure 1, the annual global anthropogenic carbon dioxide (CO_2) emissions from fossil fuel combustion, cement production and flaring have tripled [3]. With the atmospheric carbon dioxide increasing, people are facing global warming because of the so-called greenhouse effect because the carbon dioxide in atmosphere can absorb and emit radiation within the thermal infrared range thus increasing the average temperature of Earth's surface [4, 5]. Intergovernmental Panel on Climate Change (IPCC) reported that the global mean surface temperature will raise in a range from 2.5 ℃ to 7.5 ℃ above the Earth's average temperature of 1850-1900 [3]. The increased Earth's temperature might lead to increase the risks of severe ill-health, disrupted

livelihoods, food and water insecurity, extreme weather events and loss of ecosystems, biodiversity and ecosystem goods, functions and services [3].

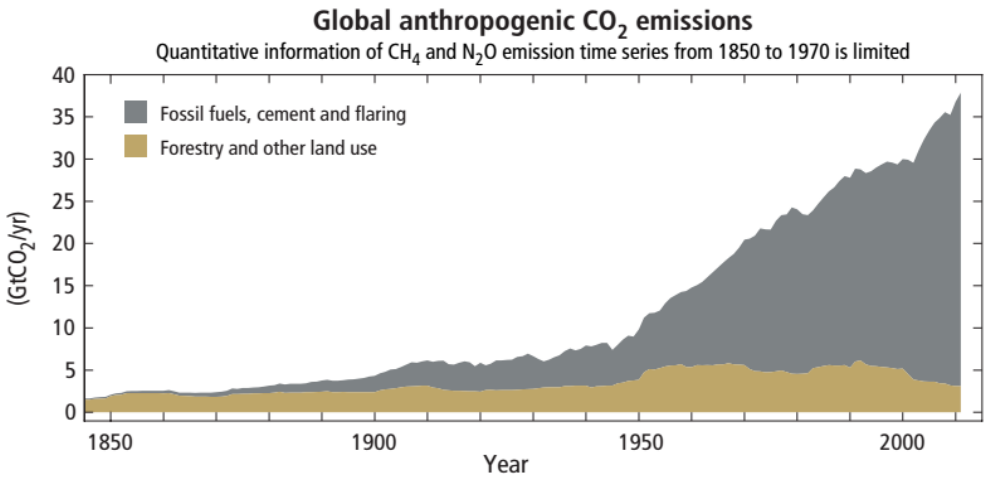

Figure 1.1: Annual global anthropogenic carbon dioxide (CO_2) emissions from fossil fuel combustion, cement production and flaring, and forestry and other land use (FOLU), 1750–2011 [3].

Fossil fuels are considered nonrenewable energy because the depletion rate of viable fossil fuels is much faster than new ones are being made. It takes millions of years to form fossil fuels through natural processes such as anaerobic decomposition of buried dead organisms. With the world energy consumption increasing, the fossil fuels will eventually run out in the future. So, it is very urgent to look for alternative energy sources to reduce our dependency of fossil fuels, thus solving the energy crisis and the environment issues.

Renewable energy resources that provide energy from the energy sources which are naturally replenished on a human timescale like sunlight, wind, tides, rain, waves and geothermal heat. They are the ideal candidates for the renewable energy sources. Compared to fossil fuels, renewable energy resources are clean and sustainable because they are continually replenished by nature and derived

directly or indirectly from the sun or other natural movements and mechanisms of the environment. Since developing renewable energy can help relief the environmental issues and energy shortage caused by fossil fuels, more and more related organizations have encouraged intensive research for exploiting renewable energy by advanced technologies. Renewable energy resources consist of different types of energy sources including wind, marine, solar, hydro, geothermal energy and bioenergy, etc. By turning these natural energy sources into electricity, these renewable energy resources have the ability to provide over 3000 times the current global energy needs as illustrated in Figure 1.2 [6].

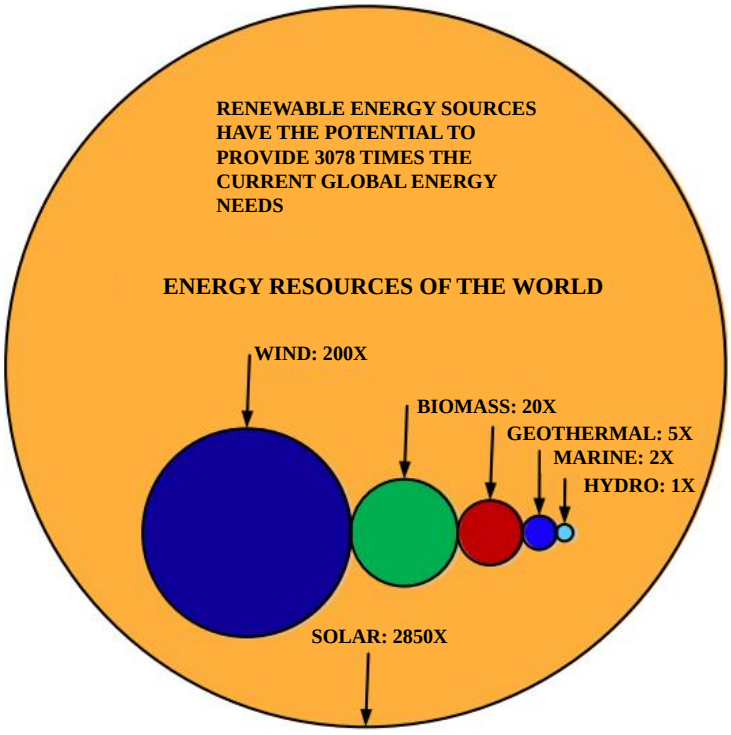

Figure 1.2: Energy sources available for the world [6].

Among all these renewable energy sources, solar energy is the most abundant source. The total amount of energy that the sunlight provides on the surface of earth every year is about twice as much as all of the Earth's non-renewable

resources, including coal, oil, natural gas and mined uranium, can provide [7]. To utilize solar energy, photovoltaic technology that converts solar energy into electricity has attracted a lot of attentions and developed for more than half a century. Photovoltaic technology is considered as a clean and elegant technology because it can directly convert sunlight to electricity without any greenhouse gas emissions during the operation. Due to the fast depletion and increasing price of non-renewable energy sources, photovoltaic technology experienced a rapid development in recently years. Figure 1.3 shows the solar PV global capacity and annual additions from 2005 to 2015 [8]. After a decade rapid development, the solar PV global capacity of 2015 reached to 227 Gigawatts (GW) which are about 40 times the value of 2005. It's worth noting that solar PV experienced another year of record growth in 2015 with the solar PV global capacity reaching to 227 GW, 50 GW higher than 2014, equivalent to an estimated 185 million solar panels.

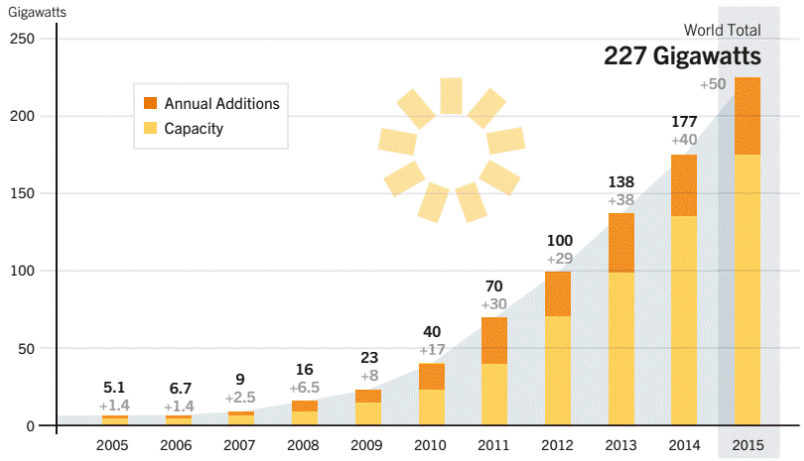

Figure 1.3: Solar PV global capacity and annual additions in the period of 2005-2015 [8].

Despite the fast growth of solar PV global capacity, the solar PV share of global and renewable electricity production is only 1.2% and 5.1%, respectively, as

shown in Figure 1.4 [8]. The low share of solar PV is because of the high costs of the PV energy as compared to the nonrenewable energy sources. To make solar PV more competitive and reliable as an alternative energy source, more efforts are needed to reduce the costs of the PV energy.

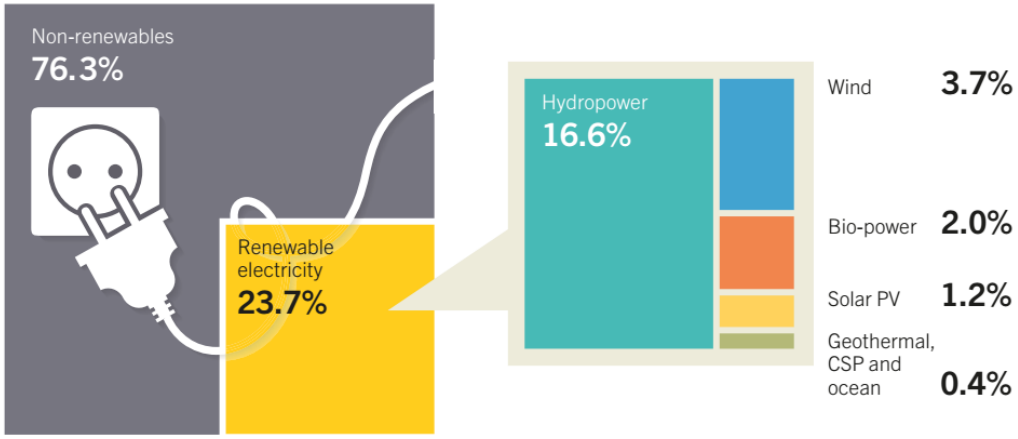

Figure 1.4: Estimated Renewable Energy Share of Global Electricity Production, End-2015 [8].

So far, the dominant PV technology is based on silicon. The best single junction terrestrial solar cells based on monocrystalline silicon have achieved a power conversion efficiency (PCE) of 26.3% by Kaneka with the highest module PCE reaching to 24.4% [9]. Besides the high PCE, the solar planes based on silicon have good stability and can operate more than 20 years. Despite these advantages, silicon dominated PV technology still cannot compete with traditional fossil fuels because the high materials and manufacturing costs impede silicon based solar cells to be widely accepted and used. As the PCE of silicon based solar cells approaching to Shockley-Queisser limit (32%), more efforts should be put on lowering the manufacturing costs to make solar PV technology cost competitive.

To make the price of solar PV energy comparable to that of nonrenewable energy, extensive research focuses on seeking for cheaper and high performance semiconductor materials for harvesting solar energy. To achieve these goals, second generation PV technologies, such as cadmium telluride (CdTe), copper indium gallium diselenide (CIGS) and amorphous thin-film silicon, have been developed. CdTe PV technology is based on using cadmium telluride thin layer to absorb and convert sunlight into electricity. The word record PCE of CdTe cell is 21.0% reported by First Solar in 2014 [10]. CIGS cell uses a thin layer of copper, indium, gallium and selenide to convert sunlight into electricity. The highest PCE of CIGS reached to 21.0% in 2014 [10]. Both CdTe and CIGS PV technologies have potential to compete with the dominant silicon based PV technology. But there are other concerns about these two PV technologies. For CdTe PV technology, the major concern is the toxic and carcinogenic cadmium and tellurium. Another concern is the extreme rarity of Te in the Earth's crust. For CIGS PV technology, its manufacturing costs still cannot compete with polycrystalline or CdTe PV technologies due to the complex structure and requirement for energy consuming deposition techniques.

Organic solar cells based on polymers or small molecular organic materials with properties, such as low material costs [11, 12], solution processability [13-15] and mechanical flexibility [16-18], have attracted lots of attentions. After decades of development, high PCE of the organic solar cells has reached to above 10% [19-27]. Another emerging solar PV technology is based on an organic-inorganic hybrid semiconductor material, perovskite. The sky-rocketing PCE of the perovskite solar cells, from 3.8% [28] in 2009 to above 20.0% in the recent two years [29-34], makes perovskite solar cells a potential promising solar PV technology to compete with the dominant silicon based PV technology.

Besides the PCE, organic solar cells and perovskite solar cells are attracting because of their potential applications into flexible devices. Flexible organic solar cells and perovskite solar cells are compatible with roll-to-roll fabrication which means they can be fabricated by a simply printing process like newspapers. In this way, the fabrication costs of organic solar cells and perovskite solar cells can be further reduced and the flexible solar cells have potential to be applied on various substrates, such as curved roofs, uneven roads and clothes.

1.2 Objectives

The objectives of my project are to develop low temperature processed interfacial organic materials and novel fabrication techniques to improve the performance of the organic solar cells and perovskite solar cells and reduce their fabrication costs. The scope of this project includes development and application of the novel organic interfacial materials, fabrication and optimization of the organic solar cells and perovskite solar cells, development of low cost printable fabrication techniques and fundamental study of the role of interfaces between active layer and electrodes in influencing the performance of organic solar cells and perovskite solar cells. The objectives of the study are summarized as follows:

(i) Low temperature processed and stable electron transporting layers (ETLs) are important for reducing the fabrication costs and commercialization of organic solar cells. Guidelines for synthesizing materials with desired properties are needed for development of highly efficient and stable ETLs in organic solar

cells. We will develop and apply novel n-type conjugated polyelectrolytes into organic solar cells as a low temperature processed ETLs. Highly efficient and stable organic solar cells based on the conjugated polyelectrolyte ETLs will be fabricated and optimized. Different conjugated polyelectrolyte ETLs will be applied into the organic solar cells and their performance will be compared. We will conduct fundamental studies to investigate the properties required for high performance conjugated polyelectrolyte ETLs.

(ii) Most high performance HTLs for perovskite solar cells require an ionic salt and cobalt based dopants. The complex doping process will increase the fabrication costs and the stability of the perovskite solar cells will be reduced after introducing the dopants. To solve these problems, we will develop a highly efficient, stable and dopant-free polymer HTL for perovskite solar cells. perovskite solar cells based on the polymer HTL will be fabricated and optimized. Different p-type polymers will be applied into the perovskite solar cells as the HTLs. Fundamental studies will be carried out to investigate how the molecular structure influenced the properties of HTLs, thus influencing the performance of perovskite solar cells. Properties required for high performance dopant-free polymer HTLs will be summarized.

(iii) The conventional deposition process for top electrodes of organic solar cells and perovskite solar cells is by E-beam or thermal evaporator and carried out in high vacuum environment. The vacuum evaporating process is not compatible with roll-to-roll process and will increase the fabrication cost of solar cells. Besides, the evaporated metal atoms have a relatively high kinetic energy and might penetrate into the thin organic interfacial layers, thus leading to increased leakage current and poor device stability. To reduce the fabrication costs and prevent damage by metal atoms penetration, we will design and

fabricate fully printable organic solar cells and perovskite solar cells by using a transfer printing technique to deposit top electrodes. We will improve the performance and stability of organic solar cells and perovskite solar cells by reducing the diffused metal atoms in the top electrodes depositing process. Characterization techniques, such as SCLC and XPS measurement, will be used to study the interfacial defects located between the top electrodes and organic interfacial layers. The influence of interfacial defects and diffused metal atoms will be studied.

1.3 Major Contribution of this Thesis

We have developed the highly efficient and stable organic solar cells and perovskite solar cells through interface engineering. We focused on improving the properties of the three interlayers or interfaces: n-type interlayer for electron transporting, p-type interlayer for hole transporting and interface between electrodes and interlayers. These interlayers or interfaces play an important role in influencing the performance of organic solar cells and perovskite solar cells. Except for improving the performance of organic solar cells and perovskite solar cells, our another goal is to reduce the fabrication costs of the solar cells. So, low temperature processed novel conjugated polyelectrolyte ETLs and polymer HTLs were applied into the organic solar cells and perovskite solar cells in this research. To further reduce the fabrication costs and improve the device performance, we have developed a transfer printing method for depositing top electrodes of, but not limited to, the organic solar cells and perovskite solar cells. We have carried out the fundamental studies on these organic solar cells and perovskite solar cells to understand how the materials'

properties and fabrication processes influenced the solar cells' performance.

Organic solar cells with an inverted structure based on a novel conjugated polyelectrolyte ETL, PFBD, have been demonstrated. In these organic solar cells, an ultrathin layer of PFBD (~2 nm) is deposited on the ITO coated glass substrates by spin coating from its methanol solution without any other additives. Only 100 ℃ is required to dry the PFBD layer after the spin coating process. The photoactive layer of the device is PTB7 and $PC_{71}BM$ blend film prepared by spin coating. Then, a 10 nm layer of MoO_3 and a 100 nm Al layer are deposited by thermal evaporator. The organic solar cells based on PFBD ETL exhibited a highest PCE of 7.21%. We compared the performance of the PFBD and another conjugated polyelectrolyte ETL, PFN, which has been reported by other researchers. Unlike PFBD, PFN's side chains don't have ionic nature thus requiring a small amount of acetic acid to facilitate it to dissolve in methanol. We have compared that the stability of the organic solar cells based on PFBD was significantly improved from that of the organic solar cells with PFN. This is because the neutral nature of PFBD's methanol solution does not corrode the photoactive layer. During the measurement of the organic solar cells based on PFBD ETL, we have observed the so-called light-soaking effects which were often observed in organic solar cells based on metal oxides ETLs. The origin of the light-soaking effect has been investigated by using different characterization techniques, such as Kelvin Probe measurement, dark current analysis, impedance measurement and AFM measurement, etc. We demonstrated that the pre-UV treatment on the PFBD layer can eliminate the light-soaking effect of the organic solar cells. Based on these results, we summarized the desired properties for high performance conjugated polyelectrolyte ETLs.

To improve the hole transporting and collecting efficiency, we have developed a dopant-free polymer HTL and applied it into the perovskite solar cells. The polymer HTL can be simply low-temperature solution processed without any doping process, thus reducing the fabrication costs of the perovskite solar cells. We have fabricated the highly efficient perovskite solar cells based on the dopant-free polymer HTL. The highest PCE of the perovskite solar cells reached to 14.02% which was higher than that of our control devices based on a commonly used small molecular HTL which requires a complex doping process. The perovskite solar cells exhibited excellent stability. After stored it in a N_2 filled glovebox in dark condition for 113 days, its PCE was still measured retained 80% of the original value. In contrast, the PCE of the control devices decreased to only 48% of their initial value. To explore the requirements for high performance dopant-free polymer HTLs, we synthesized a series of polymer HTLs. They have similar backbones but different side chains, thus exhibiting quite different performance when used them in perovskite solar cells as the HTLs. Characterizations, such as XRD, UV-vis spectra and PESA measurements, were conducted on the samples to explain the origin of their different performance. We have found that the crystalline structure of the polymer HTLs plays an important role in influencing the performance of the perovskite solar cells.

Besides the ETLs and HTLs, the interface between metal electrodes and organic interlayers is also very important for the organic solar cells and perovskite solar cells. So, we have proposed a transfer printing technique for depositing top electrodes of the organic solar cells and perovskite solar cells. This transfer printing technique is achieved by depositing metal electrodes on soft PDMS substrates first and then transfer printed on organic layers. The fabrication

process of transfer printing method is compatible with roll-to-roll process and can help reduce the fabrication costs of organic solar cells and perovskite solar cells. The best organic solar cells and perovskite solar cells with transfer printed top electrodes have highest PCEs of 2.35% and 13.72% respectively. The best perovskite solar cells with top electrodes deposited by conventional methods, thermal evaporating, has a lower PCE of 13.02%. Through some characterization techniques, such as J-V curve analysis, SCLC measurement and XPS measurement, we demonstrated that the less diffused metal atoms and interfacial defects are the key factors that lead to better performance of perovskite solar cells with transfer printed top electrodes. Besides, the perovskite solar cells with transfer printed top electrodes exhibited better stability due to less diffused metal atoms. Through this study, we demonstrated that a low cost transfer printing technique can be used to replace conventional vacuum evaporation process to deposition top electrodes of organic solar cells and perovskite solar cells.

Chapter 2 Literature Review

In this chapter, a thorough literature review in the research area of organic solar cells and perovskite solar cells will be presented. The chapter begins by introducing the fundamental working principles of solar cells. After that, working principles and development of organic solar cells and perovskite solar cells will be introduced. Then, the roles and development of interfacial materials for organic solar cells and perovskite solar cells will be presented. The last part of this chapter will focus on printable organic solar cells and perovskite solar cells, including roll-to-roll fabrication techniques and flexible organic solar cells and perovskite solar cells.

2.1 Fundamentals of Solar Cells

A solar cell is a kind of optoelectronic device that is used to directly convert sun light into electricity through the photovoltaic effect. Converting sun light directly into electricity does not produce toxic substances and greenhouse gases which are always produced in the process of burning fossil fuels to generate electricity. In a solar cell, the process of converting sun light into electricity can be divided into three steps: absorption of incident sun light photons and generation of electron-hole pairs or excitons; separation of electrons and holes; extraction of the separated electrons and holes to opposite electrodes and produce electricity in an external circuit.

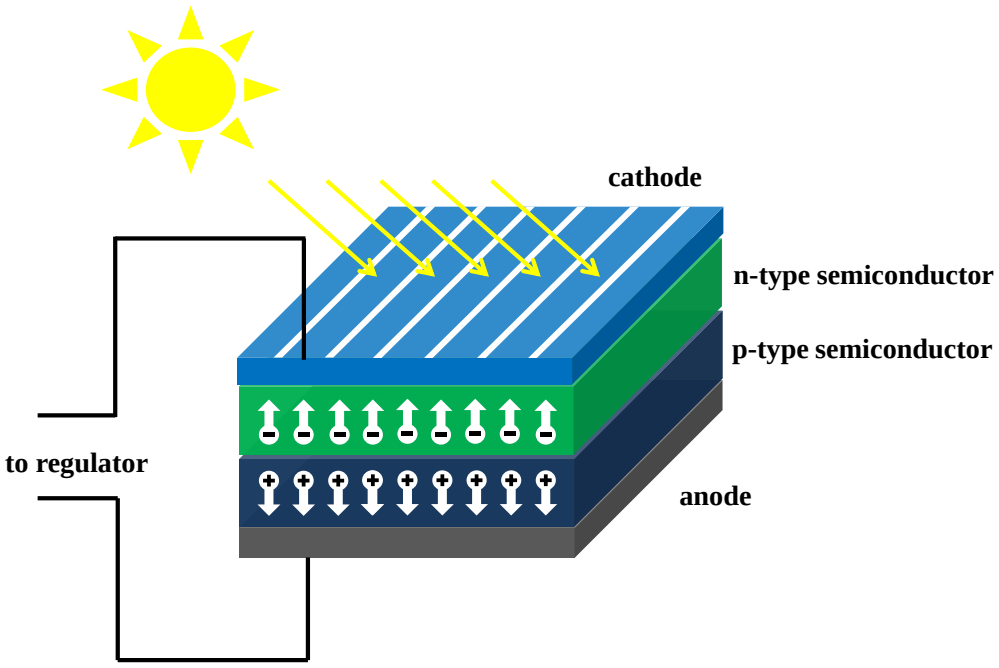

Figure 2.1: Illustration of the basic structure of a solar cell.

Figure 2.1.1 shows the basic structure of a semiconductor p-n junction solar cell. When the solar cell is illuminated by sun light, the semiconductor layers of the solar cell will absorb the incident photons with energy higher than the bandgap of the semiconductor layers. After the photons absorption, electrons in the valence band will be excited into the conduction band and the electron-hole pairs or excitons (depending on the binding energy between electrons and holes) will be generated. These electron-hole pairs or excitons will be separated by the build-in potential of the p-n junction of the cell and the separated electrons and holes will transport to their corresponding positive and negative electrodes, respectively. Some of the electrons and holes will recombine through different recombination processes, such as radiative recombination [35], Auger recombination [36] and Shockley-Read-Hall recombination [37] before they reach to the electrodes. The charge carriers that don't recombine will be collected by the electrodes and transported to an external circuit to generate

electricity.

The measurement of terrestrial solar cells is conducted under the illumination of Air mass 1.5 spectrum (AM1.5) with intensity of 100 mW/cm^2. The input power from sun light illumination is denoted as P_{in}. From the current-voltage (I-V) characteristics of the solar cells under illumination, the power conversion efficiency (PCE) of the solar cells can be obtained. Figure 2.1.2 shows a typical the I-V characteristics of solar cells under illumination and with the dark condition. The shaded area ($I_m \times V_m$) indicates the maximum power output, P_{max}, of the cell. When we set the voltage to zero, the value of current is called short circuit current, I_{sc}, of the cell When the current is set to zero, the value of voltage is called open circuit voltage, V_{oc}, of the cell. Another important parameter of solar cells is the fill factor which is defined by the following equation:

$$\mathrm{FF} = \frac{I_m \times V_m}{I_{sc} \times V_{oc}}$$

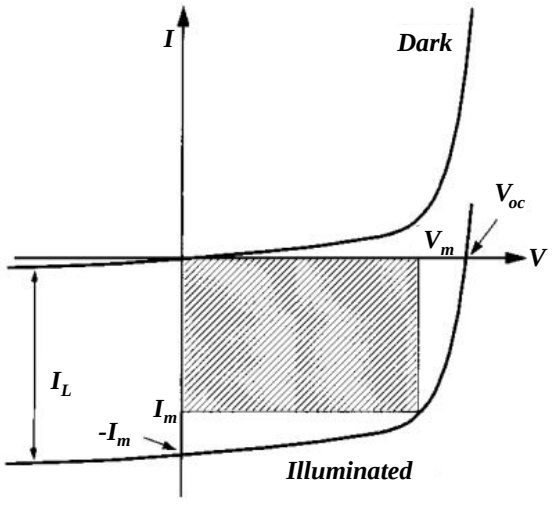

Figure 2.2: I-V characteristics of solar cell under illumination [38].

The PCE of a solar cell is given by the ratio of P_{max} and P_{in}. P_{max} which equals to the product of I_{sc}, V_{oc} and FF. If I_{sc} is replaced by current density, J_{sc}, the PCE of solar cells can be expressed as the following equation:

$$\mathrm{PCE} = J_{sc} \times V_{oc} \times \mathrm{FF}$$

2.2 Organic Solar Cells

The very first organic solar cell was invented by Tang in 1979 [39]. The organic solar cell consists a bilayer donor and acceptor planar heterojunction and had a PCE of only around 1%. The low PCE of the cell is due to the low dielectric constant of the materials and the high Frenkel exciton binding energy which is in the range of 0.3-1 eV [40, 41]. In 1995, the first organic solar cell using a bulk heterojunction structure was demonstrated by the groups of Heeger [42] and Friend [43] by adopting C_{60} fullerene and its derivatives, such as [6,6]-phenyl-C61-butyric acid methyl ester (PCBM) [44]. The bulk heterojunction structure is formed by a mixture of donor- and acceptor-materials. Using the bulk heterojunction structure can significantly increase the surface area between the donor-acceptor interfaces and improve the charge carrier separation and collection efficiency. Then after about two decades' development, the PCE of organic solar cells was pushed to a certificated 11.2% PCE [45]. The progress of organic solar cells is mainly driven by materials development, active layer morphology control and interface engineering.

Figure 2.2.1 (a) shows an illustration of the operating mechanism of the organic solar cells. The active layer of the organic solar cell consists of a polymer donor and a fullerene derivative acceptor material, PCBM. As shown in Figure 2.2.1

(a), an incident photon with energy (hγ) higher than the bandgap of the polymer is absorbed and an electron-hole pair-exciton is generated within the polymer. The exciton will be separated at the interface between the polymer and PCBM through an ultrafast electron charge transfer process which happens <100 fs [46]. After the electron-hole exciton is separated at the interface between donor and acceptor, they will be swept outside the active layer by the build-in potential created by the work function difference between the two opposite electrodes. Figure 2.2.1 (b) shows the ideal morphology model with bicontinuous interpenetration network of the donor and acceptor. The ideal width of the donor and acceptor networks is estimated to be around 20 nm which is twice of the exciton diffusion length (around 10 nm). The bicontinuous donor and acceptor networks can make sure that the separated electrons and holes can be transported to their corresponding electrodes to form electricity. The optimal thickness of the active layer for an organic solar cell is normally around 100 nm. The 100 nm active layer of an organic solar cell cannot absorb all incident photons with energy higher than the organic solar cell's bandgap, but increasing the thickness will lead to the increased charge carriers' recombination probability and resistance due to the limited charge carrier mobility and lifetime, which will reduce the performance of the device. For most organic solar cells based on polymer or small molecule donor materials, the optimized thickness of the active layer is around 100 nm. Another important factor affects the performance of organic solar cells is the interface between the active layer and electrodes. In an organic solar cell based on polymer and PCBM, the electrons are extracted from the lowest unoccupied molecular orbital (LUMO) level of the PCBM to cathode. The holes are collected by anode from the highest occupied molecular orbital (HOMO) level of the polymer. If the energy levels of the photoactive materials and electrodes don't

match, large energy barrier will be produced. So interfacial layers are often used between the active layers and electrodes to form Ohmic contacts for efficient charge carrier extraction and prevent the electron and hole recombining. The detailed roles and materials of the interfacial layers will be introduced in the section 2.4 of this chapter.

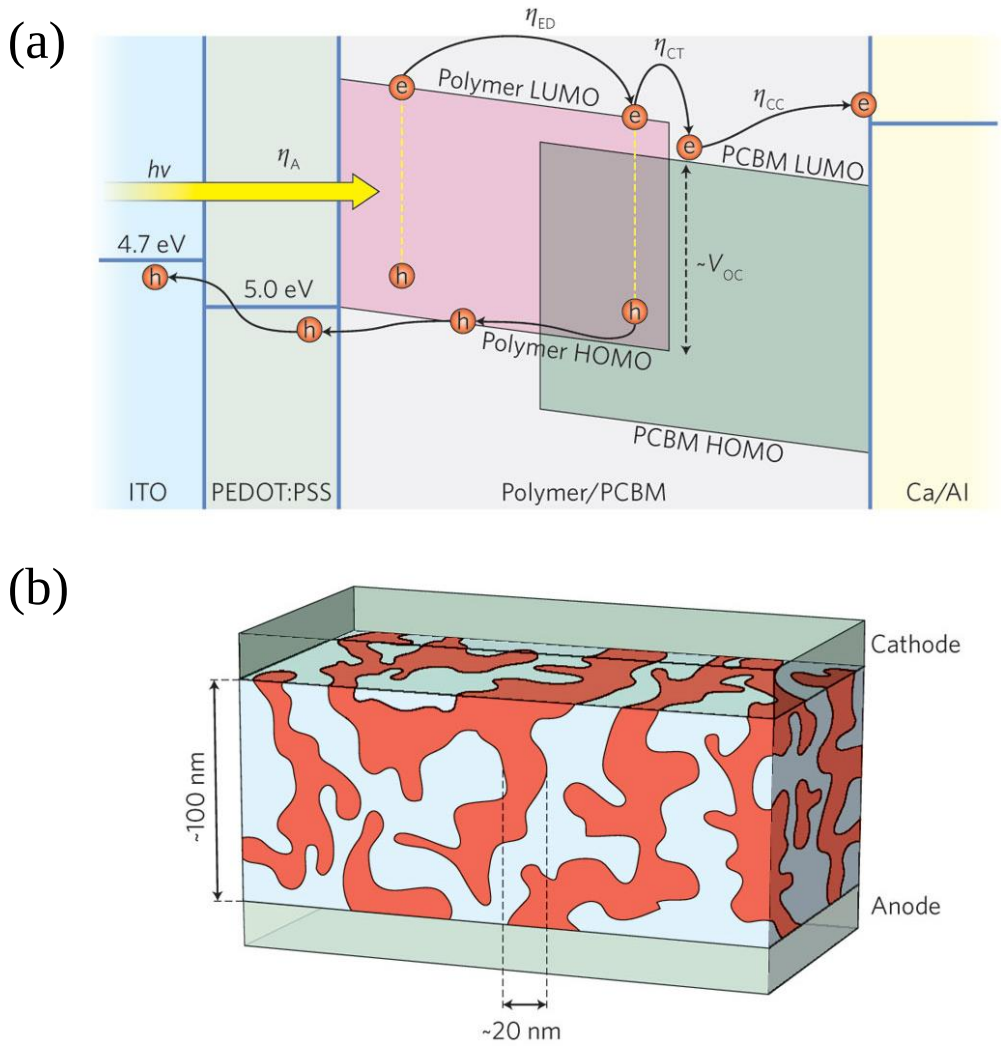

Figure 2.3: (a) Illustration of the operating mechanism of organic solar cells [13]. (b) The ideal morphology model with the bicontinuous interpenetration network of the donor and acceptor [47].

As mentioned in the section 2.1, the PCE of a solar cell is the product of V_{oc}, J_{sc}

and FF. In organic solar cells, the V_{oc} is determined by the difference between the HOMO level of donor materials and the LUMO level of acceptor material. There is an empirical equation expressing the value of V_{oc} of an organic solar cell:

$$V_{oc} = e^{-1} \times \left(\left|E_{HOMO}^{donor}\right| - \left|E_{LUMO}^{acceptor}\right| - 0.3\ eV\right)$$

where e is the elementary charge and 0.3 eV is an empirical value for efficient charge separation [48]. To increase the organic solar cells' V_{oc}, many researchers have made tremendous efforts on design and synthesis of new donor or acceptor materials with preferred energy level of HOMO and LUMO. One way to increase the V_{oc} of organic solar cells is to make the HOMO level of donor materials lower by utilizing groups that are less electron-rich [49-52]. The most popular donor material for organic solar cells is Poly(3-hexylthiophene-2,5-diyl) (P3HT) [53] which contains an electron-rich group, thiophene, as shown in Figure 2.4. The HOMO level of P3HT is around 4.9 eV and the V_{oc} of the P3HT based organic solar cells is around 0.6 V [54]. Fluorene and carbazole units are less electron-rich than thiophene. So, organic solar cells based on the donor materials using these units can achieve higher V_{oc}. For example, a polymer, PFO-DBT, demonstrated by Cao et al. contained a fluorene unit can achieve around 1.0 V of the V_{oc} as shown in Figure 2.4 [50]. Besides the energy level of donor and acceptor materials, non-radiative recombination between the donor and the acceptor can also affect the V_{oc}.

Another important parameter of organic solar cells is J_{sc}. The most straightforward way to increase the J_{sc} of organic solar cells is to make the bandgap of donor or acceptor materials narrower, so to absorb more lower energy photons of sunlight. Researchers in the chemistry and materials area

have developed some guidelines for design of low-bandgap donor materials. Alternating donor-acceptor structure using the push-pull driving forces between the donor and acceptor units can make the bandgap of narrower [55-57]. One successful donor material with this donor-acceptor structure is poly[2,6-(4,4-bis-(2-ethylhexyl)-4H-cyclopenta [2,1-b;3,4-b']-dithiophene)-alt-4,7-(2,1,3-benzothiadiazole)] (PCPDTBT) [58] as shown in Figure 2.4. The bandgap of PCPDTBT is 1.4 eV and its absorption wavelength edge can reach around 900 nm. Narrowing the bandgap cannot guarantee high J_{sc}. Some other factors can also influence the J_{sc}, such as carrier mobility, intermolecular interaction and molecular chain packing. For example, poly(4,4-dioctyldithieno(3,2-b:2',3'-d)silole)-2,6-diyl-alt-(2,1,3-benzothiadiazole)-4,7-diyl) (PSBTBT) (see Figure 2.4) is developed from PCPDTBT but has a higher crystallinity than that of PCPDTBT [59, 60]. As a result, PSBTBT based organic solar cells achieved a higher J_{sc} because of the higher crystallinity and improved hole mobility of PSBTBT. ''

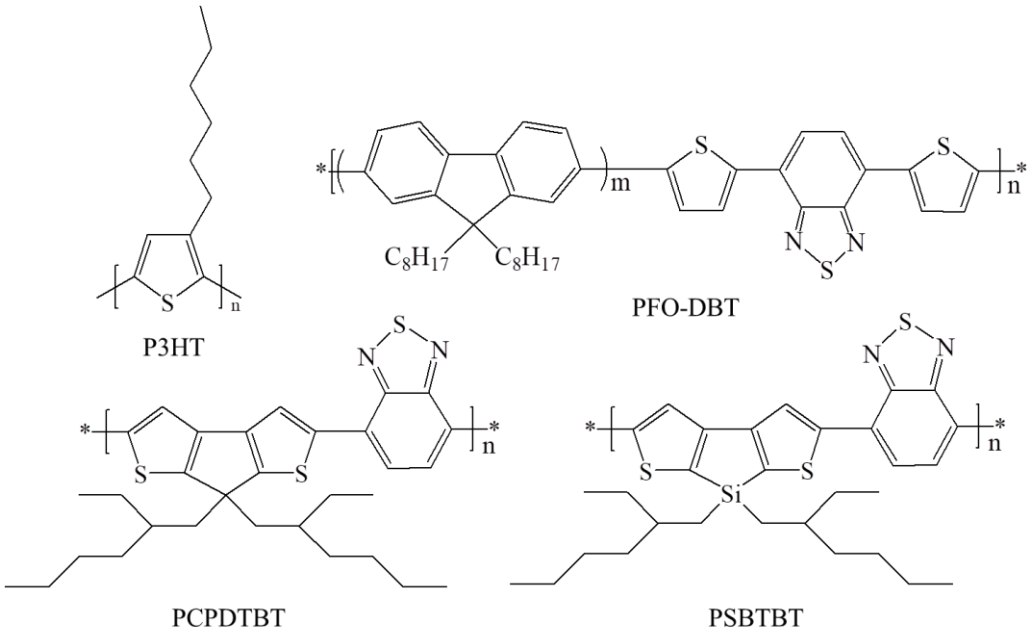

Figure 2.4: Chemical structures of representative donor and acceptor molecules used in organic solar cells.

FF is the third important parameter for organic solar cells. There are lots of factors that can influence the value of FF, such as charge carrier mobility, interface recombination, series and shunt resistances, film morphology and so on [61]. Choosing suitable interfacial layers between the active layers and electrodes can also help improve the FF of organic solar cells [62].

The above introduction focuses on improving the organic solar cells' performance by developing novel donor materials. Another aspect is to develop novel acceptors. So far, the most commonly used acceptors are fullerene derivatives, such as $PC_{61}BM$ and $PC_{71}BM$. To improve the V_{oc} of organic solar cells, one strategy is to upshift the LUMO level of acceptors. One impressive example is C_{60} with an indene bisadduct. By adding the electron-rich indene units to fullerene, the LUMO level was upshifted by 0.17 eV compared with $PC_{61}BM$. As a result, the V_{oc} of organic solar cells based on P3HT and C_{60}

bisadduct was enhanced by 40% to 0.84 V. Despite the success in improving the Voc of P3HT-based organic solar cells, it is still challenging to improve C_{60} bisadduct's compatibility with other polymer donors. Recent years, researchers are trying to replace fullerene derivatives by n-type polymers to overcome insufficiencies of fullerences, such as weak absorption of visible light and limited energy level variability. So far, the all-polymer solar cells can achieve a PCE higher than 8% [63].

2.3 Perovskite Solar Cells

The emergence of perovskite solar cells has changed the development of the third generation PV technology in recent years. In fact, perovskites are not new and have been known for over a century since it was discovered by a German mineralogist Gustrav Rose, in 1839. But it is until recent years that perovskites are applied into solar cells. A general formula ABX_3 is used to denote perovskites, where A and B are cations of different atomic radii and X is an anion. Perovskites used in solar cells often consist of a monovalent organic cation A (methylammonium ($CH_3NH_3^+$), or formamidinium ($(NH_2)_2CH^+$), a metallic cation B (Pb_2^+ or Sn_2^+) and a halide ion X (Cl^-, Br^- or I^-). Figure 2.5 shows the crystal structure of a perovskite material. An interesting property of perovskites is their tunable bandgap achieved by choosing different organic cations and halide anions [64]. In 2009, the first perovskite solar cell with a PCE of 3.8% was reported by the group of Miyasaka [28]. After two years, the group of Park increased the PCE of perovskite solar cells to 6.5% by modifying the electrolyte solvent and the perovksite deposition method [65]. In 2012, a small molecular material, Spiro-OMeTAD, was used as HTL in perovskite solar

cells and achieved 9.7% PCE of the device [66, 67]. After that, researchers worldwide have put tremendous efforts to improve the efficiency of perovskite solar cells. The improvement of perovskite solar cells mainly comes from optimization of perovskite film, interfacial engineering and structure design. So far, the highest certificated PCE of perovskite solar cells has reached to over 20% [29-34], with the highest PCE of 22.1% [68], making this the fastest-advancing solar technology to date [69].

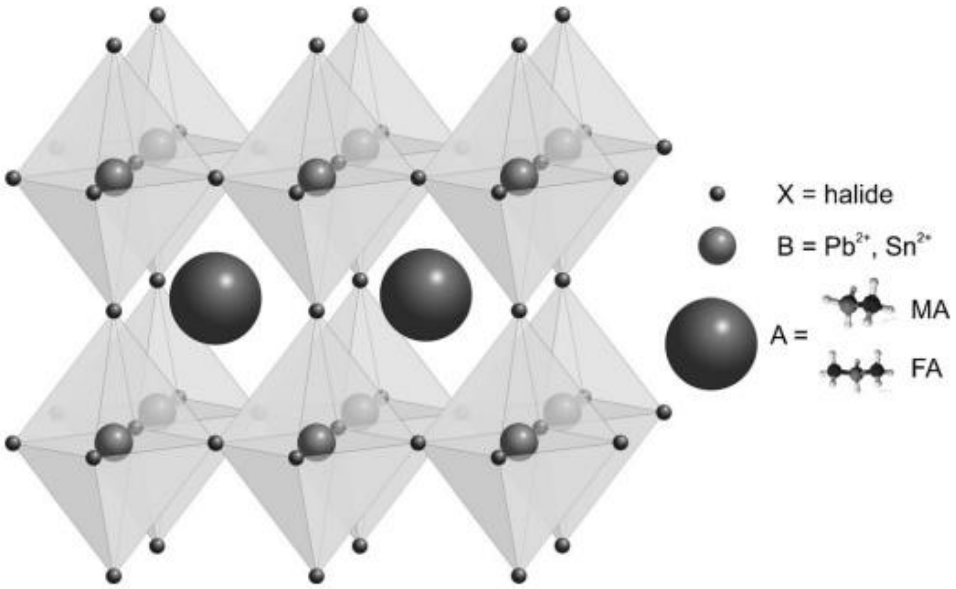

Figure 2.5: Schematic Perovskite crystal structure[70].

Perovskites have some unique properties that help perovskite solar cells achieve the high PCE above 20%. One is the strong optical absorption in the visible spectral region so the thickness of perovskite layers used in perovskite solar cells can be only around 500 nm. The photogenerated charge carriers can be efficiently collected in such thin perovskite layer. Another advantage of perovskites is that their bandgap can be tuned from 1.52 eV to 2.31 eV by changing the composition of a mixed perovskite material which contained two

organic cations (methylammonium and formamidinium), a metallic cation (Pb_2^+) and two halide ion (Br^- and I^-) [31, 71]. Figure 2.6 shows the absorbance and photoluminescence from the perovskites ($FAPbI_yBr_{3-y}$). The bandgap of the perovskites is determined to be tunable between 1.48 and 2.23 eV. With the bandgap around 1.5 eV, perovskites have wide absorption spectrum up to 800 nm. Besides, the adjustable bandgap of perovskites makes the perovskite solar cells an ideal sub-cell to be used in tandem structure solar cells. For example, the group of McGehee and Holman reported a perovskite/silicon tandem solar cell with 23.6% of the PCE [72]. Except for the optical properties, perovskites have high charge carrier mobility (66 $cm^2V^{-1}s^{-1}$) and low exciton binding energy (<10 meV) [73]. The electron- and hole-diffusion length in perovskites can be up to 1 μm due to the excellent charge carrier transport properties of the crystal structure of perovskites [74]. So, unlike organic solar cells, the electron-hole pairs generated after the photo-excitation of the perovskite light absorber can exist as free charge carriers because of their high exciton binding energy (29-50 meV for $MAPbI_3$ [75, 76] and 35-98 meV for $MAPbCl_{3-x}I_x$ [77, 78]) is comparable to the thermal energy (~25 meV) at room temperature. The generated charge carriers can be efficiently transported and collected by the corresponding electrodes.

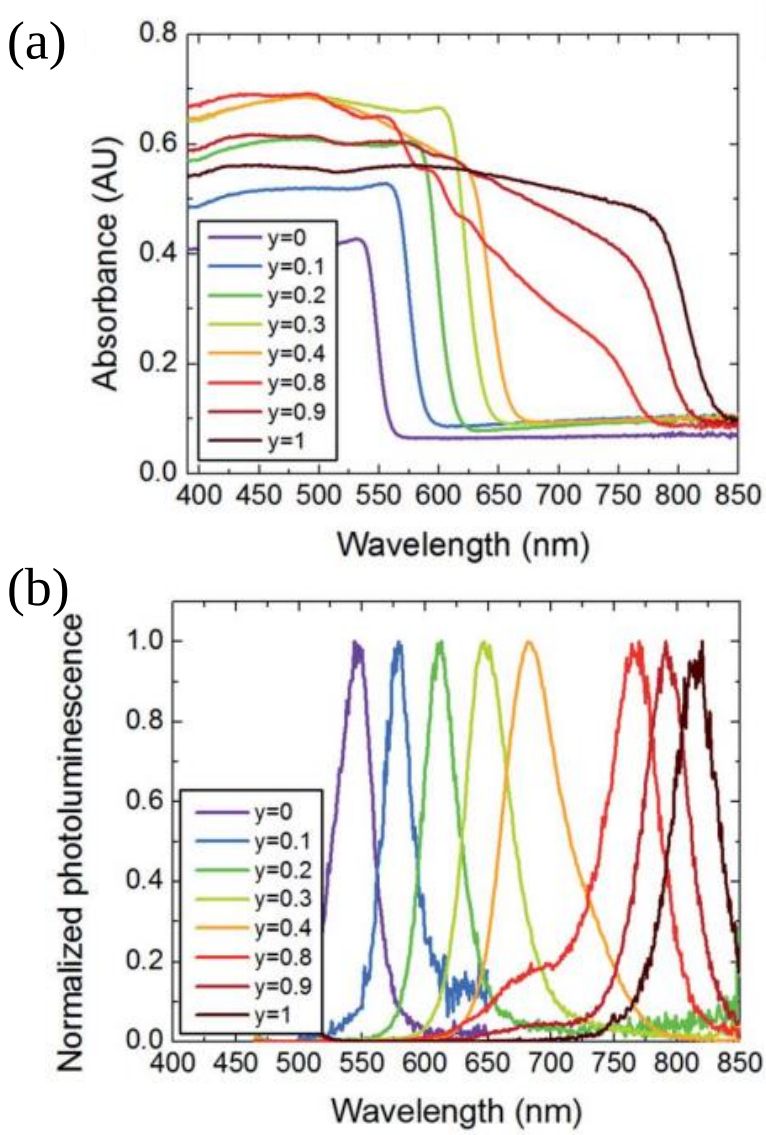

Figure 2.6. Tunability of the $FAPbI_yBr_{3-y}$ perovskite system. (a) UV-Vis absorbance of the $FAPbI_yBr_{3-y}$ perovskites with varying y, measured in an integrating sphere. (b) Corresponding steady-state photoluminescence spectra for the same films. [71]

The structures of perovskite solar cells can be divided into three different classes as shown in Figure 2.7. Figure 2.7 (a) shows the perovskite solar cell with a mesoporous structure. TCO stands for transparent conducting oxides which are commonly indium tin oxide (ITO) or fluorine doped tin oxide (FTO).

The ETL is electron transport layer and also called electron transport material (ETL). In a mesoporous structure, the ETL is often a thin titanium oxides Titanium dioxide (TiO_2) layer used. The mp-TiO_2 is a layer of mesoporous TiO_2 which was a TiO_2 scaffold filled with perovskite materials. Some other non-electron accepting, insulating dielectric oxides, such as Al_2O_3, have also been demonstrated to be used as the mesoporous scaffold [66]. On the top of mp-TiO_2 are the stacks of perovskite layer, hole transport layer (HTL) or hole transport material (HTL) and Au electrode. The thickness of HTL has a significant influence on the perovskite solar cells' performance and is dependent on the processing technique and the type of HTL. The thickness of some commonly used HTL like Spiro-OMeTAD [32] and PTAA [79] is 100~200 nm. This mesoporous structure is derived from dye-sensitized solar cell (DSSC) and the mesoporous layer is used to facilitate the electron transfer from the perovskite to the TiO_2 layer. As mentioned before, the charge carrier diffusion length can be >1 μm which is much longer than the perovskite layer's thickness (~500 nm) [80, 81]. Some researchers have reported that perovskites exhibited ambipolar behavior, so they can transport both electrons and holes [80]. These properties of perovskites indicate that the charge carriers generated within the perovskite layer can efficiently be transported to the interface between the perovskite layer and ETL or HTL even without the mesoporous layer. Figure 2.7 (b) and (c) demonstrate two different planar structures of perovskite solar cells. The structure shown in Figure 2.7 (b) has almost the same structure as Figure 2.7 (a) except that it has no mesoporous layer. The direction of electrons and holes transport is also the same as in the mesoporous structure. So, this planar structure is called regular planar structure. Another planar structure is shown in Figure 2.7 (c). In this structure, the HTL is placed at the bottom while the ETL is placed on the top of the perovskite. The

commonly used HTLs in the planar structures are PEDOT:PSS, NiO and MoO_3. The top electrodes are low work function metal, such as Ag or Al, so the direction of electrons and holes transport is reversed. This structure is called inverted planar structure. So far, most highly efficient perovskite solar cells with PCE more than 20% are based on the mesoporous structure [30-34]. After years' progress, the PCE of perovskite solar cells based planar structure can also reach to around 20% [82-84].

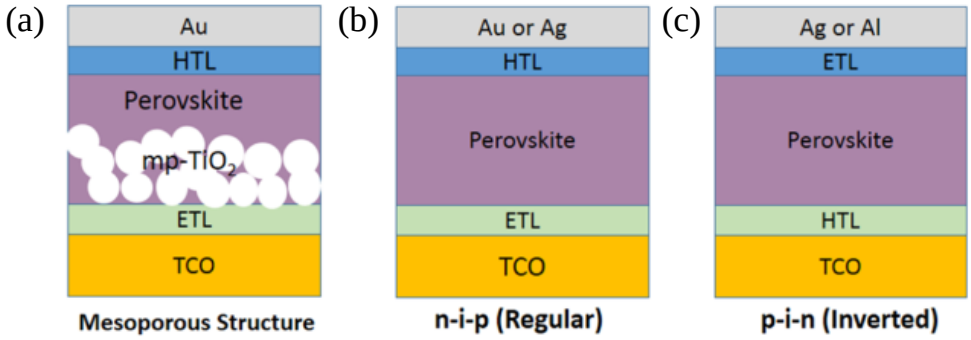

Figure 2.7: Three typical structures of perovskite solar cells: (a) mesoporous structure, (b) regular planar structure, and (c) inverted planar structure [85].

The most important factor that influences the performance of perovskite solar cells is the quality of the perovskite film. The fabrication of perovskite layers with high quality is very intriguing due to the complicated reaction during the growth of perovskite crystals. To fabricate high quality perovskite films, great efforts have been made to develop the perovskite growth techniques. So far, several growth techniques for preparation of reproducible and high performance perovskite films have been developed and utilized. Among these techniques, solvent-based methods [66, 67] and physical vapor deposition methods are the most commonly used. Physical vapor deposition methods include vacuum deposition or vapor assisted solution processing [86-88]. Figure 2.8 (a) shows

the dual-source thermal evaporation system for depositing the perovskite absorbers [88]. The cross-sectional SEM images of perovskite solar cells prepared by vapour-deposition method are shown in Figure 2.8 (b). The cross-sectional SEM images demonstrate that uniform and compact perovskite films can be prepared by the vapour-deposition method. Compared with the solvent-based methods, physical vapor deposition methods have higher manufacturing cost, so in this thesis we mainly focus on using the solvent-based methods. Perovskite layers can be deposited by one step or two step solution processes. For using two-step method to fabricate the perovskite solar cells with a mesoporous structure, a layer of PbI_2 is firstly deposited on the surface of TiO_2 mesoporous layer by spin coating [89]. Then the PbI_2 layer is immersed in CH_3NH_3I (MAI) isopropanol solution for 20 s and rinsed with isopropanol. Then the film was dried by annealing at a certain temperature which depends on the type of perovskite materials used. The one step method is much simpler than the two step method. In the simplest one step method, the perovskite precursor solution is prepared by dissolving the inorganic (PbI_2, or $PbCl_2$ or $PbBr_2$) and organic component (MAI, or MACl, or MABr) in a polar aprotic solvent (N,N-dimethylformamide (DMF), or dimethyl sulfoxide (DMSO) or γ-butyrolactone (GBL)). Then, the perovskite layer is spin coated on the mesoporous TiO_2 layer and annealed at 100 ℃ or other temperature. Incomplete coverage and large variation in morphology of the perovskite layer are normally received by using this method. To solve this problem, an anti-solvent method was utilized to modify the one step deposition process [90, 91]. In the anti-solvent method, a few drops of the nonpolar solvent, such as toluene and chlorobenzene, are added during the spin coating of the perovskite layer as shown in the Figure 2.9. The nonpolar solvent is miscible with the perovskite precursor solution but doesn't dissolve the perovskite film. Adding

the nonpolar solvent during the spin coating process can help remove the polar aprotic solvent in which the perovskite material is dissolved. During the spinning process, the nonpolar solvent will cause precipitation of the salt in perovskite precursor and formation of the intermediate phase, such as MAI-PbI_2-DMSO. After annealing the layer at 100℃ to drive out DMSO, the intermediate phase will be converted into smooth perovskite crystalline film with large grains. The anti-solvent method was first developed by Seok et al. in 2014 [91] and now is widely adopted by many other researchers to prepare high quality perovskite films because of its high reproducibility [92].

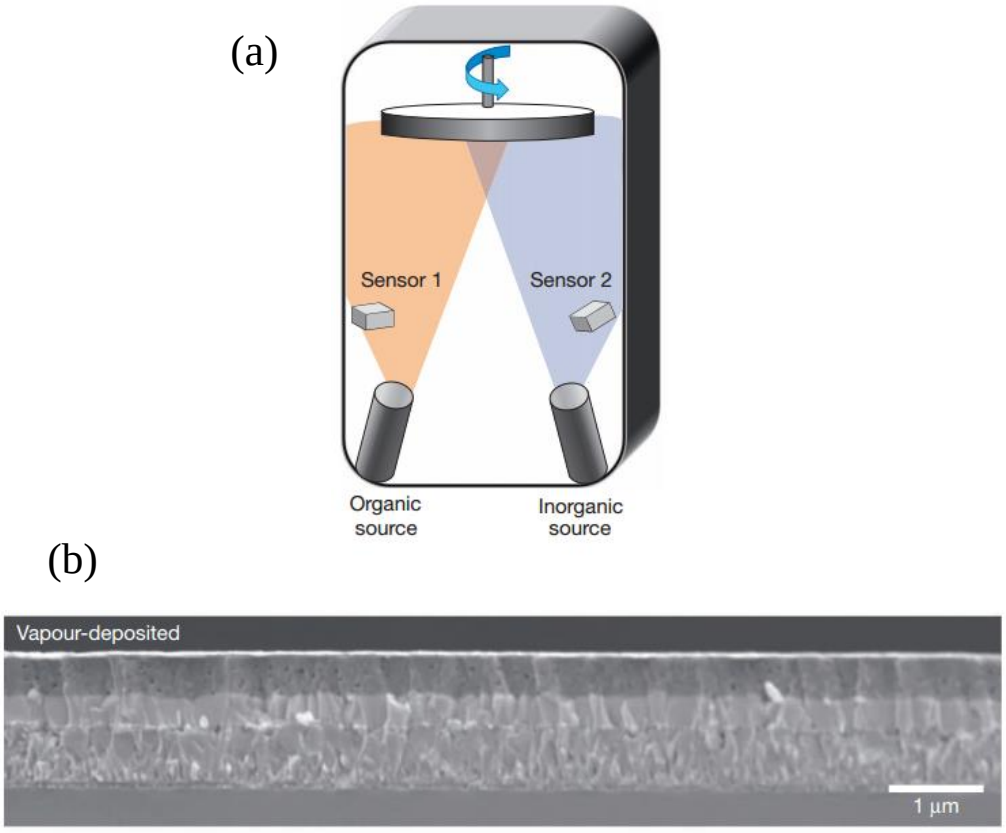

Figure 2.8: (a) Dual-source thermal evaporation system for depositing the perovskite absorbers; the organic source was MAI and the inorganic source $PbCl_2$. (b) Cross-sectional SEM images under lower magnification of completed solar cells constructed from a

vapour-deposited perovskite film. [88]

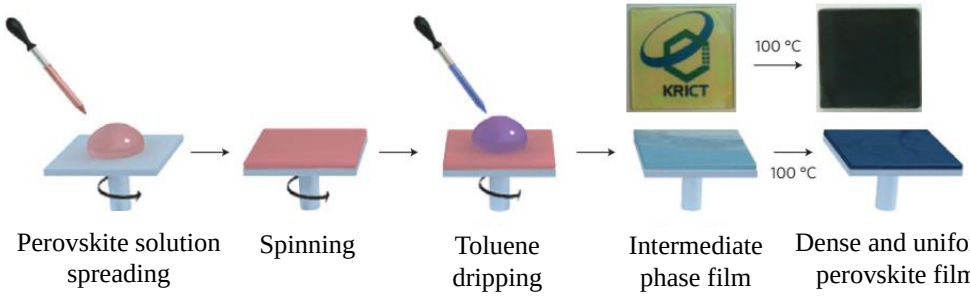

Figure 2.9: Fabrication processes for preparing an uniform and dense perovskite film by anti-solvent method. [91]

2.4 Interfacial Materials

In both of the organic solar cells and perovskite solar cells, interfacial layers are very important for achieving efficient charge carriers extraction and collection and to improve the solar cells' performance. The interfacial materials in an organic solar cell or perovskite solar cell have the following roles: to reduce the energy barrier between the active layer and the electrodes; to form a selective contact for one type of charge carriers; to prevent the chemical or physical reaction between the active layer and electrodes; to act as optical spacer for adjusting the optical field distribution within the device.

Interfacial materials are grouped as the electron transporting layers (ETL) and hole transporting layers (HTL) according to their electrical properties. ETL and HTL is used to facilitate electrons and holes to transfer from the active layer to the cathodes and anodes respectively. In the organic solar cells, the energy barrier that prevents electrons or holes transporting to the cathodes or anodes is created by the energy difference between the work function of the cathodes or anodes and the LUMO or HOMO level of the acceptor or donor in the active

layer. While in perovskite solar cells, the energy barrier for electrons or holes transport is created by the energy difference between the work function of cathodes or anodes and the valence or conduction band of the perovskite layer. Figure 2.10 shows the energy levels in an organic solar cell (a) and perovskite solar cell (b). Good interfacial layers can facilitate holes transport from the HOMO level of the donor to anode and electrons from the LUMO level of the acceptor to cathode, respectively. In the perovskite solar cell, good interfacial materials must help improve the transport of electrons from the conduction band to the cathode and the transport of holes from the valence band to the anode, respectively.

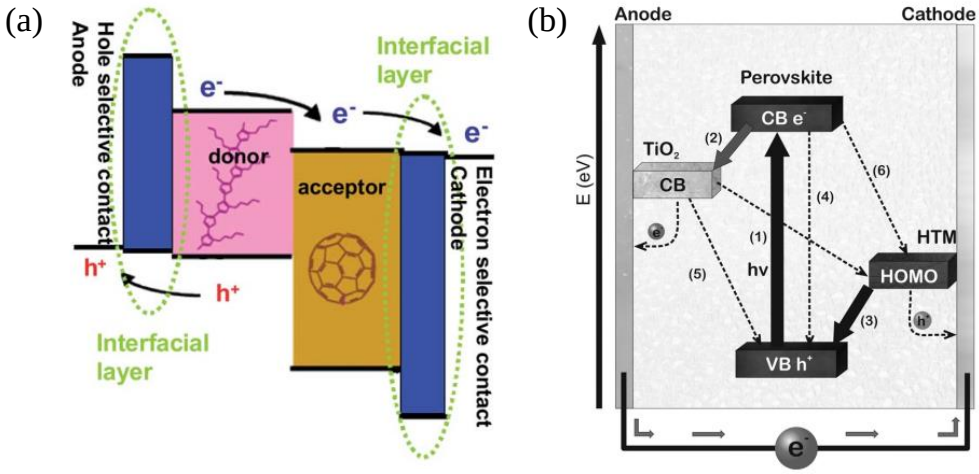

Figure 2.10: (a) Schematic illustration of energy levels in an organic solar cell [62]. (b) Schematic representation of the energy levels and electron transfer processes in perovskite solar cells [70].

2.4.1 Interfacial Materials for Electron Transport Layer

Solution processed transition metal oxides (TMO) are popular interfacial materials used in both organic solar cells and perovskite solar cells because of their good stability and electrical properties. The n-type TMO used in organic solar cells and perovskite solar cells as ETL is centered around TiO_2 and ZnO

due to their ambient stability, optical transparency, and suitable work function that matches the LUMO level of PCBM and the conduction band of perovskite. Various methods for preparing the TiO_2 and ZnO interfacial layers have been developed. But the low temperature processed sol-gel method is often preferred because it can reduce the fabrication costs and enable fabrication of solar cells on flexible substrates. Some sol-gel methods for depositing TiO_2 and ZnO layer require annealing temperature of less than 200 ℃ [22, 93-96]. ZnO nanoparticles used as the ETL in organic solar cells and perovskite solar cells can be processed at room temperature without high temperature annealing [97]. Beside using the sol-gel methods, the TiO_2 layer can also be prepared by low temperature atomic layer deposition (ALD) method at a temperature of 130-170 ℃ [98]. The pristine TiO_2 and ZnO layer often suffer from low conductivity and undesired work function. The performance of TiO_2 and ZnO layers can be effectively improved by doping them with Mg, Al, Li, Nd [21, 22, 99-104]. For example, ZnO doped with Mg by a sol-gel method exhibited better performance than the pristine ZnO ETL because of the better work function and bandgap adjusted by controlling the Mg doping content [99]. Besides the work function and bandgap, doping Mg can also improve the stability of the ZnO ETL by reducing the oxygen defects within the ZnO ETL [100]. Some other TMO ETLs include SnO_2, WO_x, etc., are also used [105, 106]. Unlike TMO ETLs, there are various TMO HTLs, such as NiO_x [107-109], MoO_x [110, 111], VO_x [112], WO_3 [113], RuO_x [114], ReO_x [115], CuO_x [116], CrO_x [117], and Fe_3O_4 [118]. The research of TMO HTLs is focused on developing solution processing techniques for large-scale and high-throughput production of organic solar cells and perovskite solar cells.

Organic interlayers are also commonly used in organic solar cells or perovskite

solar cells. Unlike some TMO interlayers which require high temperature annealing, most organic interlayers can be solution processed under a low temperature less than 150 ℃ so they can be used for fabrication of flexible organic solar cells and perovskite solar cells. The solution processed organic interlayers are compatible with roll-to-roll fabrication process, thus enabling fabrication of large area solar cells. The N-type organic electron transporting layer (ETL) can be categorized into non-fullerene oligomers, fullerene derivatives, neutral polymers, polyelectrolytes.

Non-fullerene oligomers can act as good ETL to improve the performance of organic solar cells and perovskite solar cells. DCDA and Urea, reported by Yang *et al.*, contains amino group which was coordinated with Al atoms, thus preventing undesired interactions between photoactive layer and electrode [119]. Besides, the amino groups could influence the interfacial dipole formation at photoactive layer and electrode interface, resulting in work function shifting of electrode. Some other non-fullerene oligomers also could improve the PCE of organic solar cells by forming interfacial dipoles, such as PTCDI+:PEDOT:PSS- composite [120], zwitterion Rhodamine 101 [121], F8PS [122] and 3TPA-FEP [123]. The Rhodamine 101 was used in perovskite solar cells as ETL later and achieved a PCE of 12.1% [124]. Another mechanism for non-fullerene oligomer ETLs to enhance the PCE of organic solar cells is self-doping. Gregg *et al.* reported a self-doped PETLa+OH- ETL with good conductivity [125]. PDINO ETL, reported by Li *et al.*, can be operated in a wide thickness range (6-25 nm) because of its high intrinsic conductivity and work function tuning ability, leading to a PCE of 8.35% in a PTB7:$PC_{71}BM$ based device [126]. They also applied PDINO into planar structure perovskite solar cells to improve the electron extraction properties and

achieved a high PCE of 14.0% [127]. In addition, Fang *et al.* reported that FTBTF-N can modify the photoactive layer's surface morphology, thus enhancing the PCE of PTB7:$PC_{71}BM$ device to 9.22% [128].

Fullerene derivatives have attracted lots of attention in both organic solar cells and perovskite solar cells community. Li *et al.* has modified C_{60} to be PEG end-caped C_{60} (PEGN-C_{60}) and $–NH_2$ group containing C_{60} (DMAPA-C_{60}) [129, 130]. The functional groups (PEG and $–NH_2$) help reduce the energy barrier between photoactive layer and electrode, thus achieving high PCEs of 7.45% and 7.42% in PBDTTT-C-T:$PC_{71}BM$ devices. The same group also reported on modifying the ester groups of $PC_{61}BM$ with amine end-groups to obtain a PCBDAN ETL [131]. The PCBDAN can be further modified by introducing methyl iodide, resulting in a derived salt, PCBDANI. Both of the PCBDAN and PCBDANI can be dissolved in alcohol and form interfacial dipoles at the photoactive and electrode interface. A high PCE of 7.69% of organic solar cells was demonstrated. The strategy of introducing amino group was also utilized to modify $PC_{71}BM$ [132, 133]. The amino groups in the $PC_{71}BM$ derivatives not only formed interfacial dipoles, but also induced contact doping by forming intermediate amine. Another example of contact doping is a fullerene-based ETL composite which consists of conductive fulleropyrrolidine (FPI) (Bis-OMe) and small amount of insulating PEIE [134]. This hybrid ETL has both self-doping and contact doping properties. Through contacting with the PCBMs in photoactive layer, it can improve the energy alignment between the electrode and PCBMs. As a result, the hybrid ETL-based PTB7:$PC_{71}BM$ achieved a high PCE of 9.62%. Hydrophilic triethylene glycol (TEG) functional groups were reported to modify C_{60}, leading to an alcohol soluble EGMC-CO_2H ETL [135]. FPI-based Mono-C60 and Bis-C60 ETLs, introduced by Jen et al., have good

performance [136]. Over 9% PCE was achieved when using the bis-C_{60} ETL into PIDTT-DFBT:$PC_{71}BM$ device. Bis-C60 ETL was also reported to be used in perovskite solar cells to align the energy levels at the $PC_{61}BM$ and electrode interface [137-141]. Another two high performance fulleropyrrolidines are amine and sulfobetaine substituted, C_{60}-N and C_{60}-SB, reported by Russell and Emrick *et al.* [142]. When using in the PTB7-Th:$PC_{71}BM$ devices, the highest PCEs are 8.57% and 9.35% for C_{60}-SB and C_{60}-N respectively. Besides, some other FPI ETLs, such as FN-C60 and CPTA [143, 144], were also reported to have good performance in organic solar cells. Fullerene derivatives, such as C_{60}, $PC_{61}BM$ and $PC_{71}BM$, are popular in perovskite solar cells due to their room-temperature and orthogonal solvent processability and decent electron mobility [139, 145-148]. In addition, bis-C60 surfactant has been reported to be used in perovskite solar cells for aligning the energy levels at the PC61BM and electrode interface [137-141].

Neutral polymers are promising ETLs for organic solar cells and perovskite solar cells. There are three types of neutral polymer ETLs, ethoxylated polyethylenime or branched polyethylenimine (PEIE/PEI), PFN-based and polycarbazole (PC)-based derivatives. Kippelen *et al.* reported that an ultra-tin (<10 nm) layer of insulating PEIE/PEI can modify the work function of electrodes through the intrinsic molecular and interfacial dipoles [149]. After this discovery, PEIE/PEI ETLs were widely used in organic solar cells and perovskite solar cells. Kim *et al.* reported on using PEI between ZnO and photoactive layer to obtain a PCE of 8.76% for PTB7:$PC_{71}BM$ device [150]. They attributed the high performance to improved interfacial dipoles on ZnO interface and reduced its roughness. Due to the excellent performance in modifying work function of electrodes, PEIE was also widely employed in

perovskite solar cells. Yang Yang *et al.* reported a high performance planar structure perovskite solar cells (PCE of 19.3%) based on PEIE and Yttrium-doped TiO_2 (Y-TiO_2) bilayer ETLs [84]. Brabec, C. J. *et al.* utilized PEIE at the PCBM ETL and top Ag electrode interface to reduce the work function of Ag [151]. PFN-based neutral polymers became popular ETLs for organic solar cells and perovskite solar cells after Wu *et al.* reported a 9.21% PCE in PTB7:PC_{71}BM device by using PFN to improve the Ohmic contact at the ITO and photoactive interface [152]. Later, a lot of PFN-based neutral polymers were synthesized and applied as ETLs in organic solar cells, such as PFCn6:K+ [153], PFEN-Hg [154], PFN-OX [155], PBN [156], HBPFN [157], PFPA-1 [158] and so on. Besides, Yang Yang *et al.* applied PFN into planar single junction and tandem perovskite solar cells [159, 160]. PC-based neutral polymer ETL have been investigated by several groups. Chen *et al.* synthesized two PC-based ETLs, PC-P and PCP-EP, by introducing phosphonate side chains into PC homopolymers and copolymers to improve their work function modification ability [161, 162]. Another PC-based neutral polymer, PCDTBT-N, was introduced by Huang *et al.* [132]. They used polar amino groups to functionalize the PCDTBT-N, thus improving electron extraction efficiency.

Polyelectrolytes can be easily dissolved in alcohol-based solvents making them suitable for ETL applications in organic solar cells and perovskite solar cells. Using PFN as prototype, various PFN-based conjugated polyelectrolytes were synthesized. Huang *et al.* discovered that N-oxide-functionalized PF copolymers (PNOs) had better performance than the amino functionalized polymers (PNs) [163]. The same group also reported on using PFN-Br and zwitterionic PFN-based conjugated polyelectrolytes (PFNSO) as ETL for achieving high performance organic solar cells, PCE of 8.40% and 8.74% [164,

165]. Besides PFN-based conjugated polyelectrolytes, polythiophene (PT)-based conjugated polyelectrolytes have also been investigated. Buriak *et al.* reported a P3(TBP)HT+:PEDOT:PSS- composite ETL for highly stable organic solar cells in which 97% of the original PCE could be maintained over 1000 hours of storage in air [166]. After this work, imidazolium-substituted PT-based ETLs, P3(IMD)HT-Br, were reported by Maes *et al.* [167]. Emrick *et al.* developed a series of zwitterionic PT-based ETLs, PTBTSB-1 and PTBTSB-2 [168]. They also introduced non-conjugated azulene-triazole (A-T) PATSB ETLs [169]. The optical properties and excitonic behavior can be adjusted by controlling the A-T density along the polymer chains. After optimization of the A-T density in the PATSB ETLs, a high PCE of 7.9% was achieved in the PTB7:$PC_{71}BM$ device.

2.4.2 Interfacial Materials for Hole Transporting Layer

There are various TMO HTLs reported in organic solar cells and perovskite solar cells, such as NiO_x [107-109], MoO_x [110, 111], VO_x [112], WO_3 [113], RuO_x [114], ReO_x [115], CuO_x [116], CrO_x [117], and Fe_3O_4 [118]. The research of TMO HTLs is focused on developing solution processing techniques for large-scale and high-throughput production of organic solar cells and perovskite solar cells. Among the above TMO HTLs, NiO_x is most widely studied. So *et al.* have reported on preparing NiO_x by thermolysis (275 ℃) of the precursors of nickel acetate tetrahydrate and monoethanolamine in ethanol. This NiO_x HTL enabled a high PCE of 7.82% in pDTG-TPD:$PC_{71}BM$ device [170]. Xie *et al.* developed an annealing-free NiO_x HTL achieved by using sonochemical synthesis [171]. The NiO nano particle HTL could be obtained at low temperature through ultrasonic irradiation. Guo *et al.* used a mesoporous NiO_x HTL in a conventional perovskite solar cell and obtained a PCE of 9.51%

[323]. Planar NiO HTL prepared by sol-gel NiO was reported by Yang *et al.* [324]. The PCE of the planar structure perovskite solar cells is 9.11%. Jen *et al.* improved the PCE of NiO_x-based perovskite solar cells to 15.4% by doping the NiO_x with Cu to enhance its conductivity [325]. Later, Yang Yang *et al.* reported a high performance planar structure perovskite solar cell based on NiO_x HTL prepared from nickel nitride precursors [109]. The highest PCE is 16.1% and the NiO_x-based perovskite solar cell retained about 90% of their original efficiency after 60 days storage in air at room temperature. After that, Han *et al.* developed a Li and Mg-doped NiO HTL prepared by spray pyrolysis method [172]. By using the doped NiO HTL, they obtained a certificated PCE of 16.2% in a large size (>1 cm^2) perovskite solar cell. Recently, Jen *et al.* reported a nanoparticle-based NiO_x HTL modified with para-substituted benzoic acid self-assembled monolayers (SAMs) [173]. The highest PCE of perovskite solar cells reached 18.4%.

Conductive PEDOT:PSS is the most popular p-type organic interlayers. Due to the high transparency and conductivity, organic solar cells or perovskite solar cells using PEDOT:PSS as HTL can achieve high efficiency [19, 83]. One of the drawbacks of PEDOT:PSS is its acid nature which can lead to inferior stability of solar cells. To improve the stability, a conductive conjugated polyelectrolyte, CPE-K [174, 175], has been synthesized. Compared with PEDOT:PSS, CPE-K has more suitable energy level, higher conductivity and optical transparency. Moreover, CPE-K has a neutral pH value around 7.56. So replacing PEDOT:PSS by CPE-K in organic solar cells can improve the devices' performance and stability. To unveil the doping mechanism of CPE-K, Bazan *et al.* developed two additional conjugated polyelectrolytes, $PCPDTPhSO_3Na$ and $PFBTSO_3Na$ [175]. They found $PFBTSO_3Na$ didn't have self-doping property,

thus demonstrating the importance of CPDT units on p-doping phenomenon. Gomez *et al.* reported a sulfonated poly(phenylsulfone) (SPS) HTL functioned as efficiently as PEDOT:PSS in organic solar cells [176]. The SPS localized at the anodic interface and created interfacial doping in photoactive layer. Due to the insulating nature, the SPS HTL best operated at a thickness of less than 3 nm. PEDOT:PSS is also widely used in inverted planar structure perovskite solar cells because of its high transparency, suitable energy levels and compatibility with perovskite [145, 146]. Some researchers have made efforts to improve the charge selectivity of PEDOT:PSS HTL. Bolink *et al.* developed a bilayer-type HTL consisting of polyarylamine (polyTPD) and PEDOT:PSS to improve the electron-blocking efficiency [147]. PEDOT:PSS was reported by Lee *et al.* that it could be modified by a perfluorinated ionomer [177]. The perfluorinated ionomer could self-organized on the surface of HTL, thus improving the energy level alignment between the HTL and perovskite layer. As a result, they obtained a PCE of 11.7% and 8.0% in the perovskite solar cells based on ITO and flexible substrates, respectively.

In regular structure perovskite solar cells, the most commonly used p-type interlayer is a small molecular, Spiro -OMeTAD [178, 179]. Spiro-OMeTAD was previously used in dye-sensitized solar cells (DSSCs). The intrinsic property of Spiro-OMeTAD is not good enough for acting as a HTL in perovskite solar cells, but doping cobalt based dopants and ionic salt can greatly improve the conductivity and charge carrier mobility of Spiro-OMeTAD. Perovskite solar cells using Spiro-OMeTAD as HTL have achieved more than 20% PCE [30-34]. In addition to Spiro-OMeTAD, various small molecular HTLs were developed by using Spiro-OMeTAD as prototype. Seok *et al.* systematically changed the side chain (-OMe) position in the spiro-type

arylamine HTLs and obtained a high PCE of 16.7% by linking the –OMe groups at the ortho position [180]. Besides the spiro-type HTLs, some other types of small molecular HTLs have also been reported, such as carbazole-based derivatives [181, 182], quinolizino acridine-based molecules [183] and tetrathiafulvalene derivatives [184]. Michael Saliba *et al.* synthesized a HTL with a simple dissymmetric fluorene–dithiophene (FDT) core substituted by N,N-di-p-methoxyphenylamine donor groups which can be easily modified. They proposed that the additional thiophene-iodine interaction may improve the holes' transfer at the FDT/perovskite interface, which achieved high performance of the perovskite solar cells with PCE of 20.2% [185]. Kasparas Rakstys *et al.* reported four novel star-shaped triazatruxene derivatives used as the HTL in perovskite solar cells, which achieved the best PCE of the device of 18.3% [186]. Sungmin Park *et al.* reported a high mobility small molecular HTL, PCP-TPA, and obtained the perovskite solar cells with PCE of 17.8% [187]. Polymer HTLs for perovskite solar cells can also achieve high performance. Polytriarylamine (PTAA) is the most famous polymer HTL. More than 20% PCE of perovskite solar cells has also been achieved by using PTAA as HTL [29]. Some polymers which were previously used in organic solar cells as donors in active layers have been reported to be applied into perovskite solar cells as HTLs, such as P3HT [188], PCPDTBT [79], PBDTTT-C [189] and so on. To avoid the doping process, some researchers developed dopant-free HTLs for perovskite solar cells. Yang Yang *et al.* reported a small molecule HTL, DOR3T-TBDT, which enabled a PCE of 14.9% in regular structure perovskite solar cells without using any dopants [190]. The good performance of DOR3T-TBDT was attributed to its high bulk electrical conductivity and the hole mobility. McGehee *et al.* have demonstrated a pre-oxidized Spiro-OMeTAD, spiro$(TFSI)_2$, to avoid the doping of LiTFSI

[191].

2.5 Printable Organic and Perovskite Solar Cells

One of the most attracting properties of organic solar cells and perovskite solar cells is that they can be solution processed on flexible substrates, thus enabling the fabrication by printing techniques. Using printing techniques to fabricate organic solar cells and perovskite solar cells will greatly reduce the manufacturing costs and increase their throughput.

Spin coating technique is widely used to deposit solution processed thin films with good uniformity in a small area. In a typical spin coating process, a small amount of the precursor solution to be coated is applied to a substrate which is then accelerated to a chosen rotational speed. During the spin coating process, most of the applied solution will be ejected and wasted. So the spin coating technique is not suitable for large-scale production. To prepare the solution processed thin films in large scale, many other deposition techniques have been developed, such as screen printing [12], ink jet printing [192], doctor blading [193] or knife-over-edge printing [194], slot die printing [195] and so on.

Figure 2.11 (a) shows the process of screen printing. A screen of woven material is glued to a frame under tension. The screen is filled with emulsion that is impervious to the coating solution while the pattern area is without emulsion. After filling the screen with coating solution, a squeegee is used to force the screen into contact with the substrate which is aligned under the screen. Then the squeegee is drawn linearly across the screen to force the solution through the open areas onto the substrate. The coating solution for

screen printing needs to have relatively high viscosity. Compared to screen printing, ink jet printing is a relatively novel printing process as shown in Figure 2.11 (b). The printing head is made of materials (e.g., ceramic) that are resistant to the organic solvents to be processed, thus compatible with a wide range of solvents. After loading the printing ink, the droplet will be formed by mechanical compression of the ink through a nozzle or by heating the ink. Then an applied electrical field will accelerate the charge droplet along the direction of electrical field towards the substrate. The advantage of ink jet printing technique is the ability of creating complex patterns, but in a small area. Figure 2.11 (c) shows the Knife-over-edge printing process which belongs to roll-to-roll printing techniques. The knife-over-edge printing technique works by placing a sharp blade at a fixed distance from the substrate surface that is to be coated. The coating solution is placed in front of the blade and then moves across the blade to the substrate. With the substrate moving forward, a thin wet film is left on it. In the knife-over-edge printing process, there is no waste of ink solution as all the ink supplied to the knife will be coating onto the substrate. Illustration of the slot die printing process is shown in Figure 2.11 (d). The slot die printing process is similar to the knife-over-edge printing process but it’s printing head is much more complex. A mask is used in the printing head to define the slots and disperse the ink through the individual slots. The thickness of the coated wet films is controlled by the speed of the web and the rate of feeding the ink solution to the coating head.

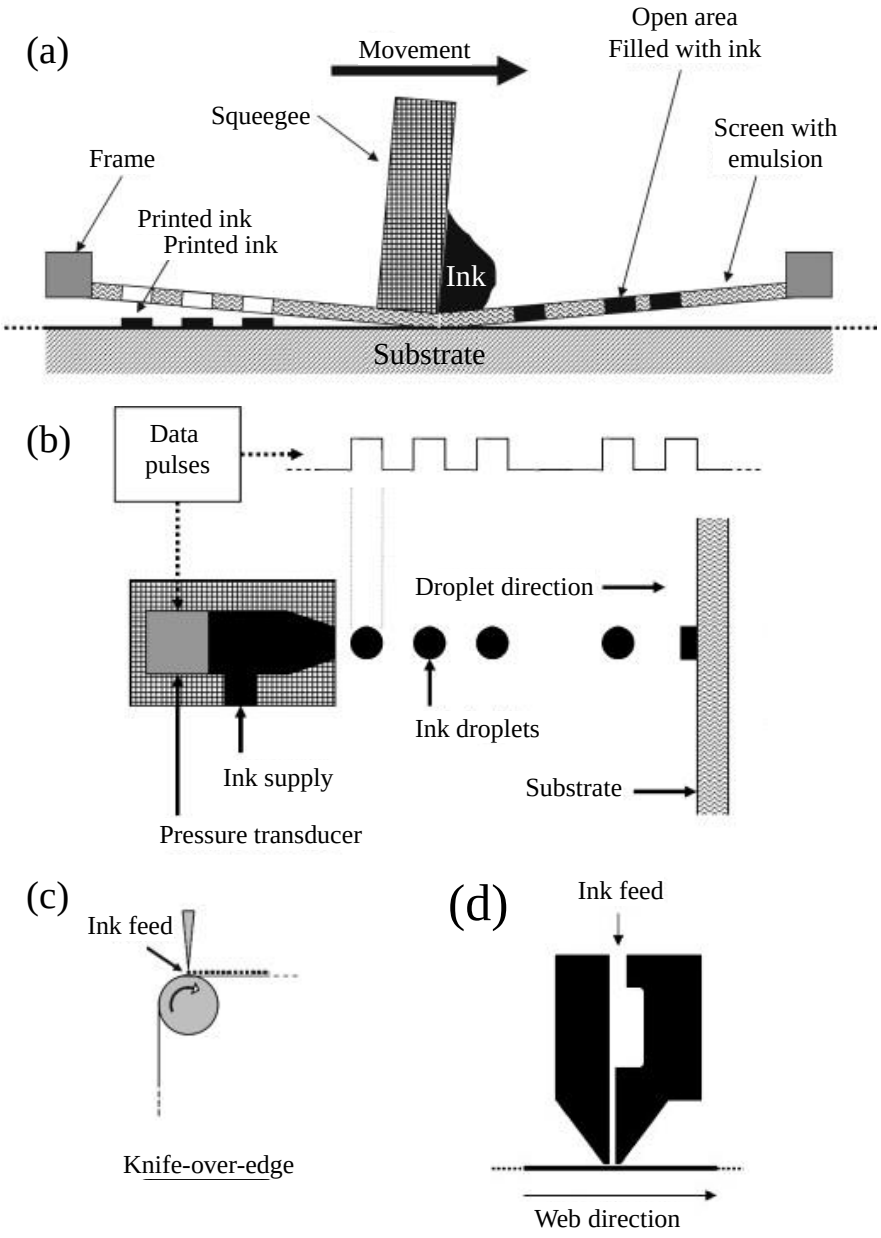

Figure 2.11: Illustrations of the screen-printing (a), ink jet printing (b), knife-over-edge printing (c) and slot die printing (d). [196]

Various printing techniques have been applied into fabrication of organic solar cells. FC Krebs et. al. reported using screen printing technique to fabricate flexible large area organic solar cells [12]. In this report, all the layers of the organic solar cells were deposited by using screen printing processes, which

demonstrated the fabrication of organic solar cells with low cost large-scale roll-to-roll process. T. Aernouts et. al. used ink jet printing technique to prepare the active layer (P3HT and fullerene blend film) of organic solar cells and achieved a PCE of 1.4% [197]. Formation of the ink solution for ink jet printing organic solar cells plays an important role in the performance of organic solar cells fabricated. Hoth, Claudia. et. al. studied the influence of the ink solution on the fabricated thin film's surface roughness and morphology of the organic solar cells' active layer [192]. They achieved the PCE of 3% of the organic solar cell by using a higher- and lower-boiling solvent mixture as the active layer solution. Knife-over-edge and slot die printing processes are often used for large-scale production of organic solar cells. FC Krebs reported using roll-to-roll methods to fabricate the polymer solar cell modules [198]. He fabricated polymer solar cell modules with an active area of 75 cm^2 by using knife-over-edge coating (for ZnO interlayer), slot die coating (for ZnO interlayer and active layer) and screen printing (for PEDOT:PSS interlayer and silver electrodes). The polymer solar cells modules with slot die printed ZnO interlayer showed the highest PCE of 0.84%. There are also some other reports on the printable perovskite solar cells in recent years. Screen printing technique was often reported to be used in the perovskite solar cells fabrication for coating the TiO_2 mesoporous layer [28, 199]. Blade coating technique can be used for both of electrodes and active layers in perovskite solar cells. Cao, K. et. al. used blade coating technique to deposit a carbon black/graphite layer as anodes in perovskite solar cells [200]. In a report by Kim JH et. al., perovskite active layer was prepared by using blade coating from a $CH_3NH_3PbI_{3-x}Cl_x$/DIO precursor solution [201]. They achieved a PCE of 12.21%, thus demonstrating that blade coating technique could be used for fabricating high performance perovskite solar cells. Instead of using roll-to-roll techniques to deposit just

interlayers or active layers, Hwang Kyeongil et. al. demonstrated that almost all of the layers of the perovskite solar cell can be prepared by slot die printing [202].

Chapter 3 A New N-type Conjugated Polyelectrolyte for Electron Transporting Layer

In this chapter, highly efficient and stable organic solar cells based on a new n-type conjugated polyelectrolyte electron transporting layer (ETL), PFBD, are demonstrated. The motivation behind using the conjugated polyelectrolyte ETL into organic solar cells will be presented first. Then, the fabrication processes of the organic solar cells, including substrates cleaning, precursor solution preparation, spin coating and thermal evaporating processes, are introduced. Following the fabrication processes of organic solar cells, thickness optimization of the conjugated polyelectrolyte layer and dark current analysis of the organic solar cells are presented. Finally, the characterizations and explanations of origin of the light-soaking effect are discussed.

3.1 Introduction and Motivation

Organic solar cells, based on a blend of conjugated polymers and fullerene derivatives, are promising candidate for clean and large-area power sources because of their potential cheap fabrication process cost. To date, organic solar cells have achieved the PCE over 10% [25, 26, 203, 204]. The advancement of this thin-film photovoltaic technology is mainly driven by developing new light harvesting materials and improving the solar radiation absorption of the materials. Development of innovative interfacial materials for the organic solar cells device structure that can be incorporated between the electrodes and the photoactive layer is also important. These interfacial materials in the device

structure can help improve the charge collection efficiency by reducing the contact resistance and the interfacial recombination loss, so to make the organic solar cell device with higher J_{sc}, V_{oc} and FF [205-211].

Conjugated polyelectrolytes are promising candidates for the interfacial modification materials. In general, conjugated polyelectrolytes are polymers which contain hydrophobic π-conjugated backbones with hydrophilic surfactant-like ionic pendant groups. Conjugated polyelectrolytes can be easily processed from the environmentally friendly polar solvents (such as alcohol or water) due to their ionic nature of the side chains, which allow the fabrication of multilayer polymer-based organic solar cells with orthogonal solubility [212-215]. Their highly polar pendant groups enable excellent interface modification functions by (1) creating strong interface and/or molecular dipoles at the metal/organic interface that lead to a substantial reduction of the electrode work function, or (2) allowing the ion motion to redistribute the electric fields within a device. These changes are able to minimize the interfacial resistances and facilitate electron transport, making them promising interfacial layer materials in organic electronic devices [152, 216-218]. In addition, the use of conjugated polyelectrolytes in the device structure can avoid high temperature device fabrication processing, which is usually required with other interfacial materials in the device structures, such as metal oxides [94, 219], hence, reduces the devices manufacturing costs [220].

The use of conjugated polyelectrolytes as the ETLs in organic solar cells has been widely reported to efficiently enhance the PCE of organic solar cells [164, 213, 218, 221-223]. For instance, cationic polythiophene, [213] and polyfluorene derivatives containing amine salts and alkoxy groups [164, 221] have been reported to be effective ETLs in solar cells. The neutral precursors of

the organic electrolytes (without ionic parts), such as, poly[(9,9-bis(30-(N,N-dimethylamino) propyl)-2,7-fluore ne)-alt-2,7-(9,9-dioctylfluorene)] (PFN) was also incorporated successfully as electron transport layer in a thieno[3,4-b]-thiophene/benzodithiophene copolymer based PSC with a high PCE of 9.2% was achieved [152].

Despite the success of using conjugated polyelectrolytes or their neutral precursors as the ETLs in organic solar cells, there are some issues to be solved before the commercialization of organic solar cells based on conjugated polyelectrolytes. One important issue is the stability of organic solar cells. To make the neutral precursors of conjugated polyelectrolyte, such as PFN, to be dissolved in polar solvents such as water and methanol, a small amount of acetic acid is added in during preparing the materials. The acetic acid is detrimental to the stability of organic solar cells. Light-soaking effects of the conjugated polyelectrolytes or metal oxides based organic solar cells have been reported [224, 225], wherein the FF and V_{oc} of the organic solar cells increased with the light illumination until they saturated. Zilberberg et al. observed the light-soaking phenomenon when they used poly(3-[6-(N-methylimidazolium) hexyl]thiophene) bromide (P3ImHT) as the ETL in organic solar cell device structure [224]. This light-soaking effect was attributed to a reduction of the ITO's work function upon UV illumination in combination with the dipole effect of the conjugated polyelectrolyte. The light-soaking effect has been recently reported in an inverted structure organic solar cells using PFN as the ETL [225]. It was attributed to the oxygen in the ITO. Understanding the fundamental mechanism of the light-soaking effects of the conjugated polyelectrolyte based organic solar cells can help develop high performance organic solar cells.

Chapter 3 A New N-type Conjugated Polyelectrolyte for Electron Transporting Layer

In this chapter, we present a new conjugated polyelectrolyte material, namely, poly[9,9-bis((60-N,N,N-trimethylamino)hexyl)-fluorene-alt-cobenzoxadiazoled ibromide] (PFBD), as the electron transport material in the thieno[3,4-b]thiophene/ benzodithiophene (PTB7) and [6,6]-phenyl C71-butyric acid methyl ester ($PC_{71}BM$) based organic solar cells. Light-soaking effect was observed in the organic solar cells. By employing a pre-UV light treatment on the PFBD layer of the device structure, the light-soaking effect of the organic solar cell can be prevented and higher efficiencies (>7%) of the device has been achieved. Through impedance analysis, we find that the pre-UV light treatment on PFBD interlayer leads to reduced series and charge transfer resistances of the inverted organic solar cells. The flat-band potential (V_{FB}) of organic solar cells is increased after the pre-UV light treatment on PFBD interlayer. As a result, the organic solar cells' FF and V_{oc} are improved. Moreover, after the pre-UV light treatment, the organic solar cells have improved stability that the maximal efficiency of the organic solar cells retains at nearly similar level for at least 26 days.

3.2 Fabrication of the Organic Solar Cells

All materials were used as received without purifications. The inverted organic solar cells fabricated in this work have a structure of ITO/PFBD/PTB7:$PC_{71}BM$/MoO_3/Al. The PTB7:$PC_{71}BM$ blends active layer were prepared from chlorobenzene at a weight ratio of 1:1.5 and total concentration of 25 mg/mL. A 3% v/v 1,8-diiodoctane (DIO) [226] solvent was also added into the final solution. The blend solution was stirred overnight at 70 ℃ in a glove box before spin-casting. PFBD was synthesized according to

previous report [227].

The complete fabrication processes are shown in the Figure 3.1. ITO substrates were cleaned using soap water and sonicating sequentially with de-ionized water, acetone and isopropanol for 15 min each. The ITO substrates were dried at 100 ℃ in oven for several hours, followed by exposure to ultraviolet light and ozone for 15 min to produce a hydrophilic surface. The cleaned ITO substrates were then transferred into a nitrogen-filled glove box. The PFBD interlayers were spin-coated on the surface of ITO substrate from a methanol solution (0.2 mg/mL) followed by drying of the films at 100 ℃ for 10 min. PTB7:$PC_{71}BM$ blend film was spin-coated at 1000 rpm for 2 min and annealed at 70 ℃ for 10 min to form an active layer with thickness of about 90 nm. A 10 nm MoO_3 layer and a 100 nm Al layer were deposited by thermal evaporation at a base pressure of 1×10^{-6} mbar to form the hole-collecting electrode. The device area was defined to be 4.5 mm^2. Inverted devices using PFN as electron transporting layer were also fabricated as a reference with a similar structure of ITO/PFN/PTB7:$PC_{71}BM$ (1:1.5 by weight)/MoO_3/Al. PFN solution with concentration of 1 mg/mL was prepared by dissolving PFN into methanol mixed with 2 μL/mL acetic acid [152].

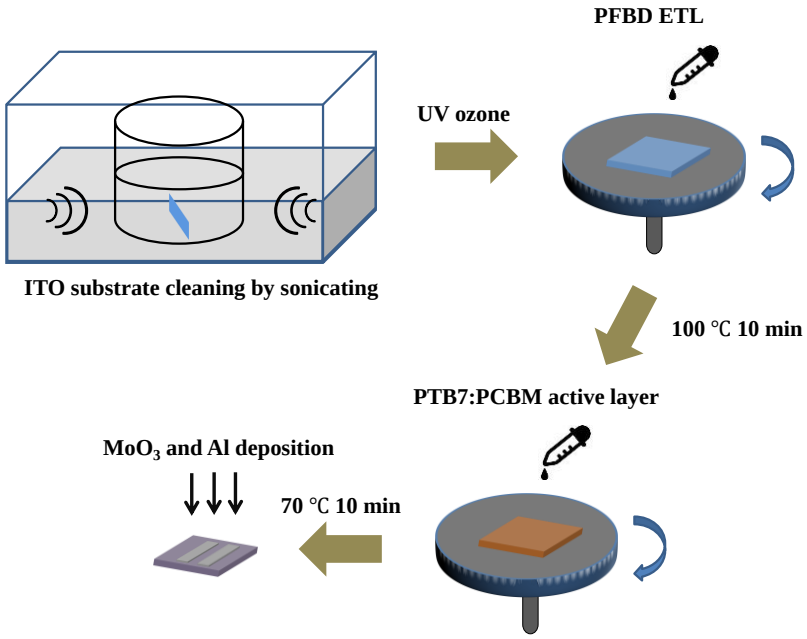

Figure 3.1: The fabrication process of organic solar cells based on PFBD ETL.

3.3 Major Characterization Techniques

Organic solar cells' photovoltaic performance measurement: The current density-voltage (J-V) characteristics of devices were measured by a Keithley 2400 parameter analyzer under one sun solar spectrum illumination (AM 1.5G) from a solar simulator with intensity of 100 mW/cm^2 calibrated via a silicon reference cell. Incident photon-to-current efficiency (IPCE) measurements were conducted on devices under short-circuit conditions through a lock-in amplifier (SR510, Stanford Research System) at a chopping frequency of 233 Hz during illumination with a monochromatic light from a Xenon arc lamp. The external quantum efficiency (EQE) is obtained from the IPCE measurement. EQE represents the ratio of the number of charge carriers collected by the solar cell

to the number of incident photons:

$$\mathrm{EQE} = \frac{electrons/sec}{photons/sec}$$

EQE displays wavelength dependent photovoltaic conversion efficiency. The J-V and IPCE measurements were carried out in a nitrogen-filled glove box.

Thickness measurement: The thickness of PTB7:$PC_{71}BM$ active layer was measured by a KLA Tencor P-16+ Surface Profiler. For the thickness measurement, the PTB7:$PC_{71}BM$ blend film and the PFBD or PFN layers were prepared on glass substrates by spin coating. The preparation process of these films was the same as that used in the organic solar cells fabrication. The thickness of PFBD layer was obtained from atomic force microscopy (AFM) measurements because the thickness of PFBD layer was too thin (less than 10 nm) to be measured by the KLA Tencor P-16+ Surface Profiler which was designed for measuring films with thickness more than 20 nm. A sharp needle was used to scratch the PTB7:$PC_{71}BM$, PFBD and PFN films to create steps for thickness measurement.

UV-vis absorption measurement: The PFBD layers were spin coated on quartz substrates for absorption measurement. A blank quartz substrate was used as the reference sample. A Shimadzu UV-3101PC UV-VIS-NIR Spectrophotometer was used to measure the absorbance of PFBD layers with wavelength ranging from 250 nm to 600 nm. First, the quartz sample coated with PFBD was used for UV-Vis absorption measurement without UV treatment. Then, the same sample was measured after UV treatment for 30 min, 1 h and 2 h.

Surface morphology measurement: The NanoWizard III instrument (JPK Instruments AG, Berlin, Germany) equipped with the NanoWizard head and

controller was used in the AFM measurement. PFBD or PFN layers were spin coated on the top of ITO/glass substrates. PTB7:$PC_{71}BM$ blend films were spin coated on the top of PFBD or PFN layers. The morphology of the model surfaces was visualized by tapping mode AFM imaging under ambient conditions using standard silicon probes (k ~ 40 N/m, Tap 300AL-G, Budget sensors). All the images were processed using the JPK data processing software (Version 4.2).

Work function measurement: The work functions of the ITO and ITO/PFBD were measured with Kelvin Probe apparatus (KP Technology, UK). Figure 3.2 (a) shows the schematic representation of Kelvin Probe measurement. The principle of Kelvin Probe measurement is to measure the difference of work function between the sample and the reference electrode (cantilever). The illustration of experimental set-up for the Kelvin Probe measurement is shown in the Figure 3.2 (b). In the Kelvin Probe measurement, the output of a frequency generator was electrically connected to the sample. So, an oscillating electrical field between the cantilever and the ITO/PFBD sample is created. Then the position of the cantilever is recorded by the position detector. This position signal is then fed into a lock-in amplifier of which the output is connected to an integrator to add a constant offset to the oscillation. This feedback loop is for minimizing the electrically induced cantilever oscillation and the potential difference between the cantilever and the sample. Then the voltage required to align the two Fermi levels is calculated by using the force applied on the cantilever, constant part of the applied voltage and the oscillating part of the applied voltage.

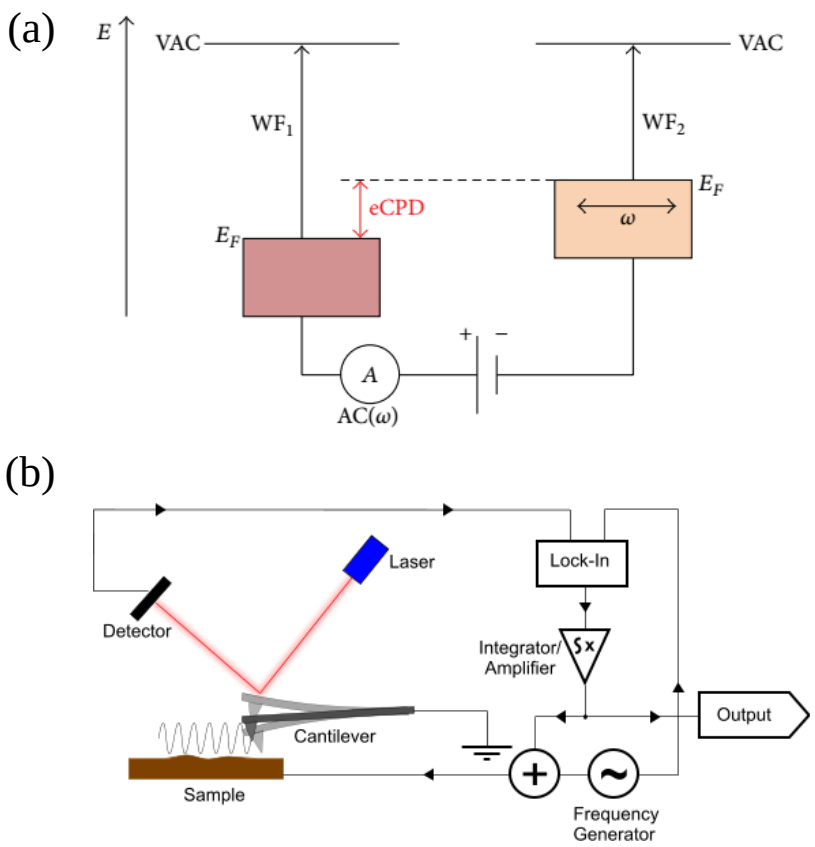

Figure 3.2: (a) Schematic representation of Kelvin Probe measurement. (b) Circuit diagram of Kelvin Probe measurement setup. [228]

The thickness, AFM, absorption and work function measurements were characterized in ambient air.

Impedance and capacitance measurement: The impedance measurement was carried out through an automated potentiostat (Solartron-analytical, 1470E) coupled with a frequency response analyzer (Solartron-analytical, 1255B) in a three-electrode electrochemical system. Figure 3.3 shows the encapsulation process of the organic solar cells. First, several drops of epoxy were applied on the top of the organic solar cells. Then the organic solar cells were covered by a glass slide and the epoxy was cured by UV light. The encapsulation process was conducted in the N_2 filled glovebox. Then the organic solar cells were taken out

of the glovebox for impedance measurement in air. The AC impedance measurement was done in Z-h mode with a fixed AC drive bias of 25 mV and the frequency varying from 500 Hz to 1 MHz, under one sun spectrum illumination. A constant DC bias which equals to the open-circuit voltage was applied and superimposed on the AC bias. The capacitance-voltage measurement was conducted in dark condition and at room temperature. The capacitance was measured at different applied bias voltages and with AC excitation amplitude of 10 mV at a frequency of 10 kHz.

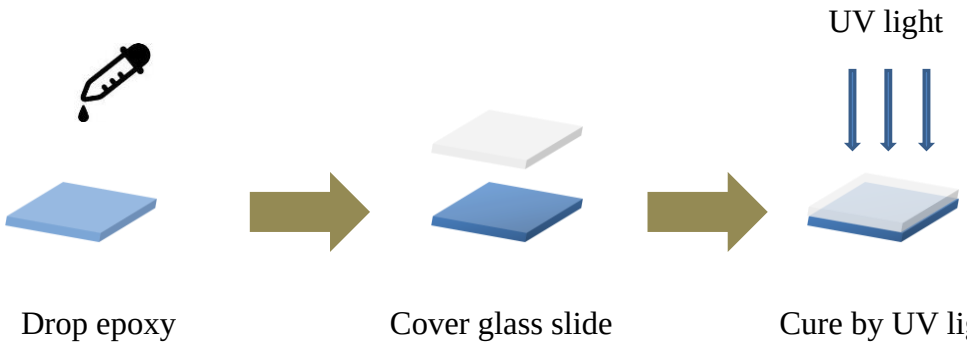

Figure 3.3: Encapsulation process of the organic solar cells.

3.4 Thickness Optimization of the Conjugated Polyelectrolyte Layer of the Organic Solar Cells

Figure 3.4 shows the schematic solar cell structure fabricated and the molecular structures of the component materials of the solar cell. The transparent ITO functions as the electron-collecting electrode while the hole-collecting electrode is Al. The bulk heterojunction polymer/fullerene photovoltaic layer of the devices is a blended film of thieno[3,4-b]thiophene/benzodithiophene (PTB7) and [6,6]-phenyl C71-butyric acid methyl ester ($PC_{71}BM$). ETL, which is

inserted between the ITO cathode and the photoactive layer, is either PFBD or PFN. MoO_3 thin layer is inserted between the photoactive layer and the top Al electrodes as the HTL layers.

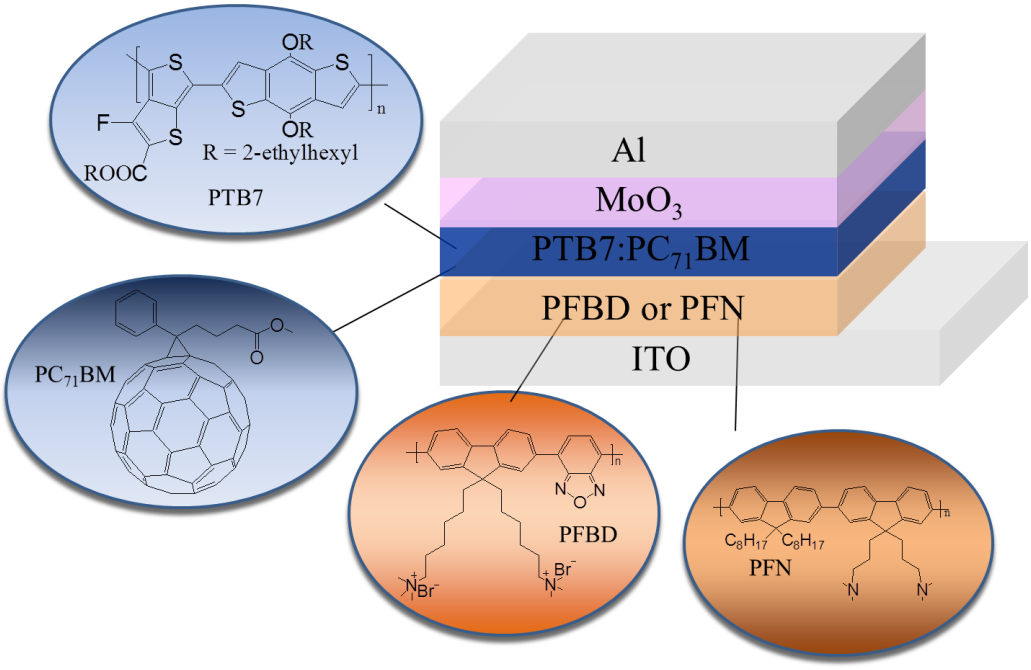

Figure 3.4: Chemical structures of the materials used in this work and schematic structure of the inverted organic solar cells.

The thickness of PFBD interlayer was optimized by varying the thickness to receive the maximum PCE of the cell as shown in Table 3.1. The measured best performance of the inverted PTB7:$PC_{71}BM$ organic solar cells using different ETLs and without the ETL (ITO-only) are compared as shown in Table 3.2. The average PCE of the devices were obtained from at least three devices for each type of the organic solar cells. For the organic solar cells using PFBD as the ETL (optimized thickness of PFBD is ~2 nm), a high PCE of 7.21% is exhibited. The measured J_{sc} is 16.44 mA/cm^2. The thickness of the PFBD ETL mainly influences the Jsc and FF of the organic solar cells. The FF of the organic solar

cells with 8 nm PFBD ETL is much lower than that of the organic solar cells with 2 nm and 1 nm PFBD ETL. This might be caused by the increased resistance of the thick PFBD layer.

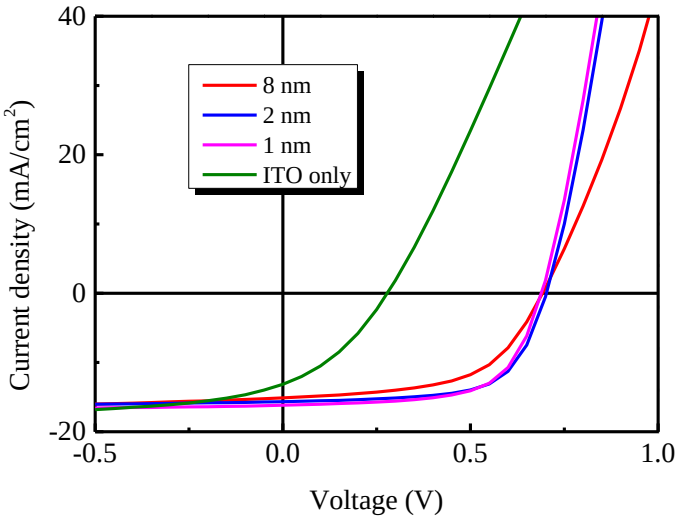

Figure 3.5: The measured J-V characteristics of the inverted organic solar cells based on PFBD interlayers with different thickness (1 nm, 2 nm, 8 nm).

Figure 3.6 shows the external quantum efficiency (EQE) spectra of the organic solar cells based on PFBD ETL with different thickness. The EQE spectra can indicate the organic solar cells' ability of generating, transporting and collecting charge carriers. The organic solar cells without any ETL exhibited the lowest EQE. The EQE of the organic solar cells with PFBD ETL is much higher because of the improved charge carrier extraction ability. The highest EQE occurs when the thickness of the PFBD ETL is 2 nm. The theoretical J_{sc} of the organic solar cells with 2 nm PFBD ETL is 16.06 mA/cm^2 obtained by integrating the product of the EQE and one sun spectrum. The J_{sc} calculated from the EQE measurement is in good agreement with that obtained from J-V

characteristic measurement demonstrating our measurement is accurate.

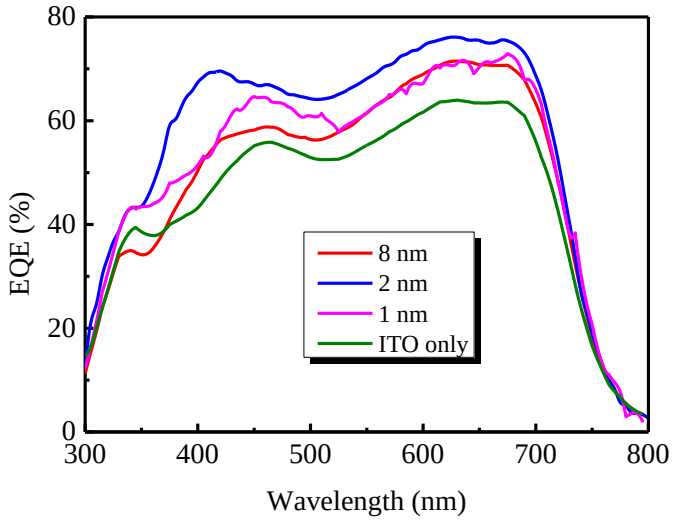

Figure 3.6: External quantum efficiency (EQE) spectra of the inverted organic solar cells based on PFBD interlayers with different thickness.

We also performed the dark current analysis to study the influence of the PFBD's thickness on the organic solar cells' performance. The dark currents of the organic solar cells were measured and shown in Figure 3.7. The dark current were fitted by using the following equation:

$$I = I_0 \left\{ exp\left[\frac{q}{nkT}(V - IR_s)\right] - 1 \right\} + \frac{V - IR_s}{R_{sh}}$$

where R_s accounts for the series resistance, R_{sh} is the shunt resistance, n is the ideality factor which represents the quality of the junction and I_0 is the saturation current of the semiconductor material. After fitting the dark current curves of the organic solar cells, the R_s and R_{sh} values were obtained and shown in Table 3.1 and Table 3.2. The low R_s value of 1.9 Ωcm^2 of the PFBD based organic solar cell suggests a good contact between the photoactive layer and ITO electrode, which facilitate free charge carrier extraction while the high R_{sh} of 1.4×10^4 Ωcm^2 indicates the ability in electron selectivity and low charge

recombination losses at the interface between the PFBD and photoactive layer. When the PFBD ETL is too thin (1 nm) or too thick (8 nm), the organic solar cells have lower R_{sh} and higher R_s, thus lower PCE. This is because the resistance of PFBD ETL is increased with increasing its thickness. The possibility of charge carrier recombination might also be increased in the thick PFBD ETL. With reducing the thickness, the resistance of PFBD ETL is decreased but it might be too thin to completely separate the ITO and PTB7:$PC_{71}BM$ photoactive layer. So there are more pathways for electrons and holes to recombine, thus leading to lower R_{sh} and higher R_s. After the optimization of the thickness of PFBD ETL, organic solar cells with good performance can be fabricated. These results indicate that PFBD is an effective ETL in inverted solar cells.

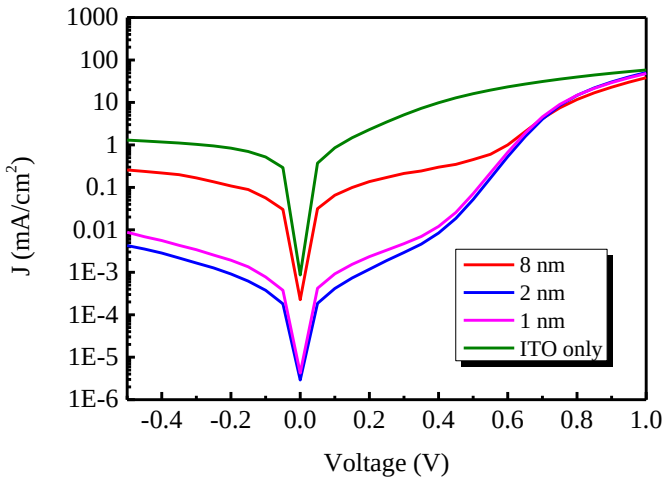

Figure 3.7: dark current of the inverted organic solar cells based on PFBD interlayers with different thickness.

Table 3.1: Photovoltaic parameters of the inverted PTB7:$PC_{71}BM$ based organic solar cells using PFBD as the ETL.

Interlayer	J_{sc}(mA/cm^2)	V_{oc}(V)	FF(%)	PCE(%)		R_{sh} (Ωcm^2)	R_s (Ωcm^2)
				Average	Best		
PFBD (8 nm)	15.27	0.70	56.69	5.91±0.10	6.03	1400	6.5
PFBD (2 nm)	16.44	0.69	63.2	7.10±0.19	7.21	14000	1.9
PFBD (1 nm)	15.19	0.71	63.57	6.78±0.07	6.86	9300	4.4

The photovoltaic performance of the organic solar cells with and without PFBD or PFN ETLs is shown in the Table 3.2. The thickness of PFBD is 2 nm. The thickness of PFN is 10 nm which is the optimized thickness of PFN ETL. The organic solar cells based on PFBD or PFN ETLs exhibit comparable performance with the best PCE of around 7.20%. In contrast, the organic solar cells without any ETL have very poor performance with the highest PCE of only 1.27%. Besides, the R_{sh} of the organic solar cells without any ETL is extremely low indicating that serious charge carrier recombination and high leakage current exists in the organic solar cells. The R_s of the organic solar cells is much higher than those of the organic solar cells based on PFBD or PFN ETLs indicating that there is a large energy barrier between the ITO electrode and the PTB7:$PC_{71}BM$ photoactive layer. Applying the PFBD or PFN ETLs can effectively reduce the energy barrier and facilitate the charge carrier transport from the PTB7:$PC_{71}BM$ photoactive layer to the ITO electrode. The

comparable performance of the organic solar cells with PFBD and PFN ETLs demonstrates that the PFBD can replace PFN as ETL for high performance organic solar cells.

Table 3.2: Photovoltaic parameters of the inverted PTB7:$PC_{71}BM$ based organic solar cells using PFBD and PFN as the ETLs, respectively. An ITO-only device without the ETL interlayer is shown as the reference.

ETL	J_{sc}(mA/cm^2)	V_{oc}(V)	FF(%)	PCE(%)		R_{sh} (Ωcm^2)	R_s (Ωcm^2)
				Average	Best		
PFBD	16.44	0.69	63.2	7.10±0.19	7.21	14000	1.9
PFN	15.24	0.72	66.7	7.15±0.13	7.27	75000	2.6
ITO only	13.15	0.28	34.8	0.95±0.28	1.27	80	10.9

3.5 Stability of the PFBD Based Organic Solar Cells

One of the advantages of using PFBD as the ETL compared to the normally used PFN ETL is that no acetic acid is needed for dissolving it in methanol during the device fabrication. Without acetic acid, the PFBD's neutral methanol solution should improve the organic solar cells' stability. To study the influence of PFBD and PFN on organic solar cells' stability, we prepared the organic solar cells using PFBD and PFN as the ETLs, respectively, in the same batch. Then the organic solar cells were stored in a N_2 filled glovebox under dark condition. The performance of the organic solar cells was measured at different days and shown in Figure 3.8. It shows the device with PFBD as the ETL displayed a good stability. Its J-V characteristic remains almost the same after stored in N_2 environment for 26 days. The PCE of the organic solar cells based on PFBD

retains 80% of the original value of PCE after 187 days. While the organic solar cell with PFN as the ETL degraded very fast. After stored in N_2 environment for 90 days, the measured PCE of the organic solar cells with PFN ETL decreased to 70% of the original PCE of the device. From the J-V characteristics of the organic solar cells with PFBD and PFN ETLs, we found that the J_{sc} and V_{oc} of the organic solar cells stayed at almost the same levels but the FF significantly decreased. After stored in N_2 environment for 26 days, the FF of the organic solar cells based on PFBD ETL decreased from 63.2% to 60.3%. The FF of the organic solar cells based on PFBD ETL further decreased to 51.9% after stored for 187 days. After stored in N_2 environment for 90 days and 250 days, the FF of the organic solar cells based on PFN ETL decreased from 67.4% to 53.7% and further decreased to 39.5%. The decreasing rate of FF of the organic solar cells based on PFBD ETL is much slower than that of the organic solar cells based on PFN ETL. As a result, the PCE of the organic solar cells based on PFBD ETL decreased slower than that of the organic solar cells based on PFN ETL. The only difference between the organic solar cells for stability measurement is that they are based on PFBD or PFN ETLs. All the other fabrication processes were the same. So the different stability performances should be attributed to the different ETLs. As we mentioned before, acetic acid is needed for dissolving the PFN in methanol, while the PFBD can be easily dissolved into methanol without the requirement of acetic acid. According to our stability measurement, the acetic acid should be detrimental to the stability of the organic solar cells. These results indicate that using the PFBD ETL can improve the stability of organic solar cells compared with the organic solar cells based on PFN ETL. So the PFBD ETL has great potential to be used for commercialization of organic solar cells in the future because of the good photovoltaic performance and stability of the organic solar cells based on it.

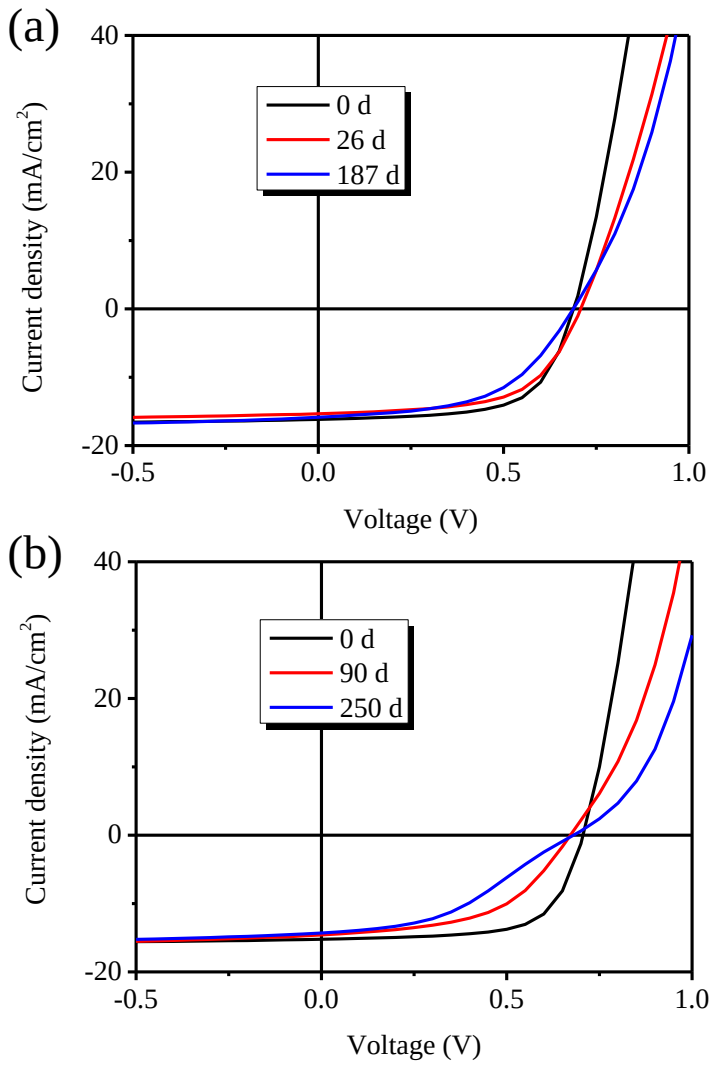

Figure 3.8: The J-V graphs of the inverted solar cells based on PFBD (a) and PFN (b) interlayers measured on different days.

3.6 Light-soaking Effect of the PFBD Based Organic Solar Cells

Light-soaking effect was observed when measuring the performance of the organic solar cells with the PFBD ETL. While for the organic solar cells with PFN ETL or without ETL, this light-soaking effect was not observed. By using

a pre-UV treatment during the device fabrication, this light-soaking effect of the PFBD based organic solar cells can be successfully eliminated. Using various techniques, the light-soaking effects of the PFBD based organic solar cells have been investigated in details.

3.6.1 Light-soaking Effect of the PFBD Based Organic Solar Cells

As shown in Figure 3.9, an S-shaped current-voltage (J-V) characteristics of the inverted PTB7:PC71BM organic solar cells with the PFBD as ETL upon illumination. At the beginning, the measured V_{oc} of the device was 0.62 V, the J_{sc} was 16.33 mA/cm^2 and the FF was measured 44.0%. The PCE of the organic solar cell was only 4.5%. However, when the illumination time increased, the measured device parameters became better and the S-shape J-V characteristics disappeared. A high efficiency of ~6.9% of the device with 16.16 mA/cm^2 J_{sc}, 0.70 V V_{oc} and 63.2% FF was received after 15 minutes of continuous illumination of the device.

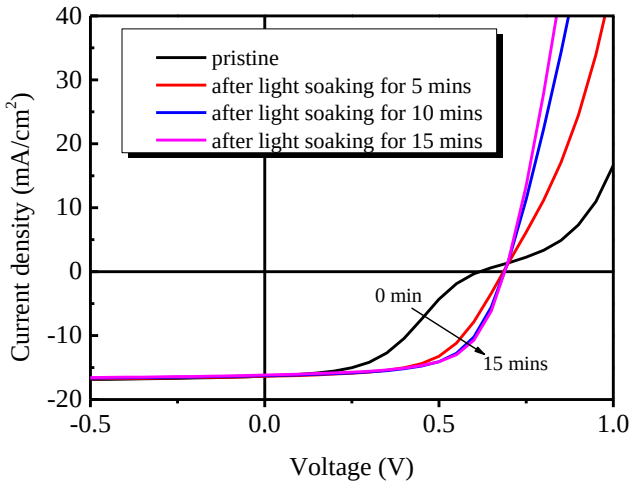

Figure 3.9: J-V characteristics of the inverted organic solar cells with the

PFBD ETL with different illumination time.

The light-soaking effect was not observed in the inverted organic solar cells with PFN ETL interlayer fabricated in the same batch (Figure 3.10 (a)). Before illumination, the PCE of the organic solar cells with PFN ETL was 6.11% with 14.15 mA/cm^2 J_{sc}, 0.70 V V_{oc} and 61.7% FF. After 3 min illumination, the PCE of the organic solar cells with PFN ETL remained almost the same, 6.49%, with 14.09 mA/cm^2 J_{sc}, 0.70 V V_{oc} and 65.8% FF. For the control device without the ETL (ITO only), little change of the J-V characteristics of the device was observed after continuous illumination (Figure 3.10 (b)). The photovoltaic performance of the organic solar cells without the ETL was very poor. Before the illumination, the PCE of the organic solar cells without the ETL was 0.93% with 13.59 mA/cm^2 J_{sc}, 0.20 V V_{oc} and 34.1% FF. After the illumination, the PCE of the organic solar cells slightly increased to 1.35% with 14.53 mA/cm^2 J_{sc}, 0.25 V V_{oc} and 37.2% FF. No S-shaped J-V characteristics were observed during measuring the photovoltaic performance of the PFN ETL based and ITO only organic solar cells. These results show that this light-soaking effect of the organic solar cell is not because of the Al/MoO_3 contact, the adsorbed oxygen species on ITO electrode [224, 229] or the photoactive layer. Otherwise, the light-soaking effect should be observed during the measurement of the performance of PFN ETL based and ITO only organic solar cells. So we suspected that the light-soaking effect of the organic solar cells with the PFBD ETL was because of the ITO/PFBD interface and/or the PFBD layer itself.

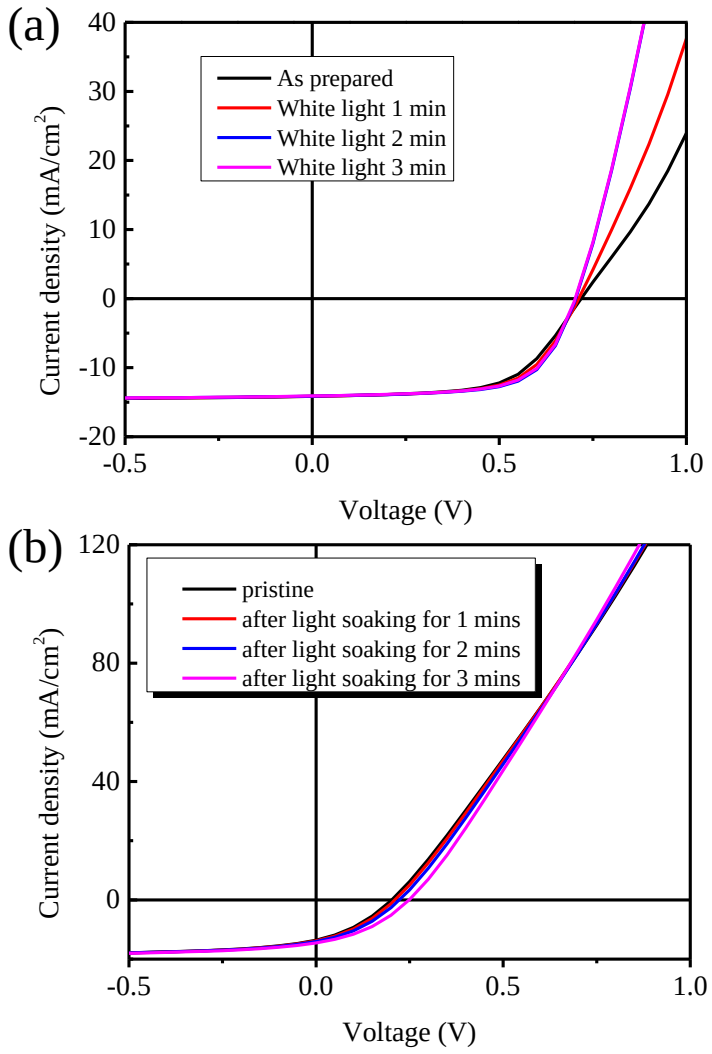

Figure 3.10: J-V characteristics of the inverted organic solar cells with (a) the PFN ETL interlayer and (b) without the ETL (ITO only) with different illumination time.

3.6.2 Pre-UV Treatment Effects on the Light-soaking Effects

To investigate the effects of the UV exposure on the light-soaking effect, the PCE of the PFBD ETL based organic solar cells under illumination were measured with and without introducing an UV spectral component during the

measurement. In this experiment, an UV long-pass filter with the cutoff wavelength at 430 nm was used in front of the devices when carried out the J-V measurement under illumination. Figure 3.11 shows the measured PCE of the devices changes with the illumination time with and without introducing the UV filter. The PCE of the PFBD ETL based organic solar cells increased from 4.5% to 6.9% when the UV cutoff filter was not used. When the UV cutoff filter was applied, the PCE of the PFBD ETL based organic solar cells was increased from 4.2% to only 6.0%. In particular, we note that the improved J-V characteristics (see Figure 3.12) after light-soaking (with UV spectral components) are stable. We stored the PFBD based organic solar cells in dark condition in a N_2 filled glovebox for 24 hours. Then the J-V characteristic of the PFBD based organic solar cells was measured. We found that its performance didn't return to its initial S-shape state over time, providing the first indication that a permanent photochemical modification of PFBD has occurred upon light illumination.

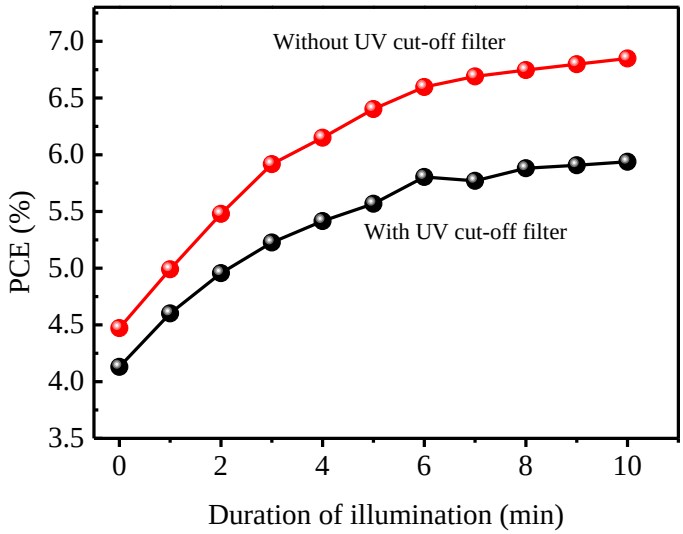

Figure 3.11: Power conversion efficiency of the PFBD based organic

solar cells as a function of illumination time with and without the UV filter.

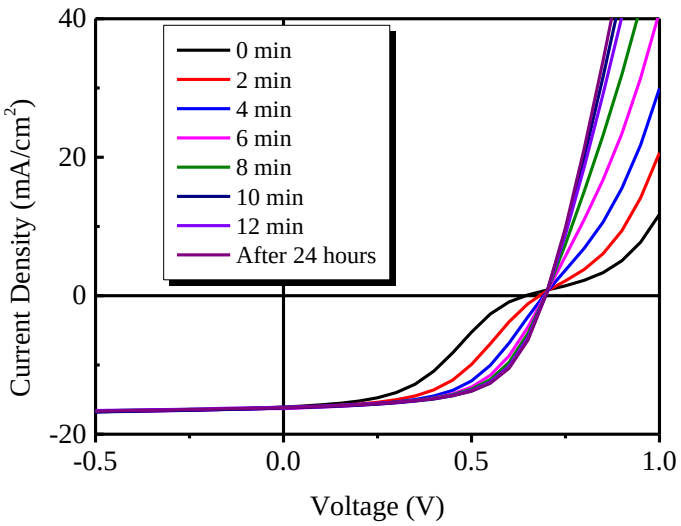

Figure 3.12: J-V characteristics of the PFBD ETL based organic solar cells under different illumination time with UV component.

To further ascertain the hypothesis that the UV spectral components is the main factor for the improvement in device performance, a pre-UV light treatment was performed on the PFBD coated ITO substrate, followed by completion of the device fabrication. The PFBD ETL interlayer was spin coated on the top of ITO substrates. Then the sample was illuminated by UV light for 30 min, 60 min and 120 min. After the pre-UV light treatment, the following fabrication processes were the same as those described in the organic solar cells' fabrication. The behavior of detailed photovoltaic parameters of inverted organic solar cells with and without pre-UV treatment is plotted in Figure 3.13. Compared to the characteristics exhibited by devices without pre-UV treatment of PFBD (as prepared), the initial V_{oc} and FF of devices with 30 min of pre-UV treatment are substantially higher. The efficiency of the organic solar cell with 30 min pre-UV treatment quickly saturates from 6.7% to 7.2%, and the organic

solar cell displays negligible light-soaking effect. It is clear that light-soaking problem is from the influence of UV spectral components on the PFBD layer, which was successfully solved after introducing the pre-UV treatment method.

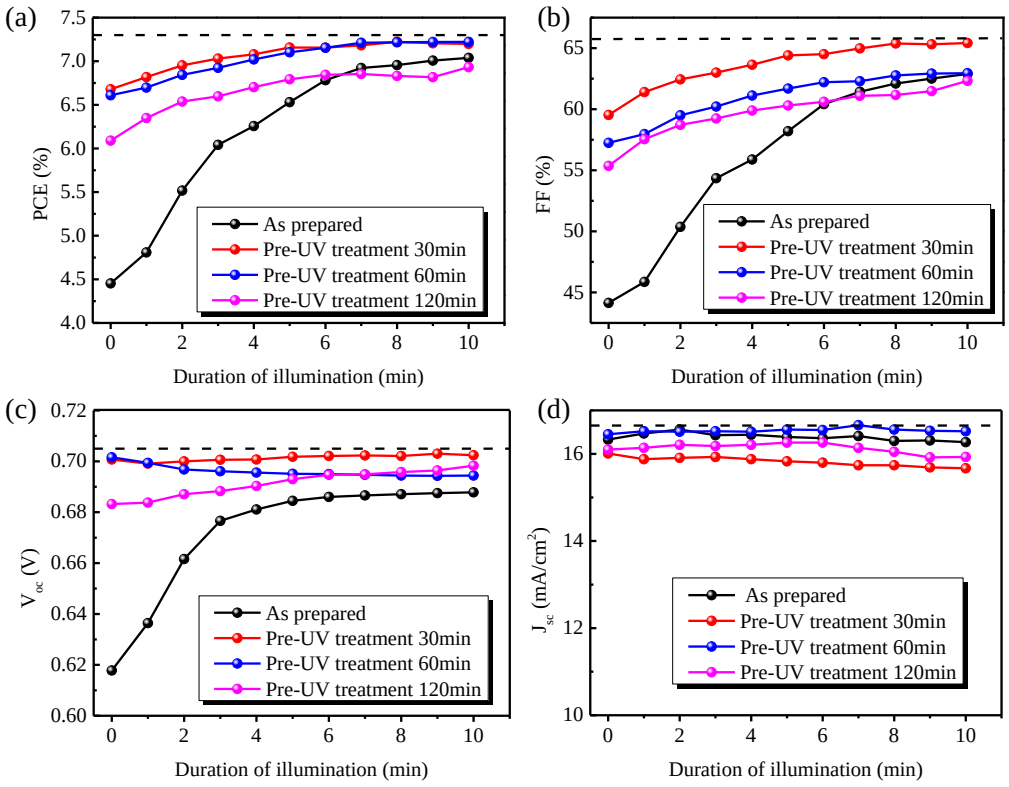

Figure 3.13: Photovoltaic parameters, (a) PCE, (b) FF, (c) V_{oc} and (d) J_{sc} as a function of different illumination time, of the inverted organic solar cells based on PFBD ETL interlayer with and without UV treatment on the PFBD layer.

3.6.3 ITO Work Function Modification and Surface Morphology of the PFBD ETL

To study the influence of pre-UV treatment on the properties of PFBD ETL, Kelvin Probe measurements were conducted on ITO and ITO/PFBD electrodes

with and without pre-UV treatment. The measured work functions of ITO/PFBD with and without pre-UV treatment are shown in Figure 3.14. The work functions of bare ITO and as-prepared ITO/PFBD are 5.2 eV and 4.9 eV respectively while the work function of ITO/PFBD is further reduced to 4.6 eV after 30 min of pre-UV treatment. The lowered work function of ITO/PFBD matches well with the LUMO level of $PC_{71}BM$ (~4.3 eV) [152], enabling a more efficient charge collection and hence higher efficiency. The PFBD without pre-UV treatment can only reduce the work function of ITO by 0.3 eV. So without UV-treatment, a large energy barrier, 0.6 eV, exists between ITO and $PC_{71}BM$. That is the reason that the S-shaped J-V characteristics occurred when measuring the organic solar cells based on PFBD ETL with short illumination time. After illumination of UV light, the work function of ITO/PFBD was reduced to 4.6 eV. So the S-shaped J-V characteristics disappeared because of the reduced energy barrier between ITO and $PC_{71}BM$.

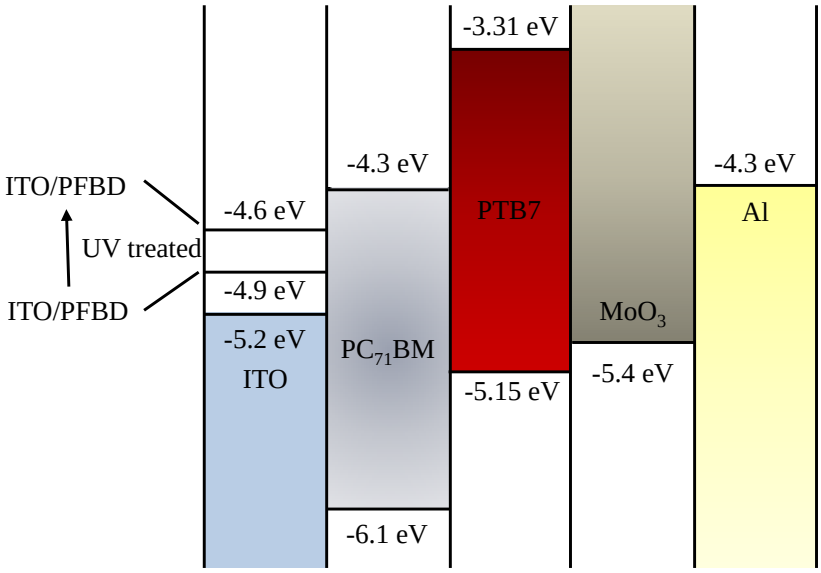

Figure 3.14: Energy levels of the inverted organic solar cells based on PFBD ETL with and without pre-UV treatment.

Since the PTB7:$PC_{71}BM$ morphology can be potentially affected by the surface

energy of the underlying PFBD layer after UV treatment, AFM measurement was conducted on the as-prepared and 30 min pre-UV treated PFBD layers (see Figure 3.15 (a)-(d)) as well on the corresponding PTB7:$PC_{71}BM$ active layers (see Figure 3.15 (e) and (f)). The PFBD layers uniformly cover the surface of ITO as shown in Figure 3.15 (c) and (d). The as-prepared PFBD interlayer displays a smoother morphology with root-mean-square (rms) roughness of 0.54 nm. Similar rms roughness of the UV treated PFBD layer (~0.57 nm) is observed, indicating that the UV treatment doesn't influence the surface topography of PFBD layer. The PTB7:$PC_{71}BM$ blend film on top of the as-prepared PFBD interlayer is also very uniform and smooth with rms of 1.24 nm. No obvious change is observed in PTB7:$PC_{71}BM$ blend film on the top of UV treated PFBD interlayer (rms ~1.18 nm). The performance difference between the organic solar cells with as-prepared and pre-UV treated PFBD ETL interlayers couldn't be caused by the surface morphology change. The small difference between the rms of the as-prepared and pre-UV treated PFBD ETL and PTB7:$PC_{71}BM$ layers shouldn't have great influence on the organic solar cells' performance. From the AFM results, it can be concluded that UV illumination doesn't change the surface morphology of PFBD layer and the surface morphology of PTB7:$PC_{71}BM$ blend film is independent on the pre-UV light treatment of the underlying PFBD layer. The unchanged morphology of PFBD before and after UV-treatment also indicates that the UV treatment doesn't induce polymer chain realignment or change the polymer packing property. The change of polymer chain realignment or packing properties after annealing the polymer film is always accompanied by the morphology change observed by AFM measurement[54, 230]. The AFM measurement results rule out the possibility of change of morphology, polymer chain realignment and packing properties. So the light-soaking effect and the work function change of

the ITO/PFBD layers after pre-UV treatment should be caused by other factors.

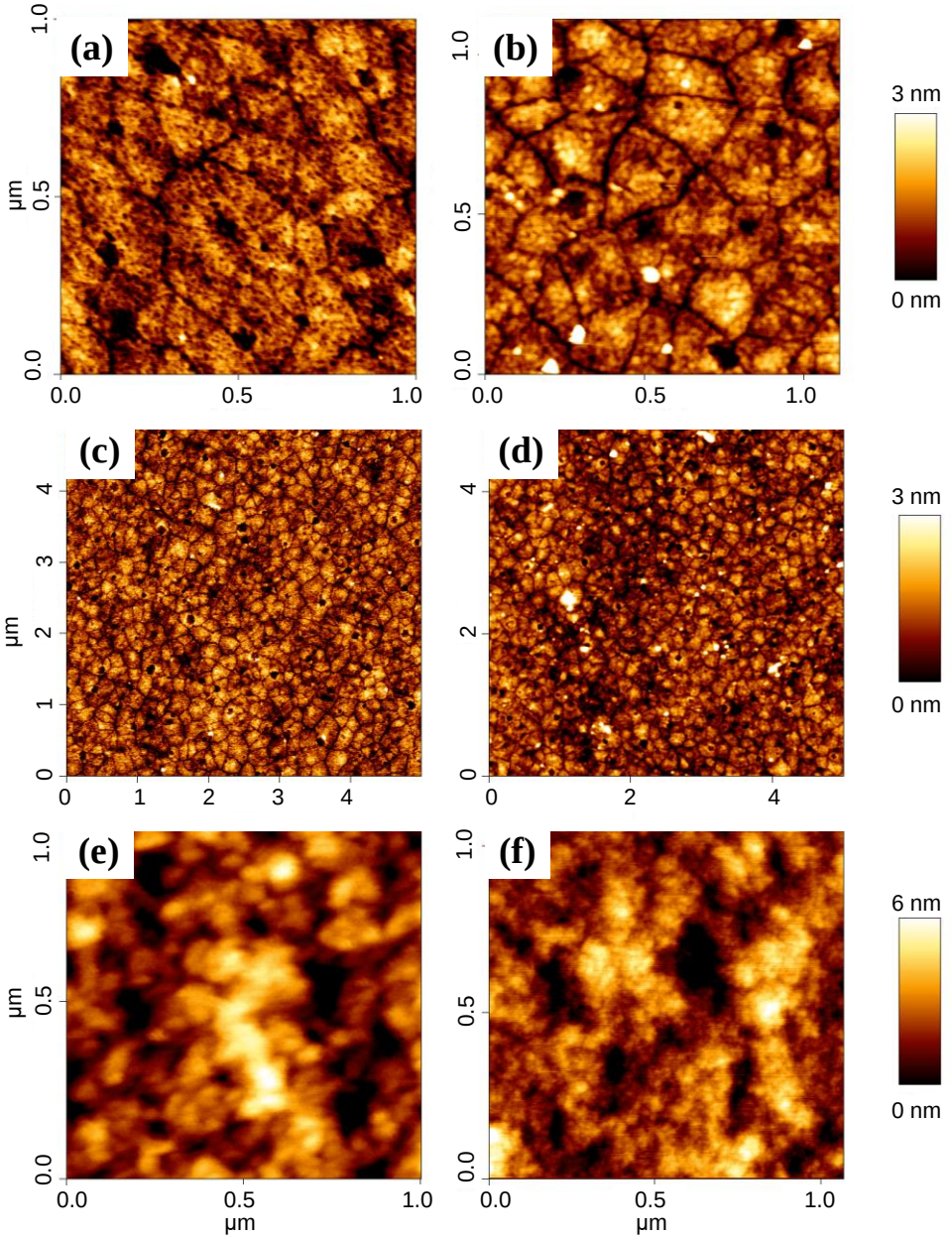

Figure 3.15: AFM topographic images of (a, c) as-prepared and (b, d) 30 min UV treated PFBD interlayer on ITO and PTB7:$PC_{71}BM$ blend film on the top of (e) as-prepared and (f) 30 min UV treated PFBD interlayer.

3.6.4 Impedance Analysis of the Organic Solar Cells Based on the PFBD ETL before and after UV Treatment

To further understand the influence of UV-treatment on device performance, the series and bulk resistance of the PFBD ETL based inverted organic solar cells were measured by impedance analysis. The Nyquist plots of the measured impedance of the organic solar cells based on as-prepared and 30 min pre-UV light treated PFBD ETL interlayers are shown in Figure 3.16. The series resistance R_s of the organic solar cells can be obtained from the Nyquist plots by extrapolating the curves to x-axis at high frequency on the left side. From the Figure 3.16, we obtained that the R_s of the organic solar cell with as-prepared PFBD layer is 4.9 Ωcm^2, while the R_s of the organic solar cell with pre-UV treated PFBD layer is reduced to 2.2 Ωcm^2. Besides the series resistance, another important characteristic change, charge transfer resistance, can be obtained from the Nyquist plots. The charge transfer resistance is indicated by the radius of the semicircle in Nyquist plot. The charge transfer resistance of the organic solar cells with as-prepared PFBD layer is much higher than that of the organic solar cells with pre-UV treated PFBD layer. The charge transfer resistance originates from the interfaces through which charge transfer occurs. In this study, there are three interfaces for charge transfer: PFBD-$PC_{71}BM$; PTB7-$PC_{71}BM$; PTB7-MoO_3. In the previous experiments, we have already demonstrated that the light-soaking effect is not caused by the photoactive layer and Al/MoO_3 contact. So we can rule out the possibility that the changed charge transfer resistance comes from the PTB7-$PC_{71}BM$ and PTB7-MoO_3 interfaces. Since the UV treatment is not affecting the latter two, it is most likely resulting from the change in charge transfer efficiency through PFBD-$PC_{71}BM$ interface. This is consistent with the observed reduction in

work function of ITO/PFBD after pre-UV treatment from Kelvin Probe measurements. The reduced work function of ITO/PFBD is associated with the improvement in FF and reduction in R_s identified from dark I-V curves because of the reduced barrier against electron collection from $PC_{71}BM$ to ITO electrode.

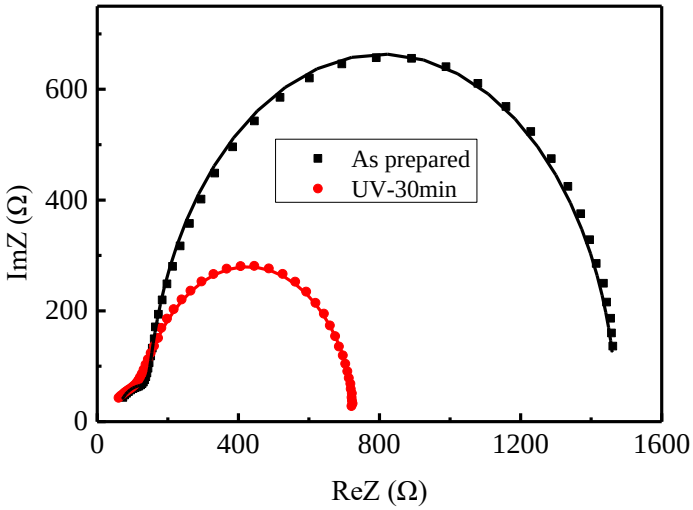

Figure 3.16: Nyquist plots of the impedance of inverted PTB7:$PC_{71}BM$ solar cells based on as-prepared and 30 min pre-UV light treated PFBD interlayers.

The corresponding Mott-Schottky characteristics of inverted organic solar cells with the as-prepared and 30 min pre-UV treated PFBD interlayers are shown in Figure 3.17. The flat-band potential (V_{FB}) is obtained by extrapolating the curve to x-axis in the linear region [231]. The V_{FB} of the organic solar cell with as-prepared PFBD ETL is 0.53 V while the organic solar cell with 30 min pre-UV treated PFBD ETL has a much higher V_{FB} (0.68 V). The enhancement of V_{FB} correlates well with the higher V_{oc} value after illuminating the organic solar cells. In the previous experiments, we have observed that the V_{oc} of the

organic solar cells with PFBD ETL increased from 0.62 V to 0.70 V after 15 minutes of continuous illumination of the device. The enhancement of the PFBD ETL based organic solar cells' V_{oc} can be explained by the improvement of V_{FB} after one sun illumination or pre-UV treatment. From the impedance analysis results, it can be concluded that UV-treatment improves the device performance by reducing the bulk and series resistance and increasing the V_{FB}. The improvement of the V_{FB}, bulk and series resistance originates from the PFBD-$PC_{71}BM$ interface.

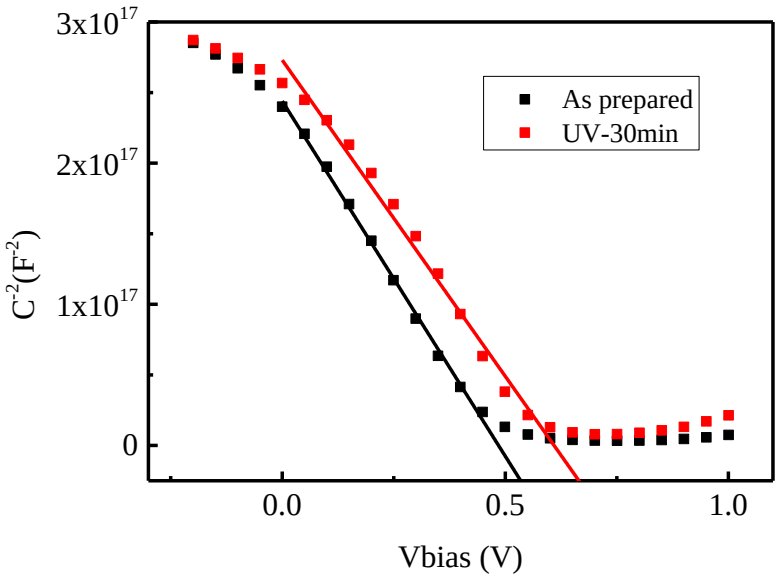

Figure 3.17: Mott-Schottky characteristics of inverted devices based on as-prepared and 30 min pre-UV light treated PFBD interlayers.

3.6.5 Optical Properties of PFBD Layer under UV Illumination

To study the influence of pre-UV treatment on the PFBD ETL itself, we carried out optical measurements to analyze the UV light treated PFBD films. The

PFBD films were prepared on clean quartz substrates. The as-prepared PFBD coated quartz substrates were measured before pre-UV treatment. Then the same samples were illuminated by UV light for different time and measured. First, we have tried to study the influence of pre-UV treatment on PFBD films by Fourier transform infrared (FT-IR). However, no obvious peak was found in Fourier transform infrared (FT-IR) spectra due to thin thickness of PFBD film. Then we measured the absorption spectra of PFBD film prepared on quartz substrate (Figure 3.18). The absorption maximum of the as-prepared PFBD films (black line) occurs at 325 nm and 480 nm, corresponding to the localized π-π* transitions of the conjugated backbones and the intramolecular charge transfer (ICT) from the donor of fluorene to the acceptor of benzoxadiazole (BD) units, respectively. After UV-treatment for various times, ranging from 30 min to 2 hour, the absorbance of the PFBD films at longer wavelength (480 nm) decreased accompanied with gradual blue-shift, indicating that the ICT effect has decreased. The absorbance at 325 nm remains almost the same, implying that the fluorene units are not affected by the UV-treatment. The highly localized electron densities in the LUMO on electron-deficient BD units would be expected to decrease the electron mobility in PFBD [231]. Hence, one possible explanation for the role of UV treatment is that some of the BD units are broken down by UV irradiation and result in increased electron mobility in PFBD films which corroborates well with the observed low series resistances obtained from dark current analysis and impedance analysis. This finding is in good agreement with our observation that the PFBD ETL based organic solar cells have a good stability indicating that the UV light causes permanent change within the PFBD layer. From Figure 3.18 we cannot find any vibronic absorption shoulder before and after UV treatment which often occurs when the polymer chain ordering degree increases [54, 232, 233]. So these results also

support the conclusion that the light-soaking effect should not be caused by the change of polymer chain alignment or packing properties. Except for the influence on electron mobility, decomposed BD units might also improve the work function tunning ability by producing more interfacial dipoles. It has been reported that the interfacial model can be used to explain the work function tuning of conjugate polyelectrolyte ETLs with a thickness less than 10 nm [218, 234]. In the interfacial dipole model, the Br^- ion located on the ITO surface during the film formation process while the N^+ functionalities in the alkoxy side chains are tethered to be Br^-, thus covering ITO surface. As a result, permanent dipoles are formed pointing outward from the ITO surface. In the PFBD ETL, the BD units could interact with the Br^- ions because of the electron-deficient nature of BD units. As a result, these Br^- ions cannot form interfacial dipoles. While after UV treatment, some BD units decomposed, thus releasing the Br^- ions which could contribute to more interfacial dipoles. So the increased interfacial dipoles improved the work function tuning ability of PFBD ETL, thus leading to the light-soaking effect. The optical measurement results indicate that the structure of the polymer backbone of PFBD plays an important role in determining its photovoltaic performance. With less BD units on the PFBD's backbone, the PFBD ETL has improved ability of reducing the work function of ITO. So our study suggests that further improvement of the performance of the PFBD ETL based organic solar cells can be achieved by introducing less BD units into the polymer backbone of PFBD or replacing BD units by other stable and electron-rich units.

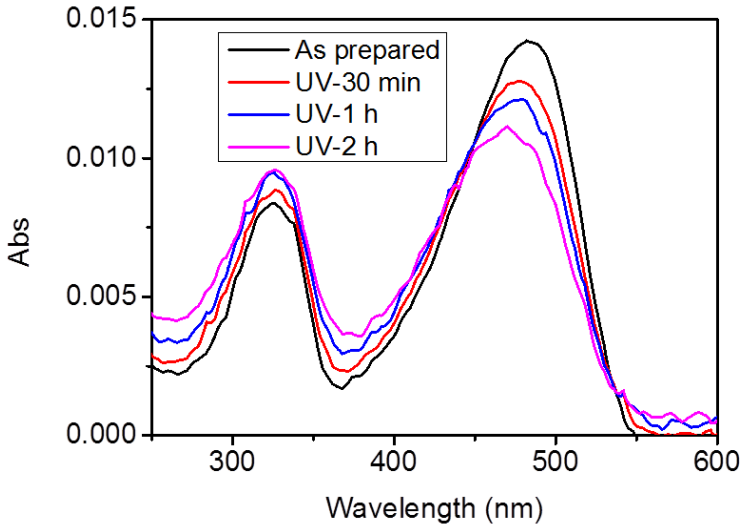

Figure 3.18: UV-vis absorption spectra of PFBD films at various UV illumination durations.

3.7 Conclusion

In summary, we have demonstrated inverted organic solar cells using a thin conjugated polyelectrolyte, PFBD, as ETL and they can be as efficient (>7%) as the inverted organic solar cells using the commonly used PFN ETL. The PFBD ETL based organic solar cells exhibited much better stability that the maximal efficiency of these solar cells retains at a similar level after stored in a N_2 filled glovebox for at least 26 days. We have also shown that the light soaking issue can be remedied by employment of a pre-UV treatment on the PFBD layer. The pre-UV treatment of PFBD leads to reduced work function, decreased series resistance and charge transfer resistance, and higher V_{FB}, thus enabling a more efficient electron collection. Our studies suggested that proper selection of the conjugated main chains is critical for the development of conjugated polyelectrolytes as interfacial materials and the interfacial property can be

well-modified by employment of UV treatment. The low-temperature processed PFBD ETL is a promising candidate for fabrication of highly efficient and stable organic solar cells. Further improvement of the PFBD ETL can be achieved by the modification of the polymer backbone.

Chapter 4 A New Dopant-free P-type Polymer as the Hole Transporting Layer in Perovskite Solar Cells

A new type dopant-free p-type polymer has been synthesized and used as the hole transporting layer for high performance perovskite solar cells applications. Using the new dopant-free p-type polymer can help improve the performance and stability of the perovskite solar cells compared with the perovskite solar cells based on Spiro-OMeTAD HTL. The use of the polymers for fabrication of perovskite solar cells will be presented first in this chapter. Then, the operation and performance of the perovskite solar cells are characterized. Finally, the properties of these p-type polymers, such as absorption spectrum, crystalline structure, working function, etc., are investigated and their applications in the perovskite solar cells have been compared.

4.1 Introduction and Motivation

Solution processed organic-inorganic lead halide perovskite solar cells have attracted much attentions after experienced a sky-rocketing power conversion efficiency (PCE) in recent years. Within few years' development, the highest PCE of perovskite solar cells has been enhanced from 3.8% [28] to above 20% [29, 30, 32, 34, 235]. Such dramatic PCE enhancement of the solar cells has never happened before in any other photovoltaic technologies. The reported PCE of perovskite solar cells is comparable or higher than that of silicon solar

cells. Benefiting from the solution processability, the manufacturing costs of perovskite solar cells are much cheaper when compared to the silicon based photovoltaic techniques. The high PCE and low manufacturing costs make perovskite solar cells a promising candidate to compete with the currently silicon dominated photovoltaic technology.

The structure of perovskite solar cells can be grouped into two: mesoscopic structure and planar structure. In the mesoscopic structure, a mesoporous TiO_2 scaffold layer is used for fast extraction of electrons from the perovskite layer [236]. While in the planar structure, there is no mesoporous TiO_2 scaffold layer, instead, only a layer of compact TiO_2 [237] or other n-type materials, such as [6,6]-Phenyl-C61-butyric acid methyl ester ($PC_{61}BM$) and C_{60} (in inverted planar structure) [83, 159, 238, 239], is used as the electron transport material (ETL). Compared with mesoscopic structure perovskite solar cells, planar perovskite solar cells have lower PCE and often suffer from the notorious hysteresis phenomenon of which the origin is still under debate [240-243]. So far, the highest reported PCE of the planar perovskite solar cells is lower than that of the mesoscopic perovskite solar cells. In this study, we focus on the mesoscopic perovskite solar cells. Except for the ETLs, another indispensable component of a perovskite solar cell structure is the hole-transporting material (HTL). HTL is deposited on the top of perovskite layer in mesoscopic perovskite solar cell structure to extract holes from the perovskite layers and transport them to the anodes. The most commonly used HTL is a small molecular material, 2,20,7,70-tetrakis(N,N0-di-p-methoxyphenylamine)-9,90-spirobifluorene (Spiro-OMeTAD) which was first reported by Grätzel et al two decades ago [178, 179]. The intrinsic semiconducting properties of Spiro-OMeTAD are not optimum for perovskite

solar cells. But after doping cobalt based dopants and ionic salt, Spiro-OMeTAD's semiconducting properties can be significantly improved. Using using Spiro-OMeTAD as the HTL, the PCE of the mesoscopic perovskite solar cells has achieved higher than 20% [30-34]. However, fabrication of the Spiro-OMeTAD based perovskite solar cells is complicated and the perovskite solar cells' stability is sacrificed after doping the ionic salt into Spiro-OMeTAD [244-249]. Another disadvantage of using Spiro-OMeTAD in perovskite solar cell is its lengthy, expensive synthesis process in preparation. Also, to receive the Spiro-OMeTAD, it needs costly sublimation steps to purify the material [250]. Besides Spiro-OMeTAD, many other small molecular HTLs have also been synthesized and used for perovskite solar cells. Some of them have good performance when they were used in perovskite solar cells. The PCE of the devices achieved above or close to 20%. Michael Saliba et al synthesized a HTL with a simple dissymmetric fluorene-dithiophene (FDT) core substituted by N,N-di- p-methoxyphenylamine donor groups which can be easily modified. They proposed that the additional thiophene-iodine interaction may improve hole transfer at the FDT/perovskite interface, thus leading to high performance of the perovskite solar cells with the PCE of 20.2% [185]. Kasparas Rakstys et al reported four novel star-shaped triazatruxene derivatives used as the HTL in perovskite solar cells. The best perovskite solar cell using this HTL has a PCE of 18.3%, which was benefited from the good interfacial properties between the HTL and perovskite layer [186]. Sungmin Park et al reported a high mobility small molecular HTL, PCP-TPA, and obtained the perovskite solar cells with the PCE of 17.8% [187]. Compared to small molecular HTLs, using polymer HTLs in perovskite solar cells were much less reported. So far, the most successful polymer HTL in perovskite solar cells is polytriarylamine (PTAA). The PCE of the perovskite solar cells using it as the HTL achieved 20.2% [29].

Beside, some p-type polymers such as poly(3-hexylthiophene) (P3HT), poly-[2,1,3-benzothiadia- zole-4,7-diyl[4,4-bis(2-ethylhexyl)-4H-cyclo penta[2,1-b:3,4-b'] dithiophene- 2,6-diyl]] (PCDTBT), Poly[2,6-(4,4-bis-(2-ethylhexyl)-4H-cyclopenta [2,1- b;3,4-b'] dithiophene)-alt-4,7(2,1,3- benzothiadiazole)] (PCPDTBT) and so on, are widely used as HTLs in organic photovoltaic (OPV) cells. They were also reported to be used as the HTLs in perovskite solar cells. Unfortunately, all the mentioned small molecular and polymer HTLs require ionic salt doping to obtain good performance. Only a few dopant-free small molecular HTLs have been reported to be used in mesoscopic perovskite solar cells. The PCE of the devices was reported ranging from 8.60% to 13.40% [246, 247, 251-254]. The reports for dopant-free polymer HTLs are rarer. To our best knowledge, the highest reported PCE of mesoscopic perovskite solar cells is 12.32% by using a diketopyrrolopyrrole (DPP) based polymer [255]. Most of the reported perovskite solar cells with the dopant-free polymer HTLs can only achieve less than 10% of the PCE [256-258]. To achieve high performance dopant-free polymer HTLs, polymers with proper HOMO and LUMO levels and charge carrier transport properties are needed. Incorporating thiazolothiazole fused rings into the backbone of polymers might be a good choice for high performance dopant-free polymer HTLs for perovskite solar cells because of their excellent charge carrier transport properties. There have been many reports on thiazolothiazole-containing copolymers with good OFET and OPV performance [259-269]. Sang Kyu Lee et al. reported a new thiazolothiazole-containing copolymer PCDTTz [268]. When the PCDTTz was used in OFET, the mobility was one order higher than another polymer without thiazolothiazole units. Selvam et al. also reported thiazolothiazole-linked polymers have better OFET performance than a benzobisthiazole-linked

copolymer [265]. The better performance was attributed to better solid state molecular packing and crystallinity of thiazolothiazole-linked polymers. Besides the backbone [262], side chain [259, 261, 263, 264, 267, 269], processing methods [260] and molecular weight [266] can also influence the thiazolothiazole-containing copolymers' charge carrier transport properties, HOMO level and stability, thus influencing their OFET and OPV performance. Despite so many reports on applying thiazolothiazole-containing copolymers into OFET and OPV, to our best knowledge thiazolothiazole-containing copolymers have never been reported to be used in perovskite solar cells as HTLs so far.

In this work, we synthesized a series of new dopant-free thiazolothiazole-containing copolymers and used them as the HTLs in perovskite solar cells. Their performance has been studied. The perovskite solar cells with these new polymer HTLs have good photovoltaic performance without introducing any dopants into the polymer HTLs. We have achieved the PCE of the perovskite solar cell of 14.02% by using the polymer Jl-2-38 as the HTL in the perovskite solar cell. Three polymers have been prepared. The three polymer HTLs have similar molecular structure, while the other two polymer HTLs, Jl-2-19 and Jl-2-21, have lower PCE with only 10.26% and 8.47%. We investigated the factors that can influence the performance of polymer HTLs in perovskite solar cells. Through XRD measurement, we found that the crystallinity of polymer HTLs is an important factor that can influence the perovskite solar cells' performance. We carried out TRPL measurement to investigate the charge carrier extraction ability of the polymer HTLs. Then we found that the Jl-2-38 HTL had the best charge carrier extraction ability as indicated by its short PL decay time. As a result, the PSCs based on Jl-2-38 have the best performance.

Use the dopant-free polymer HTL, Jl-2-38, can improve the perovskite solar cells' stability. After storing in a N_2 filled glove box for 113 days, the PCE still retained 80% of the original value. These findings will be useful for synthesis of more highly efficient and stable dopant-free polymer HTLs in the future.

4.2 Fabrication of the New Polymer HTL Based Perovskite Solar Cells

Figure 4.1 shows the fabrication processes of the new polymer HTL based perovskite solar cells. To fabricate the perovskite solar cells with the new polymer HTLs, fluorine doped tin oxide (FTO) substrates were cleaned using soap water and followed by sonicating sequentially with de-ionized water, acetone and isopropanol for 10 min each. After drying at 60 ℃ in oven for several hours, the FTO substrates were exposed to ultraviolet light and ozone for 15 min. After being exposed to ultraviolet light and ozone, a TiO_2 compact layer was spin coated from a titanium isopropoxide solution at 6000 rpm for 30 seconds followed by sintering at 450 ℃ for 20 min. The TiO_2 precursor solution was prepared by mixing 1 mL titanium isopropoxide and 10 uL HCl (12 M) solution in 10 mL ethanol. After cooling down to room temperature, a mesoporous scaffold of TiO_2 nanoparticles was deposited by spin coating at 6000 rpm with an acceleration of 500 rpm/s for 30 s. The TiO_2 paste (Dyesol 30 NR-D) was bought from Dyesol. The TiO_2 precursor solution was prepared by dissolving the TiO_2 paste in ethanol (150 mg/mL). The substrate with TiO_2 mesoporous layer was sintered at 500 ℃ for 20 min and then cooled to room temperature. The perovskite precursor solution was prepared by dissolving PbI_2, $PbBr_2$, CH_3NH_3Br (MABr) and $NH{=}CHNH_3I$ (FAI) in a mixed solvent of

anhydrous dimethyl formamide (DMF) and anhydrous dimethyl sulfoxide (DMSO). The molar ratio of PbI_2:$PbBr_2$:MABr:FAI was 1.05:0.19:0.19:1. The volume ratio of DMF to DMSO was 4:1. The perovskite precursor solution was spin coated on the substrate in an N_2 filled glovebox to form the perovskite layer: firstly, it was spun at 2000 rpm for 10 s; then, continued spun at 6000 rpm for another 30 s. During the spin coating process, 110 μL chlorobenzene was dropped on the spinning substrate 20 s before the end of the procedure. The sample was then annealed at 100 ℃ for 60 min and then cooled to room temperature followed by spin coating the polymer HTLs (Jl-2-21, Jl-2-19, Jl-2-38) at 1000 rpm for 30 s on the perovskite layer. The polymer HTLs solution was prepared by dissolving 6 mg polymer in 1 mL 1,2-Dichlorobenzene. The polymer HTL solution was heated at 70 ℃ for 15 min and then filtered through a 0.45 μm PTFE filter before it was used for the spin coating. The Spiro-OMeTAD layer was prepared by spin coating its solution at 3000 rpm for 30 s on the perovskite layer. The Spiro-OMeTAD solution was prepared by dissolving 72 mg Spiro-OMeTAD in 1 ml chlorobenzene doped with 17.6 μl Li-TFSI (1.8 M in acetonitrile), 29.2 μl tert-butylpyridine and 29.2 μl Co[t-BuPyPz]$_3$[TFSI]$_3$ (FK209) acetonitrile solution (100 mg/ml). The device fabrication was completed by depositing Au top electrodes on the polymer HTLs by a thermal evaporator with the chamber pressure of 2×10^{-6} mbar. The initial deposition rate was kept less than 0.5 Å/s until 10 nm Au was deposited. The final thickness of Au is 80 nm. The device active area was defined by a shadow mask to be 0.09 cm^2. The fabricated perovskite solar cells structure are shown in the Figure 4.2 (a).

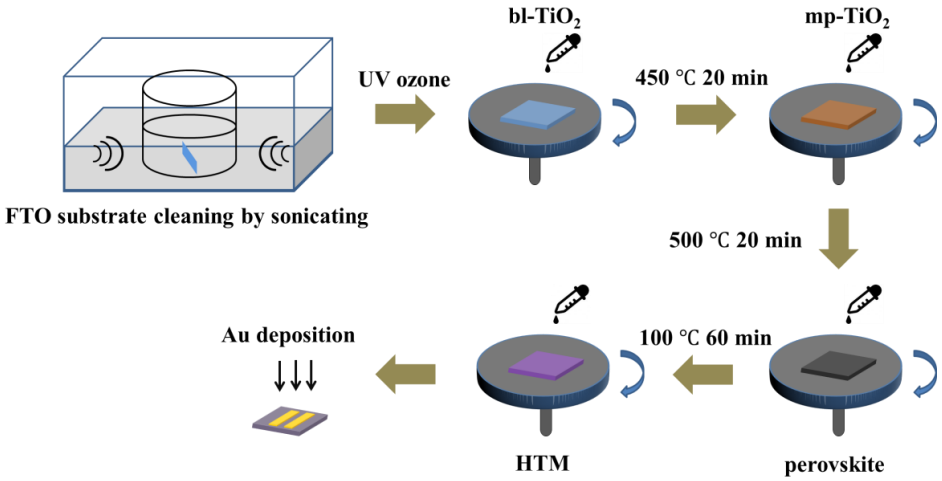

Figure 4.1: The fabrication process of perovskite solar cells based on the dopant-free polymer HTLs.

Figure 4.2 (b) shows the molecular structure of the Jl-2-38 HTL used in this study. The other two polymers have a similar molecular structure but with different side chains. The polymer backbone contains thiophene and thiazolothiazole units. The synthesis procedure of the polymers with similar molecular structure has been reported before [269]. These thiazolothiazole-containing copolymers have been used for high performance OTFT and OPV. The high charge carrier mobility and stability of these polymers made them good candidates for dopant-free HTLs of the perovskite solar cells.

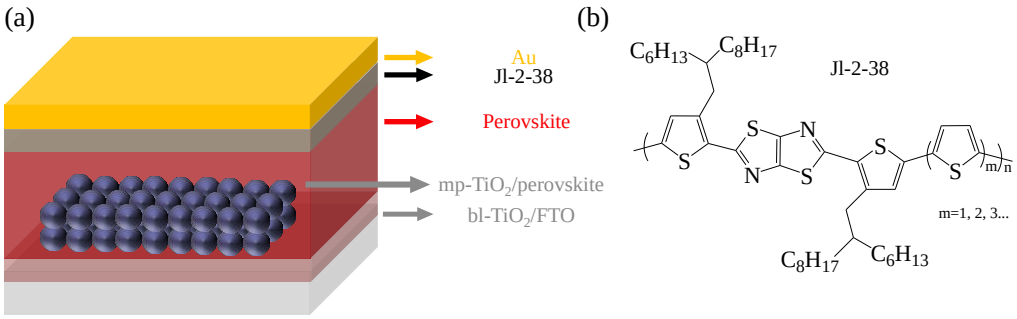

Figure 4.2: (a) Schematic illustration of the perovskite solar cell configuration. (b) Molecular structure of the Jl-2-38 HTL used in this study.

4.3 Major Characterization Techniques

Perovskite solar cells' photovoltaic performance measurement: The J-V characteristics and external quantum efficiency (EQE) were measured by the methods described in chapter 3. The only difference is that the IPCE measurements were conducted on perovskite solar cells under short-circuit conditions at a chopping frequency of 8 Hz during illumination with a monochromatic light from a Xenon arc lamp. This is to avoid the hysteresis effects on the EQE measurement. All the J-V characteristics and IPCE measurements were conducted in a N_2 filled glovebox.

Scanning electron microscopy (SEM) measurement: The cross sectional SEM image of the perovskite solar cells was taken by a scanning electron microscopy (JEOL-JSM-7600F) at an accelerating voltage of 5 kV. The fabricated perovskite solar cells with the dopant-free polymer HTLs were used for SEM measurement. After preparation of the perovskite solar cells, the samples were broken by using a glass cutter to cut from the glass sides.

UV-vis absorption measurement: The samples were prepared by spin coating the three polymer HTLs' 1,2-Dichlorobenzene solution on quartz substrates. The concentrations of the solutions are 6 mg/mL which are the same as those used for the fabrication of the perovskite solar cells. The absorption spectra of the polymer HTLs films were measured by a Shimadzu UV-3101PC UV-VIS-NIR Spectrophotometer.

Photo-Electron Spectroscopy in Air (PESA) measurement: The samples for PESA measurement were prepared by spin coating the polymer on glass substrates. The measurement was carried out by using Riken Photoelectron

Spectrometer (Model AC-2). This measurement is to measure the HOMO levels of the polymer HTLs. In the PESA measurement, the surface of the sample is illuminated by UV light. With increasing the energy of UV light to more than a certain value, photoelectrons will start to emit from the surface of the sample. Then the HOMO level of the polymer HTLs can be obtained from the onset energy level of photoelectron output.

X-ray diffraction (XRD) measurement: The crystallinity of the polymer HTLs was measured by XRD measurements were carried out on a 2D GADDS X-ray diffractometer. The polymer HTL thin films were prepared on glass substrates by spin coating from their 1,2-Dichlorobenzene solution. In the XRD measurement, monochromatic X-ray beams were generated from Cu X-ray tube with Graphite monochromator. The diffracted beams from the polymer/glass samples were captured with HI-STAR Area detector which is a two dimensional multi wire proportional counter.

Time-resolved photoluminescence (TRPL) measurement: Time-resolved photoluminescence (TRPL) measurements were performed using a home-build set-up as shown in Figure 4.3. The samples were illuminated by a 405 nm picosecond pulsed laser. The PL signals were collected in a conventional backscattering geometry and detected by a charge-coupled device array (Princeton Instruments, PixisTM 400B) coupled to a monochromator (Acton, Spectra ProTM 2500i). The TRPL signal were collected using the time correlated single-photon counting (TCSPC) technique. The samples for TRPL measurement have a structure of glass/perovskite/HTL. The TRPL measurement was carried out in ambient environment at room temperature.

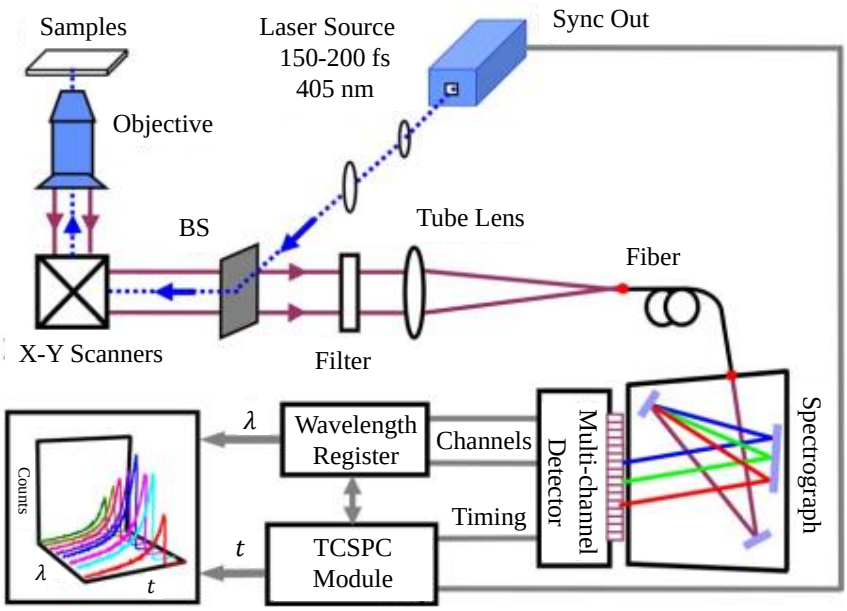

Figure 4.3: Schematic of the time-resolved photoluminescence (TRPL) system.

Stability measurement: The stability of the perovskite solar cells with the dopant-free polymer HTLs was carried out in a N_2 filled glovebox. For each polymer HTL, at least 10 devices were fabricated for stability measurement.

4.4 Characterization of Solar Cells' Performance

Figure 4.4 shows the schematic illustration (a) and cross sectional SEM image of a mesoscopic perovskite solar cell based on Jl-2-38 HTL. The perovskite solar cell has a structure of glass/fluorine-doped tin oxide (FTO)/block layer TiO_2 (bl-TiO_2)/mesoporous TiO_2 (mp-TiO_2)/mixed perovskite/HTL/gold. The 30 nm bl-TiO_2 layer is to prevent the perovskite layer from contacting the FTO electrode, otherwise high leakage current and poor FF will occur. A layer of mp-TiO_2 with a thickness of around 150 nm is used to increase the area of the interface between perovskite and TiO_2 layers. In the spin coating process of

perovskite layer, the perovskite precursor solution is infiltrated into the mp-TiO_2 layer. Some of the perovskites crystals will be formed within the pores of the mp-TiO_2 layer, thus increasing the contact area between the perovskite and TiO_2 layer. So the generated charge carriers will be efficiently transferred into the FTO/TiO_2 cathodes. The mixed perovskite layer has a composition of $FA_{0.81}MA_{0.15}PbI_{2.5}Br_{0.45}$ (FA= formamidinium, MA= methylammonium) which was prepared by one-step method with anti-solvent (chlorobenzene) [30]. The thickness of the perovskite layer is around 450 nm. The Jl-2-38 HTL was inserted between the perovskite layer and Au electrode by spin coating from its solution in 1,2-Dichlorobenzene. As shown in the cross sectional SEM image, a Jl-2-38 layer with thickness around 50 nm well covered the surface of perovskite layer and prevented the direct contact between perovskite and Au layer. Finally, the fabrication of the perovskite solar cells was completed by depositing a 80 nm layer of Au.

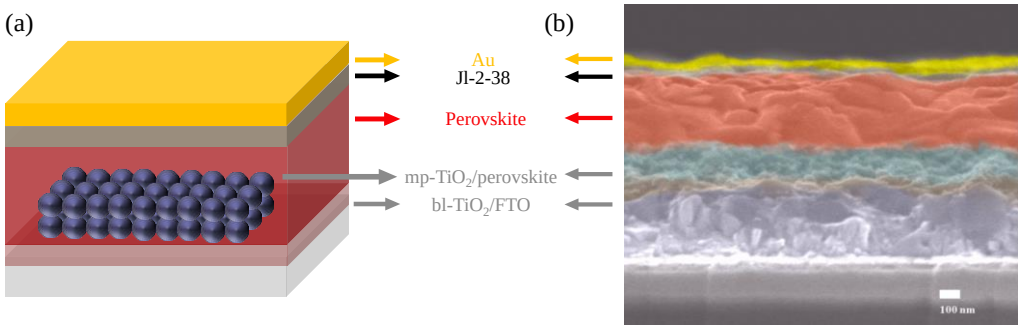

Figure 4.4: (a) Schematic illustration of the perovskite solar cell configuration. (b) A high-resolution cross sectional SEM image of a complete solar cell.

Figure 4.5 shows the J-V characteristic of the best perovskite solar cell based on the Jl-2-38 and Spiro-OMeTAD HTL. The Jl-2-38 HTL was used without any dopants, while the Spiro-OMeTAD HTL was doped. The detailed photovoltaic parameters of the perovskite solar cells are summarized in Table 4.1. The best Jl-2-38 HTL based perovskite solar cell can achieve a PCE of 14.02% under the

reverse voltage sweep direction. A slight hysteresis phenomenon was observed when measuring the performance of the perovskite solar cells. The highest PCE of the perovskite solar cells in the forward voltage sweep direction is 12.46%. From the J-V curve shown in Figure 4.3, the hysteresis effect in the perovskite solar cells led to a 1.56% PCE difference when scanning in different voltage sweep directions. The average PCEs of the perovskite solar cells obtained from at least 20 cells are 11.80% and 13.03% for forward and reverse voltage sweep directions, respectively. The highest PCE of the Spiro-OMeTAD HTL based perovskite solar cells is 13.02% under reverse voltage sweep direction. The hysteresis phenomenon was also observed during the measurement of the Spiro-OMeTAD based perovskite solar cells. The lower PCE of the Spiro-OMeTAD HTL based perovskite solar cells is because their lower FF, 0.63. The high FF of the Jl-2-38 HTL based perovskite solar cells around 0.70 indicates that the Jl-2-38 HTL can effectively extract holes and block electrons from the perovskite layer and transfer the holes to Au electrodes.

Table 4.1: Photovoltaic parameters of the perovskite solar cells based on Jl-2-38 HTL.

HTL	Voltage sweep direction	V_{oc} (V)	J_{sc} (mA/cm^2)	FF	PCE (%) Best	PCE (%) Average*
Jl-2-38	Forward	1.00	19.01	0.64	12.46	11.80±0.36
	Reverse	1.01	18.67	0.69	14.02	13.03±0.52
Spiro-OMeTAD	Forward	0.99	20.32	0.53	10.66	10.30±0.88
	Reverse	1.02	20.26	0.63	13.02	12.10±0.64

*The average PCE is obtained from at least 20 cells.

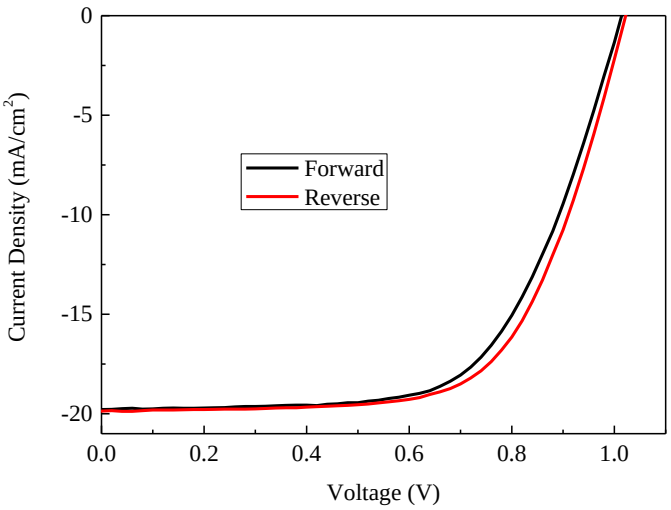

Figure 4.5: J-V characteristics of the perovskite solar cells based on the Jl-2-38 HTL under forward and reverse voltage sweep directions.

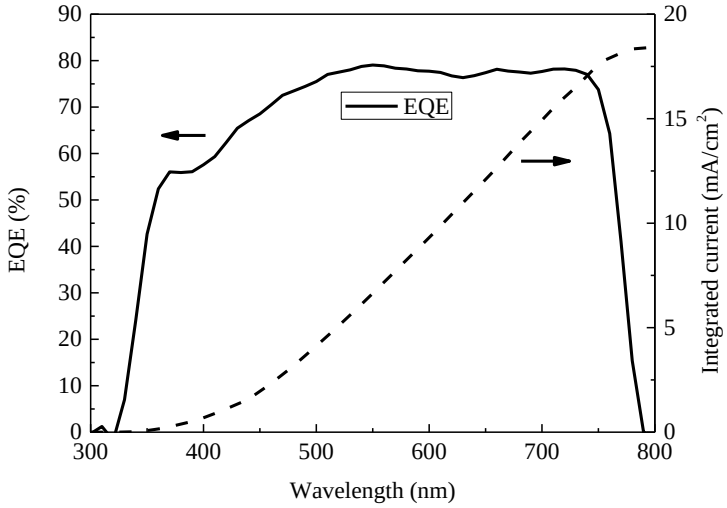

Figure 4.6: Solid line: EQE curve of the perovskite solar cells from 300 nm to 800 nm. Dashed line: J_{sc} calculated from the overlap integral of the EQE spectrum with the standard AM1.5 solar emission.

Figure 4.6 shows the measured EQE spectrum (solid line) and the calculated J_{sc}

(dashed line) of the perovskite solar cells based on Jl-2-38 HTL. The theoretical J_{sc} was calculated to be 18.38 mA/cm^2 by integrating the product of EQE and AM1.5 spectrum. Under reverse voltage sweep direction, the J_{sc} of the perovskite solar cell obtained from the J-V characteristic measurement is 18.67 mA/cm^2 which is in good agreement with that calculated from the EQE curve.

Figure 4.7 shows the box charts of the photovoltaic parameters of the perovskite solar cells based on Jl-2-38 HTL. The photovoltaic parameters were obtained from at least 20 cells fabricated in different batches. The small variation of the photovoltaic parameters of the perovskite solar cells with the Jl-2-38 HTL demonstrates that our results are highly reproducible. These results indicate that the Jl-2-38 is suitable for applying in perovskite solar cells as HTL and fabricating highly efficient perovskite solar cells.

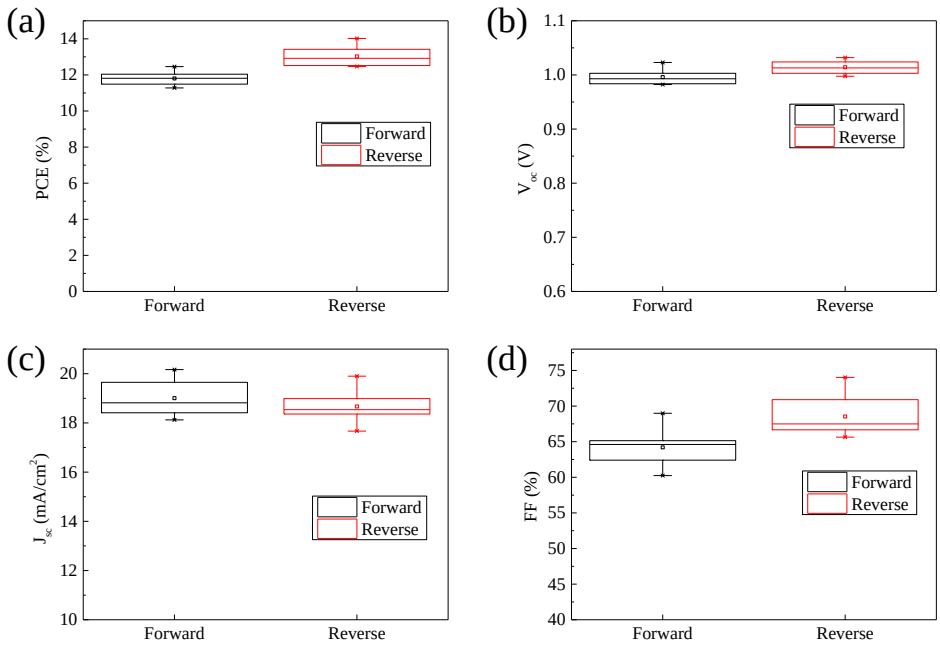

Figure 4.7: Box charts of the photovoltaic parameters of the perovskite solar cells based on Jl-2-38 HTL.

The other two polymers, Jl-2-19 and Jl-2-21, were also applied into perovskite solar cells as HTLs. The perovskite solar cells with Jl-2-19 and Jl-2-21 HTLs have the similar structure as shown in Figure 4.2 (a). The Jl-2-19 and Jl-2-21 HTLs were prepared by spin coating their 1,2-Dichlorobenzene solutions with a concentration of 6 mg/mL. The spin coating process is same as that used for spin coating the Jl-2-38 HTL. The thicknesses of the three polymer HTLs are the similar and around 50 nm. To do a fair comparison, the perovskite solar cells based on the different polymer HTLs were fabricated under the same conditions in the same batch. Table 4.2 and Figure 4.8 show the photovoltaic parameters and the J-V characteristics of the perovskite solar cells based on the three different polymer HTLs under reverse voltage sweep direction. The best perovskite solar cell with the Jl-2-38 HTL has a PCE of 13.21%. The highest PCE of the perovskite solar cells based on Jl-2-21 and Jl-2-19 HTLs can only achieve 8.47% and 10.26%, respectively. J_{sc} of the perovskite solar cells based on Jl-2-21 and Jl-2-19 HTLs calculated from the EQE results (Figure 4.8 (b)) are 15.82 mA/cm^2 and 16.65 mA/cm^2 respectively and lower than the J_{sc} of perovskite solar cells based on Jl-2-38. The lower EQE and J_{sc} of the perovskite solar cells with Jl-2-21 and Jl-2-19 demonstrate that the generated charge carriers cannot be efficiently collected by the Au electrodes because of the poor charge carrier extraction properties of the Jl-2-21 and Jl-2-19 HTLs. Besides, we notice that the V_{oc} and FF of the perovskite solar cells based on Jl-2-21 and Jl-2-19 HTLs are also lower. The V_{oc} of the perovskite solar cells with Jl-2-21 and Jl-2-19 HTLs are 0.90 V and 0.94 V. The FF of the perovskite solar cells with Jl-2-21 and Jl-2-19 HTLs are 0.57 and 0.62. These results are also evidences that the properties of the Jl-2-21 and Jl-2-19 HTLs are not as good as those of the Jl-2-38 HTL for achieving highly efficient perovskite solar cells.

Table 4.2: Photovoltaic parameters of perovskite solar cells based on Jl-2-21, Jl-2-19 and Jl-2-38.

HTLs	V_{oc} (V)	J_{sc} (mA/cm^2)	FF	PCE (%)
Jl-2-21	0.90	16.47	0.57	8.47
Jl-2-19	0.94	17.62	0.62	10.26
Jl-2-38	1.02	19.87	0.65	13.21

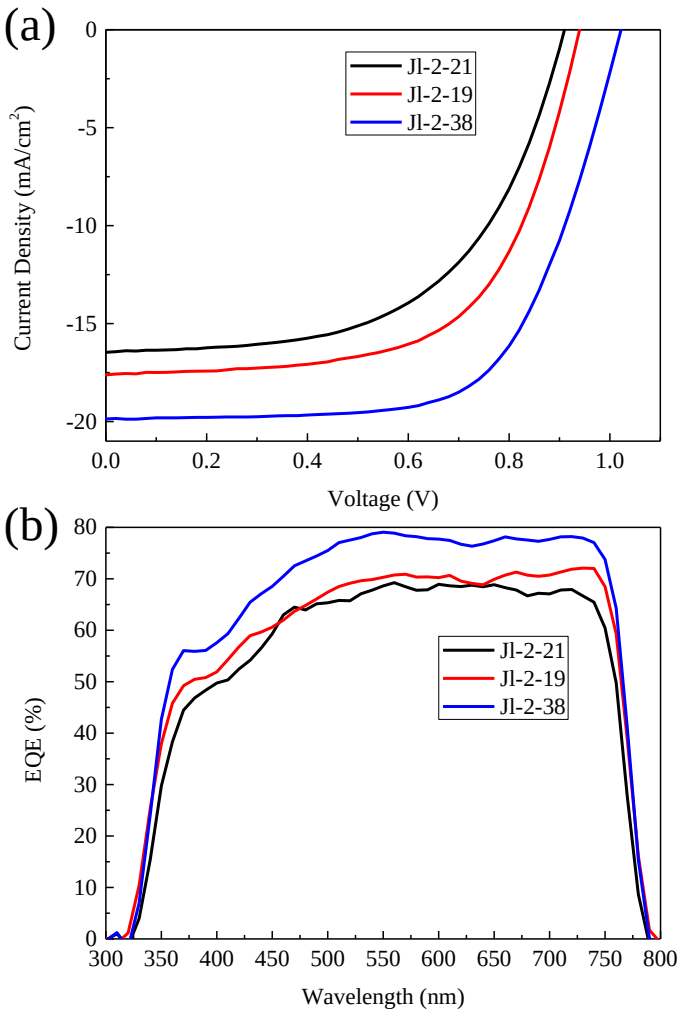

Figure 4.8: Measured (a) J-V and (b) EQE curves of the perovskite solar cells with different polymer HTLs.

4.5 Characterization of the P-type Polymer HTLs

We have demonstrated that the Jl-2-38 has the best photovoltaic performance when used in perovskite solar cells as HTL. In this section, we will investigate and find out what properties of the Jl-2-38 polymer make it act as a good HTL in perovskite solar cells.

4.6.1 Band Energy Levels and Optical Properties of the P-type Polymer HTLs

The measured J-V curves of the perovskite solar cells with different polymer HTLs show that Jl-2-21 and Jl-2-19 HTLs based perovskite solar cells have much lower V_{oc} than that of the Jl-2-38 HTL based perovskite solar cells. It was suspected that the Jl-2-38 HTL had better band alignment with the perovskite layer. To investigate the band alignment of the different polymers, we used UV-vis absorption measurement and Photo-Electron Spectroscopy in Air (PESA) measurement to determine their highest energy occupied molecular orbital (HOMO) and lowest energy unoccupied molecular orbital (LUMO) levels. Figure 4.9 shows the UV-vis absorption spectra of the three different polymer thin films deposited on glass substrates. The absorbance of the polymer HTLs was normalized to the peak value at the main absorption peak located at the wavelength of 624 nm. Another absorption peak with a vibronic absorption shoulder located at 572 nm. The absorption maxima ($\lambda_{abs,max}$) at 624 nm and 572 nm correspond to 0-0 and 0-1 transitions [269]. The optical bandgap (E_g) of the polymer HTLs was calculated from the onset of absorption spectra (λ_{onset}). As shown in the Table 4.3, the optical bandgaps of Jl-2-21, Jl-2-19 and Jl-2-38

are 1.84 eV, 1.88 eV and 1.83 eV. The optical bandgap of Jl-2-19 is the largest among the three polymers and is in agreement with its slightly red shifted absorption curve. Despite the small difference of the optical bandgap, all of the three polymers have similar UV-vis absorption characteristics.

Table 4.3: Optical properties and HOMO/LUMO levels of HTLs.

HTLs	λ_{onset} (nm)	E_{HOMO} (eV)	E_g (eV)	E_{LUMO} (eV)
Jl-2-21	674.18	-5.20	1.84	-3.36
Jl-2-19	659.33	-5.21	1.88	-3.33
Jl-2-38	678.64	-5.19	1.83	-3.36

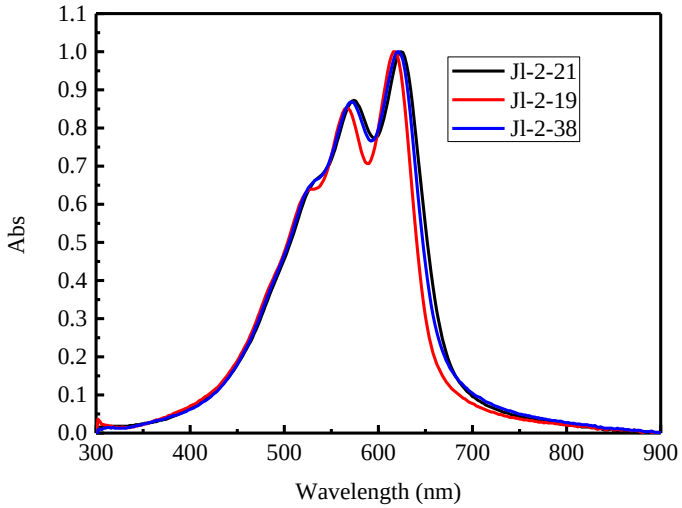

Figure 4.9: The measured UV-vis absorption spectra of the different polymer HTL thin films deposited on glass substrate.

The HOMO levels of the polymer HTLs were determined by PESA measurement as shown in Figure 4.10. The collected photoelectrons are plotted

as a function of the energy of the incident UV light. The HOMO levels of the polymer HTLs were obtained by extrapolating the curves of emitted photoelectrons to the horizontal level of the collected photoelectrons curves. Then E_{LUMO} of the polymer HTLs can be obtained by adding up the E_g and E_{HOMO}. The HOMO and LUMO levels of the polymer HTLs are summarized in the Table 4.3. All the three polymer HTLs have similar E_{HOMO} levels, around 5.20 eV, which is very close to the reported HOMO level of Spiro-OMeTAD (5.22 eV) [180]. This means that the three polymer HTLs should have similar band alignment with the perovskite layer. So we can rule out that possibility that the low PCE of perovskite solar cells with Jl-2-21 and Jl-2-19 HTLs comes from large energy barriers between the perovskite layer and the HTLs. The poor performance of the perovskite solar cells based on the Jl-2-21 and Jl-2-21 HTLs should come from other factors rather than the energy barrier.

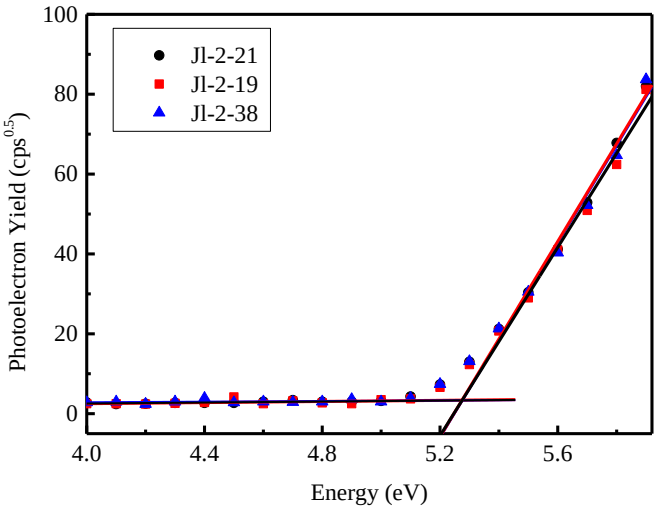

Figure 4.10: Photoelectron yield as a function of the incident UV light energy measured by PESA.

4.6.2 XRD Measurement

The crystallinity of polymer HTL thin films can greatly influence the charge carrier transport, thus influencing the perovskite solar cells' performance. So we carried out X-ray diffraction (XRD) measurement to study the crystallinity of the three polymer HTLs. We prepared the three polymer thin films on glass substrates for XRD measurement. The measured XRD curves of the polymer films on glass substrates are shown in Figure 4.11. The broad and amorphous hump observed in the XRD patterns of the three polymer HTLs is attributed to the glass substrates. Both Jl-2-21 and Jl-2-19 polymer HTLs exhibited diffraction peaks at 4.38°. Different from the less discernable peaks of Jl-2-21 and Jl-2-19, the Jl-2-38 polymer HTL has a sharp and prominent diffraction peak at 4.24°, indicating that the Jl-2-38 has higher crystallinity. The higher crystallinity of Jl-2-38 indicates that the charge carriers might be better extracted and transferred from the perovskite layer to the Jl-2-38 HTL then to the Au electrodes.

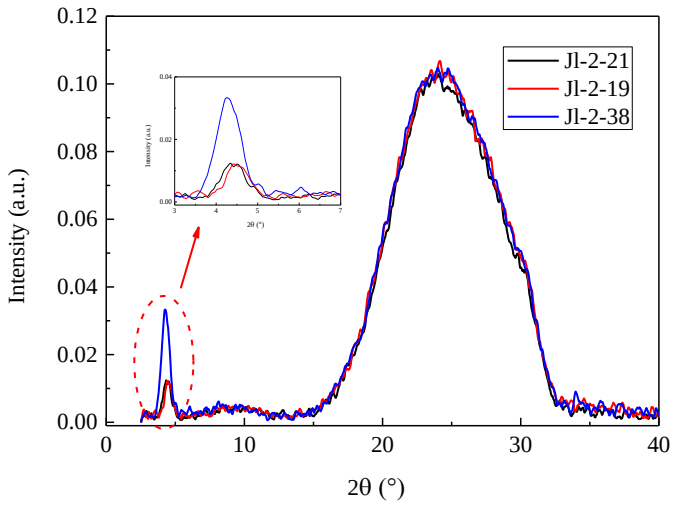

Figure 4.11: XRD patterns of the polymer thin films on glass substrates.

4.6.3 Time-resolved Photoluminescence Measurement

From the XRD measurement, we have already observed that the Jl-2-38 has the highest crystallinity among the three polymers. To study the charge carrier transfer properties at the interface between the perovskite layer and the polymer HTLs, we carried out time-resolved photoluminescence (TRPL) measurement. The samples used for this investigation were prepared by depositing the perovskite layer on the glass substrate followed by depositing another layer of the polymer HTL to be investigated. The TRPL decay curves of the samples with different polymers are shown in Figure 4.12. It shows that the PL quenching of the glass/perovskite/Jl-2-38 sample has the fastest rate. While the PL quenching rate in the glass/perovskite/Jl-2-21 was the lowest. These results indicate that the charge carriers injection from perovskite into the Jl-2-38 is faster than into the other two polymer HTLs, Jl-2-38 and Jl-2-19. The efficient charge carrier injection from perovskite to Jl-2-38 is in good agreement with the highest efficiency of perovskite solar cells based on Jl-2-38 HTL. We also fitted the PL decay by using a bi-exponential decay function as shown below [270]:

$$\mathrm{I}\,(\mathrm{t}) = A_1 \exp(-\frac{t}{\tau_1}) + A_2 \exp(-\frac{t}{\tau_2})$$

The smaller time constants τ_1 is caused by the initially photogenerated intrachain excitons' migration to defects while relaxing toward lower energy states. The larger time constant τ_2 represents the exciton lifetime of perovskite. The PL decay times and the decay amplitudes (A_1 and A_2) are shown in Table 4.4. The average PL decay times (τ_{ave}) values are calculated by using the following equation [271]:

$$\tau_{ave} = \frac{A_1\tau_1^2 + A_2\tau_2^2}{A_1\tau_1 + A_2\tau_2}$$

The τ_{ave} of glass/perovskite/Jl-2-21 is 22.78 ns which is much longer than that of glass/perovskite/Jl-2-38, 11.32 ns. So the Jl-2-38 HTL has the best charge separation ability among the three polymers. The shorter PL decay time and faster charge transfer rate are beneficial for efficient extraction of charge carriers from perovskite to HTL and suppressing the charge recombination at the perovskite and HTL interface. The TRPL results match with the photovoltaic performance of the perovskite solar cells with the three polymer HTLs. The higher V_{oc}, FF and J_{sc} of the perovskite solar cells with Jl-2-38 HTL could be caused by the suppressed recombination of charge carrier. So we can conclude that the good photovoltaic performance of the Jl-2-38 HTL used in the perovskite solar cells comes from its good charge extraction ability.

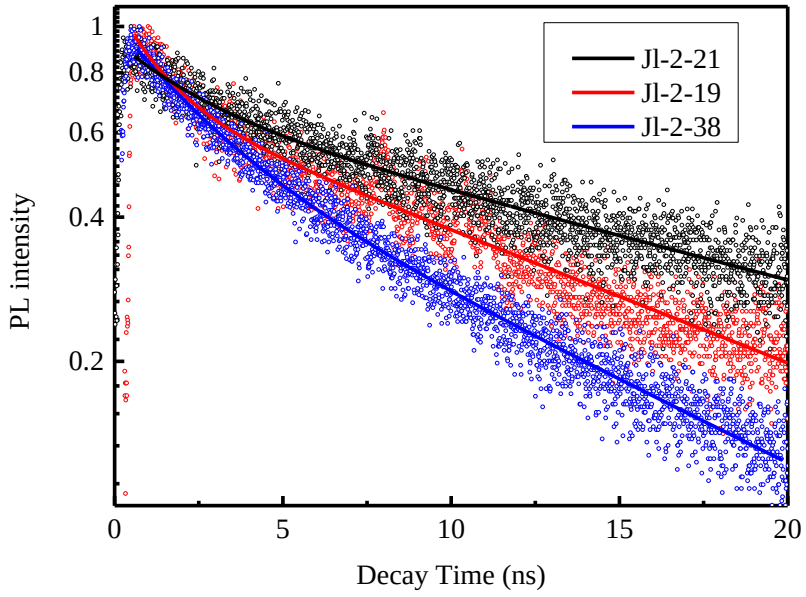

Figure 4.12: TRPL decay curves of glass/perovskite/HTL.

Table 4.4: Summary of the parameters from fitting to the TRPL decay data.

HTLs	A_1	τ_1 (ns)	A_2	τ_2 (ns)	τ_{ave} (ns)
Jl-2-21	0.692	23.53	0.244	2.45	22.78
Jl-2-19	0.713	15.63	0.408	1.42	14.93
Jl-2-38	0.600	12.60	0.424	2.62	11.32

4.6 Stability Measurement

As mentioned before, one of the serious issues of Spiro-OMeTAD is the requirement for cobalt based and ionic salt dopants which lead to poor stability of perovskite solar cells. In contrast, the Jl-2-38 polymer HTL can achieve 14.02% PCE without using any dopants. To study the stability of the perovskite solar cells based on Jl-2-38, we stored the perovskite solar cells in a N_2 filled glovebox and kept recording the performance in a period of 113 days. At the same time, we also prepared control devices of the perovskite solar cells with Spiro-OMeTAD HTL. The perovskite solar cells with Spiro-OMeTAD HTL were stored under the same condition. The preparation method of the perovskite solar cells with Jl-2-38 and Spiro-OMeTAD HTL is the same except the deposition of HTLs. Figure 4.13 (a) shows the PCE of the perovskite solar cells with JL-2-38 and Spiro-OMeTAD HTLs plotted as a function of time. The perovskite solar cells based on Jl-2-38 exhibited excellent stability. After storing for 113 days, PCE of the perovskite solar cells still retained 80% of the original value, from 13.28% to 10.52%. In contrast, PCE of the perovskite solar cells with Spiro-OMeTAD HTL decreased from 12.14% to 4.84% after stored for 97 days. The better stability of the Jl-2-38 based perovskite solar cells demonstrates that the stability of perovskite solar cells can be improved by using dopant-free HTLs. The J-V characteristics of the as-prepared and stored

for 113 days perovskite solar cells are shown in Figure 4.13 (b). We observed that the V_{oc} and J_{sc} of the perovskite solar cells based on the Jl-2-38 HTL reduced from 1.01 V and 19.54 mA/cm^2 to 0.90 V and 17.49 mA/cm^2 after stored for 113 days. Although the V_{oc} and J_{sc} decreased, the FF of the perovskite solar cells retained 95% of the initial value that the FF decreased from 0.68 to 0.65. The stable FF value demonstrates that the Jl-2-38 HTL can keep its good charge carrier extraction ability even after the perovskite solar cells are stored for 113 days. From Figure 4.14 (b), (c) and (d), we found that the main factors that influenced the PCE of perovskite solar cells using Spiro-OMeTAD HTL are J_{sc} and FF. Figure 4.14 (b) shows that the V_{oc} values of both of the Jl-2-38 and Spiro-OMeTAD HTLs-based perovskite solar cells remained almost unchanged. According to Figure 4.14 (c) and (d), the J_{sc} and FF of Spiro-OMeTAD HTL-based perovskite solar cells decreased very fast. After stored for 97 days, the J_{sc} and FF values of the Spiro-OMeTAD HTL-based devices decreased from 20.06 mA/cm^2 to 14.14 mA/cm^2 and 60.32% to 32.75%, respectively. The Jl-2-38 HTL-based devices are much more stable with J_{sc} and FF decreasing from 19.71 mA/cm^2 to 18.04 mA/cm^2 and 67.14% to 63.84%, respectively. The stable J_{sc} and FF of perovskite solar cells using Jl-2-38 HTL indicate that the Jl-2-38 HTL could keep its good hole transporting and electron blocking properties for a longer period than Spiro-OMeTAD. The decreased PCE of perovskite solar cells could be caused by the decomposition of perovskite films or the degradation of HTL materials [272-274]. In our stability study, we observed that the V_{oc}, J_{sc} and FF of the perovskite solar cells using Jl-2-38 HTL remained almost the same. The V_{oc} of the device using Spiro-OMeTAD HTL slightly increased after stored for 97 days but the J_{sc} and FF decreased very fast. This phenomenon has also been observed by Zhang et al. [275]. This could be caused by the Spiro-OMeTAD HTL itself and the dopants in it. It has been

reported that pinholes would form in spin-coated Spiro-OMeTAD film dopedwith Li-TFSI and tert-butylpyridine, thus leading to decomposition of perovskite layer [244, 276]. Besides, Li-TFSI absorbs moisture in the air and tert-butylpyridine can react with the perovskite [277]. These factors might all contribute to the poor stability of the perovskite solar cells using doped Spiro-OMeTAD HTL. The stability measurement results indicate that the dopant-free polymer HTL, Jl-2-38, can be used for fabrication of highly stable perovskite solar cells.

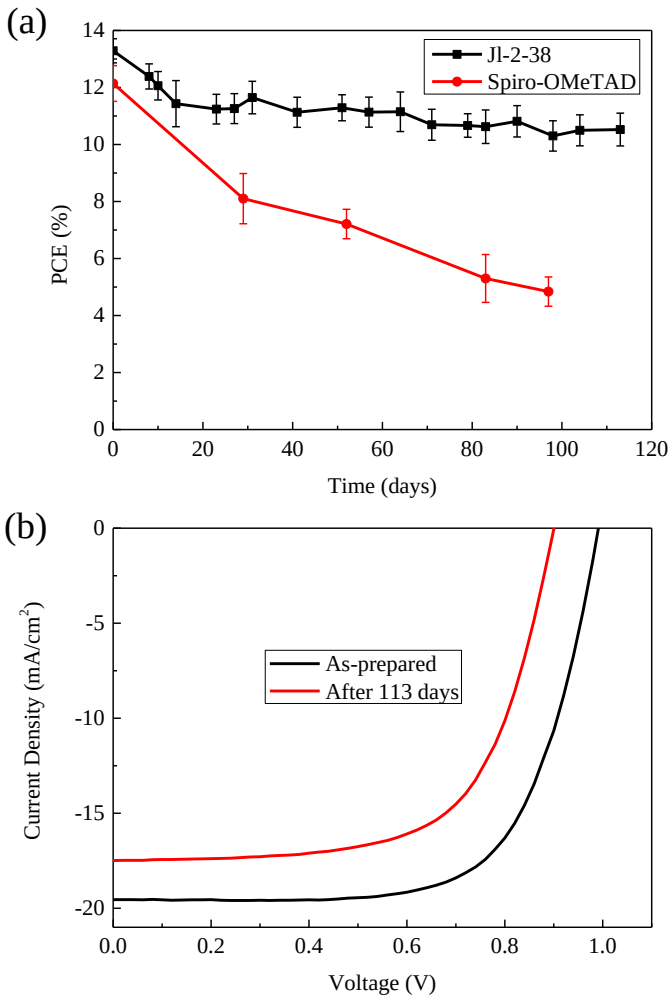

Figure 4.13: (a) PCE of perovskite solar cells with Jl-2-38 and

Spiro-OMeTAD HTLs plotted as a function of time. (b) J-V characteristics of the perovskite solar cells stored for 113 days.

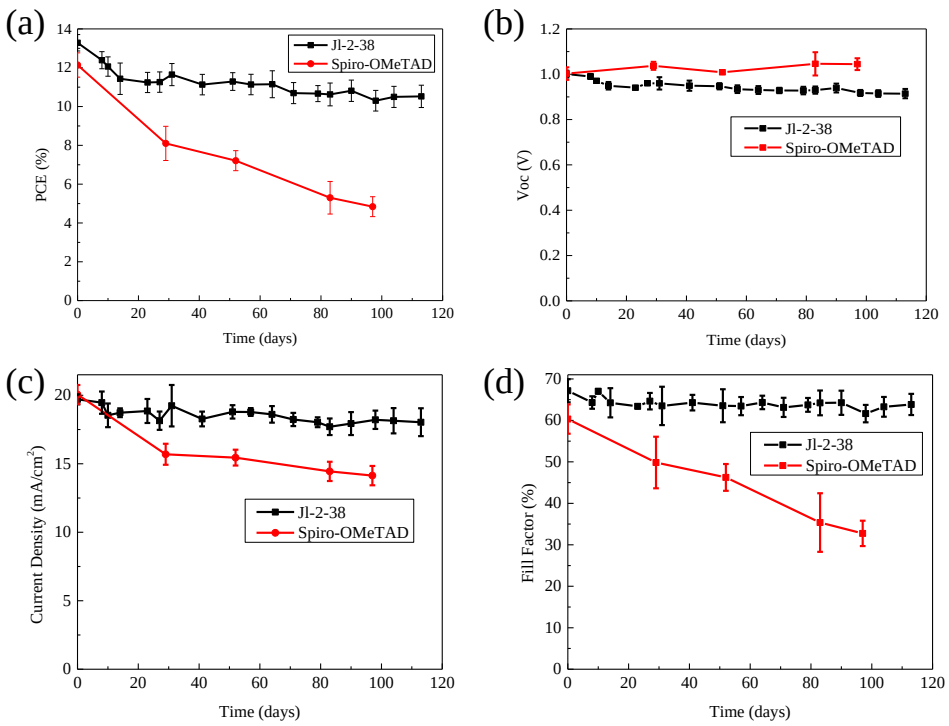

Figure 4.14. Detailed photovoltaic parameters of perovskite solar cells with Jl-2-38 and Spiro-OMeTAD HTLs plotted as a function of time.

4.7 Conclusion

In summary, we have successfully developed a series of new dopant-free polymer HTLs for highly efficient and stable perovskite solar cells. The best perovskite solar cell based on the Jl-2-38 HTL, has a PCE of 14.02% and the PCE can retain 80% of the original value after storing in a N_2 filled glovebox for 113 days. We also applied the other two similar polymers, Jl-2-21 and Jl-2-19, into perovskite solar cells as HTLs, but they can only achieve highest PCEs of 8.47% and 10.26%, respectively. Then we carried various characterization techniques to investigate the factors that influence the

performance of the perovskite solar cells. Through UV-vis absorption and PESA measurement, we found that the three polymer HTLs have almost the same band energy level. So we ruled out the influence of energy barrier caused by the mismatch between the polymer HTLs' HOMO levels and the valence band of perovskite layer. From the XRD measurement, we observed that the Jl-2-38 HTL had much higher crystallinity than those of the other two polymer HTLs. We conducted TRPL measurement to study the charge carrier extraction properties of the polymer HTLs. Then we found that the Jl-2-38 HTL had the best charge carrier extraction ability among the three polymer HTLs as indicated by its short PL decay time. In this study, we demonstrated the importance of the crystallinity of polymer HTLs and the influence of the crystallinity on the charge carrier extraction ability. The dopant-free Jl-2-38 polymer is a promising candidate for replacing the costly Spiro-OMeTAD in perovskite solar cells as HTL. Without the requirement of dopants, the perovskite solar cells with Jl-2-38 HTL exhibited excellent stability. We hope that this study could provide some guidelines for chemists and material scientists to synthesize more efficient and stable dopant-free polymer HTLs. Besides the energy levels of the polymer HTLs, attentions should also be paid to improve the polymer HTLs' crystallinity for better charge carrier extraction.

Chapter 5 Fully Printable Organic and Perovskite Solar Cells with Transfer-printed Flexible Electrodes

In the previous two chapters, we have demonstrated that the performance of the organic solar cells and perovskite solar cells can be improved by applying novel polymer interfacial layers. In these studies, we focused on improving the charge carrier extraction properties at the interfaces between the photoactive and interfacial layers. In an OPV or perovskite solar cell device, the top metal electrode does not only transfer the electricity generated from the device to the external load. The interface between the metal electrode and the interfacial layer of the device plays very important role in the performance of the device. In this chapter, we demonstrate the high performance perovskite solar cells and organic solar cells with good stability with their top metal electrode being fabricated using a low-cost transfer printing method to deposit the top metal electrodes. The advantages of using this transfer printing method to fabricate the electrode over that fabricated using the conventional thermal evaporation method are presented. It is demonstrated that the transfer printing technique has potential to replace the high-cost vacuum deposition method for fabricating highly efficient and stable perovskite solar cells and organic solar cells.

5.1 Introduction and Motivation

In developing the perovskite solar cells and organic solar cells, most research focused on developing and optimizing solution or printable process for

fabrication of active layers and buffer layers while less attention was paid to electrodes which are also important components in perovskite solar cells and organic solar cells. The top electrodes of perovskite solar cells and organic solar cells are normally fabricated by depositing a gold layer on top in high vacuum environment using thermal or E-beam evaporator in high vacuum environment. The commonly used hole transporting layers of perovskite solar cells, such as Spiro-OMeTAD [33, 278] and PTAA [29, 279-281], in perovskite solar cells are very thin ~200 nm, due to their limited conductivity and charge carrier mobility. The optimal thickness of the photoactive layer in the state-of-art organic solar cells is around 100 nm because of a trade-off between photons absorption and photogenerated charge carriers collection efficiency [26]. To prevent excess metal atoms penetrating into the soft and thin organic films underneath of the perovskite solar cells or organic solar cells, the initial metal deposition rate during the top metal electrode evaporation is normally very low and precisely controlled [282, 283]. The excess metal atoms penetrating into the organic films will lead to increasing the leakage current [284, 285] and poor device stability [286-289]. Besides, the vacuum evaporation process is not compatible with the roll-to-roll production of perovskite solar cells and organic solar cells. It will significantly increase the fabrication costs. To achieve fully printable perovskite solar cells and organic solar cells fabrication, alternative methods of depositing metal top electrodes of the devices that are compatible with roll-to-roll fabrication process and will not induce excess metal penetration are attractive. Transfer printing method is a potential candidate for replacing the traditional method by using E-beam or thermal evaporator for the devices' top electrode fabrication because it is fast, robust and applicable to various materials and substrates [290-295]. The transfer printing method has been widely used in thin film transistors (TFTs) [290, 296-298], light emitting diodes (LEDs) [299, 300]

and solar cells [15, 301-307]. PEDOT:PSS, graphene and silver nanowires have been successfully transfer printed as top electrodes of perovskite solar cells and organic solar cells [14, 15, 304, 305, 308]. But the reports on transfer printing metal thin films as top electrodes of perovskite solar cells and organic solar cells are rare.

In this study, we have developed and investigated the transfer printing Au electrode of the perovskite solar cells and organic solar cells. The Au top electrodes of perovskite solar cells were deposited by transfer printing the Au layer from a soft polydimethylsiloxane (PDMS) substrate onto the top of Spiro-OMeTAD layer of the perovskite solar cell device structure. The highest PCE of the perovskite solar cells with the transfer-printed Au electrodes was measured 13.72% which is higher than that of the control device with the thermally evaporated Au electrodes. The interface between the Spiro-OMeTAD and the transfer-printed Au electrode has been evaluated less defects than that between the Spiro-OMeTAD and thermally evaporated Au electrode as indicated by the space charge limited current (SCLC) analysis. Through X-ray photoelectron spectroscopy (XPS) measurement, we have found that less Au atoms diffused into the Spiro-OMeTAD layer when the Au electrode was deposited by using the transfer printing method. It has also been measured that the perovskite solar cells with the transfer-printed Au electrodes showed excellent stability. They retained 71% of their initial PCE after storing them in N_2 environment for 97 days without any encapsulation. We have also demonstrated the universality of this transfer printing method by successfully fabricating the P3HT-based organic solar cells with the transfer printed Au top electrode. They showed good performance and stability.

5.2 Fabrication of Organic Solar Cells and Perovskite Solar Cells Using Transfer Printing Method

Figure 5.1 shows the procedure of transfer printing Au layer from PDMS onto the top of Spiro-OMeTAD to form the Au top electrode of a perovskite solar cell. An 80 nm Au layer was deposited on the top of PDMS strips by using an E-beam or thermal evaporator. The PDMS/Au sample was attached to a glass slide. Details of preparation of device with a structure of FTO/TiO_2 compact layer/TiO_2 mesoporous layer /perovskite layer/spiro-OMeTAD can be found in the following parts of this section. The PDMS/Au sample was placed on the top of Spiro-OMeTAD, then, the two parts were firmly laminated together by two long tail clips. To facilitate the Au layer to be transferred from PDMS to the Spiro-OMeTAD, the whole sample was heated at 90 ℃ for 2 h. The heating step can accelerate the surface hydrophobic recovery in the PDMS, thus to reduce the PDMS substrate's surface energy and adhesion between PDMS and Au interface [293]. After the heating process, the PDMS strips were slowly peeled off and the Au film was left on the top of the Spiro-OMeTAD.

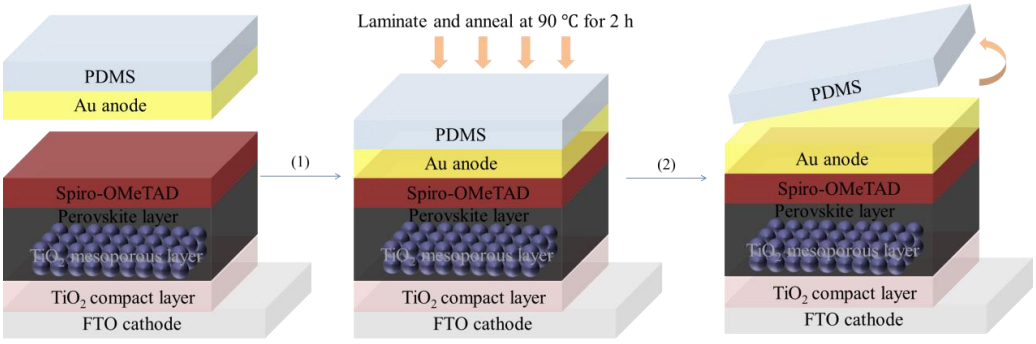

Figure 5.1: The fabrication procedure of the transfer-printing Au top electrodes of the perovskite solar cells.

Perovskite solar cells fabrication: FTO substrates were cleaned using soap

water and sonicated sequentially with de-ionized water, acetone and isopropanol for 10 min each. After drying at 60 ℃ in oven for several hours, the FTO substrates were exposed to ultraviolet light and ozone for 15 min. After being exposed to ultraviolet light and ozone, a TiO_2 compact layer was spin coated from a Titanium diisopropoxide bis(acetylacetonate) solution at 6000 rpm for 30 s followed by sintering at 450 ℃ for 20 min. After cooling down to room temperature, a mesoporous scaffold of TiO_2 nanoparticles was deposited by spin coating a solution of TiO_2 paste in ethanol (150 mg/ml) at 6000 rpm with an acceleration of 500 rpm/s for 30 s. The substrate with TiO_2 mesoporous layer was sintered at 500 ℃ for 20 min and then cooled to room temperature. The perovskite precursor solution was prepared by dissolving PbI_2, $PbBr_2$, CH_3NH_3Br (MABr) and $NH{=}CHNH_3I$ (FAI) in a mixed solvent of anhydrous dimethyl formamide (DMF) and anhydrous dimethyl sulfoxide (DMSO) [309]. The molar ratio of PbI_2:$PbBr_2$:MABr:FAI was 1.05:0.19:0.19:1. The volume ratio of DMF to DMSO was 4:1. The perovskite precursor solution was spin coated in a N_2 filled glovebox: first, 2000 rpm for 10 s; second, 6000 rpm for 30 s. During the spin coating process, 110 μl chlorobenzene was dropped on the spinning substrate 20 s before the end of the procedure. The substrate was then annealed at 100 ℃ for 60 min and then cooled to room temperature followed by spin coating Spiro-OMeTAD at 3000 rpm for 30 s on the perovskite layer. The Spiro-OMeTAD solution was prepared by dissolving 72 mg Spiro-OMeTAD in 1 ml chlorobenzene doped with 17.6 μl Li–TFSI (1.8 M in acetonitrile), 29.2 μl tert-butylpyridine and 29.2 μl $Co[t\text{-}BuPyPz]_3[TFSI]_3$ (FK209) acetonitrile solution (100 mg/ml). The device fabrication was completed by depositing Au top electrodes on Spiro-OMeTAD by transfer printing method as shown in Figure 5.1. For the control device, an 80 nm Au layer was deposited by a thermal evaporator at the pressure of 2×10^{-6}mbar.

The initial deposition rate was controlled less than 0.5 Å/s until 10 nm Au was deposited. The device active area was defined by a shadow mask to be 0.2 cm^2.

Organic solar cells fabrication: ITO substrates were cleaned using soap water and sonicated sequentially with de-ionized water, acetone and isopropanol for 10 min each. After drying at 60 ℃ in oven for several hours, the ITO substrates were exposed to ultraviolet light and ozone for 15 min. The fabrication procedure of the organic solar cells followed other people's report [14]. A 30 nm ZnO layer was prepared by spin coating ZnO sol-gel precursor at 2500 rpm for 30 s on ITO substrates, which were then annealed at 150 for 1 h in the air. The ZnO sol-gel precursor was prepared by dissolving zinc acetate dihydrate ($Zn(CH_3COO)_2 \cdot 2H_2O$) and ethanolamine ($NH_2CH_2CH_2OH$) in 2-methoxyethanol ($CH_3OCH_2CH_2OH$). The molar ratio of zinc acetate dihydrate to ethanolamine was 1:1 and the Zn concentration in 2-methoxyethanol was 0.5 M. The solution was stirred overnight in air and then passed through a 0.2 μm PTFE filter before spin coating. Then the substrates were transferred into a N_2 filled glovebox. A P3HT and $PC_{60}BM$ (weight ratio 1:1) blend solution with a total concentration of 40 mg/ml in 1,2-dichlorobenzene was spin coated at 800 rpm for 60 s. After annealing at 120 ℃ for 10 min, a ~200 nm P3HT and $PC_{60}BM$ blend film was obtained. After being filtered through 0.45 μm PVDF filter and sonicated, PEDOT:PSS (Al 4083) mixed with 1 vol % Zonyl surfactant (FSO-100) was spin coated on P3HT and $PC_{60}BM$ blend film at 5000 rpm for 50 s followed by annealing at 110 ℃ for 10 min. The device fabrication was completed by transfer printing Au top electrodes on PEDOT:PSS layer. For the control device, an 80 nm Au electrode was deposited by a thermal evaporator at the pressure of 2×10^{-6}mbar. The initial deposition rate was controlled less than 0.5 Å/s until 10

nm Au was deposited. The device active area was defined by a shadow mask to be 0.09 cm^2.

5.3 Sample Preparation for Characterization and Major Characterization Techniques

Space-charge limited current-voltage (SCLC) measurement: In SCLC measurement, a hole-only or electron-only device is required. In the hole-only or electron-only device, only one type of charge carriers (holes or electrons) must be efficiently injected from at least one electrode while the other type of charge carriers must be efficiently blocked. Applying a voltage to the diode can result in a build-up of space-charge because of unipolar charge injection. After sufficient time (greater than the charge carrier transit time), the electric field at the injecting contact will be diminished by the space-charge. Finally the amount of the charge carriers inside the device will saturate that a new charge carrier can only be injected when one is extracted by the opposite electrode. In this condition, the SCLC model can be used to calculate the charge carrier mobility in the device at low voltage [310-313]:

$$J = \frac{9}{8}\varepsilon_0\varepsilon_r\mu\frac{V^2}{L^3} \quad (1)$$

where J is the measured current density, $\varepsilon_0\varepsilon_r$ is the permittivity of the component, μ is the charge carrier mobility, L is the thickness of the active layer of the device.

Hole-only device: The hole-only device with a structure of ITO/PEDOT:PSS/Spiro-OMeTAD/Au was fabricated by spin coating PEDOT:PSS (Al 4083) solution filtered through 0.45 μm PVDF filter on

UV-ozone treated ITO substrate at 5000 rpm with an acceleration of 4000 rpm/s for 50 s followed by annealing at 140 ℃ for 10 min. The Spiro-OMeTAD solution was prepared by dissolving 72 mg Spiro-OMeTAD in 1 ml chlorobenzene doped with 17.6 μl Li–TFSI (1.8 M in acetonitrile), 29.2 μl tert-butylpyridine and 29.2 μl Co[t-BuPyPz]3[TFSI]3 (FK209) acetonitrile solution (100 mg/ml). Spiro-OMeTAD was spin coated on the top of PEDOT:PSS layer following the same procedure described in perovskite solar cells fabrication part. The thickness of Spiro-OMeTAD was around 170 nm determined by surface profiler. Hole-only device based on P3HT:PC_{60}BM was fabricated by replacing ZnO layer in organic solar cells by PEDOT:PSS layer. The PEDOT:PSS layer was spin coated on ITO substrate at 5000 rpm with an acceleration of 4000 rpm/s for 50 s from a PEDOT:PSS (Al 4083) solution filtered through 0.45 μm PVDF filter followed by annealing at 140 ℃ for 10 min. The other fabrication process for the hole-only device was the same as that of the organic solar cells. All hole-only devices were completed by deposition of a 80 nm layer of Au top electrodes by using transfer printing or thermally evaporating method.

Thickness measurement: A KLA Tencor P-16+ Surface Profiler was used to measure the thickness of Spiro-OMeTAD and P3HT:PC_{60}BM blend films in the hole-only devices. The films to be measured were prepared on clean glass substrates. The preparation methods for the Spiro-OMeTAD and P3HT:PC_{60}BM blend films followed those used for fabrication of their hole-only devices. After the preparation of the films, steps for the thickness measurement were created by using the sharp needle to scratch the surface of the films.

X-ray photoelectron spectroscopy (XPS) measurement: XPS spectra of the samples were obtained with a monochromatic Al Kα radiation (VGESCALAB

200i-XL). The samples for XPS measurement were prepared by depositing perovskite films on clean glass substrates first. Then a layer of Spiro-OMeTAD was spin coated on the top of the perovskite layers. For the control device, a 80 nm Au layer was deposited on the Spiro-OMeTAD layer by a thermal evaporator. The initial deposition rate was controlled less than 0.5 Å/s until 10 nm Au was deposited. For the device by transfer-printing method, a 80 nm Au layer was deposited by transfer-printing method from PDMS substrates. After the device preparation, the Au electrodes were peeled off by using Kapton tape to expose the buried Spiro-OMeTAD surface for XPS measurement. Figure 5.2 shows the illustration of the setup for XPS measurement. The prepared samples were excited by a monochromatic Al Kα radiation and the photoelectrons were emitted from the surface of the samples. The emitted photoelectrons were collected and analyzed by an electron energy analyzer. According to the binding energy and the intensity of a photoelectron peak, the elemental identity, chemical state, and quantity of a detected element can be determined.

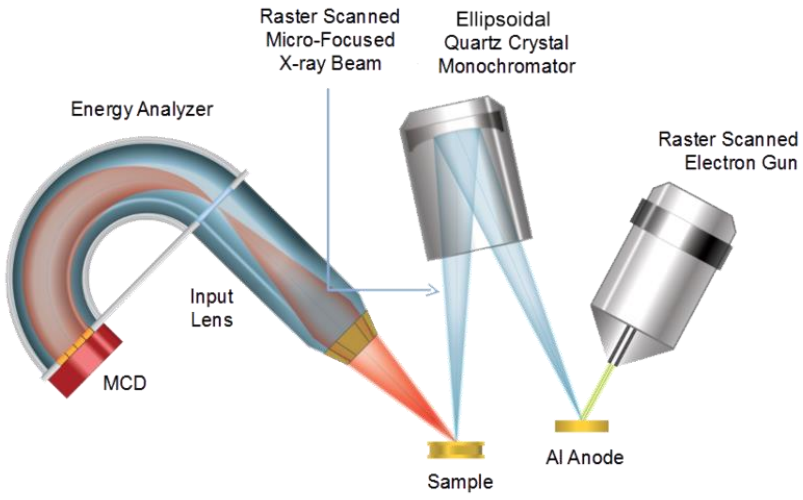

Figure 5.2: Illustration of the setup for XPS measurement.

5.4 Characterization of Solar Cells' Performance

To compare the performance of the perovskite solar cells with Au electrodes fabricated by different methods, perovskite solar cells with the transfer-printed and thermally evaporated Au electrodes were fabricated in the same batch. All the fabrication processes of the perovskite solar cells were the same except the method of depositing the Au top electrodes. Figure 5.3 shows the J-V characteristics of the perovskite solar cells with transfer-printed and thermally evaporated Au electrodes under reverse voltage sweep direction. The detailed photovoltaic parameters are summarized and shown in the Table 5.1. As shown in Table 5.1, the highest PCE of the perovskite solar cells with the transfer-printed Au electrodes is 13.72% which is slightly higher than that of the perovskite solar cells with the thermally evaporated Au electrodes, 13.02%. The perovskite solar cells with either transfer-printed or thermally evaporated Au electrodes exhibit hysteresis effects as shown in Table 5.1. The average PCEs (obtained from at least 24 cells) of the perovskite solar cells with transfer-printed Au electrodes are 11.01% and 13.18% under forward and reverse voltage sweep directions. The average PCEs of the perovskite solar cells with thermally evaporated Au electrodes are 10.26% and 12.18% under forward and reverse voltage sweep directions. Since the hysteresis effects exist in all the perovskite solar cells, it should be caused by other factors rather than using the transfer printing process. The better performance of perovskite solar cells by transfer printing method mainly comes from the slightly higher V_{oc} and J_{sc} which might be a result of better interface properties between Au and Spiro-OMeTAD. Besides, we have observed that the shunt resistance, R_{sh}, of the thermally evaporated devices is smaller than that of the transfer printed devices. The R_{sh} was calculated from the reciprocal value of the J-V curves'

slope near V=0. After analyzing the J-V curves of all the 24 cells, the average R_{sh} of the thermally evaporated and transfer printed devices are received $1838.33 \pm 274.54\ \Omega cm^2$ and $2634.45 \pm 564.22\ \Omega cm^2$, respectively. In agreement with the smaller R_{sh}, the perovskite solar cells with thermally evaporated Au also have smaller average FF. The average FF of the perovskite solar cells with thermally evaporated Au is 0.61 which is lower than that of the perovskite solar cells with transfer-printed Au, 0.62. The smaller R_{sh} and FF of the thermally evaporated devices indicate that the thermal evaporation process might introduce excess metal penetration into the Spiro-OMeTAD layer and increased leakage current of the perovskite solar cells.

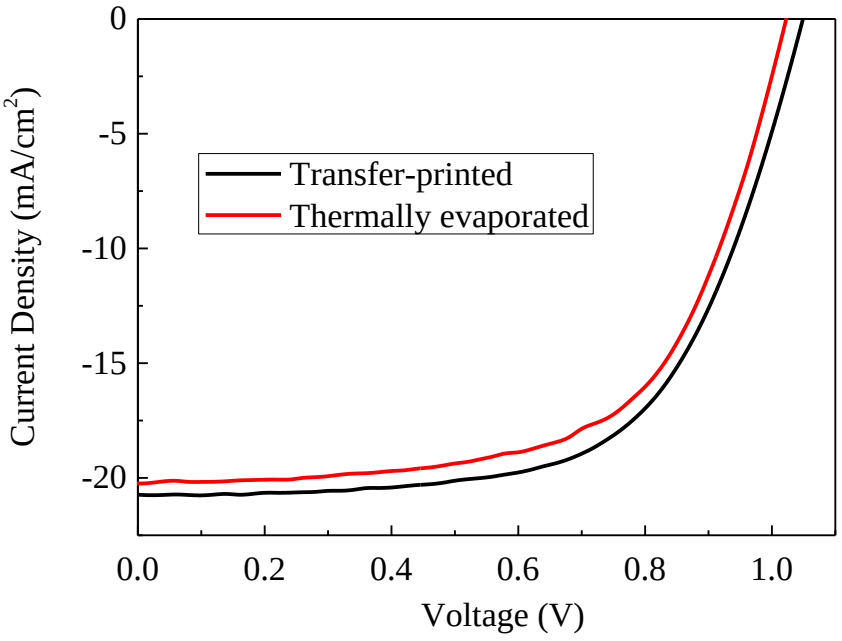

Figure 5.3: J-V characteristics perovskite solar cells with transfer-printed or thermally evaporated Au electrodes under reverse voltage sweep direction.

Figure 5.4 shows the EQE spectrum of the perovskite solar cells with transfer-printed and thermally evaporated Au electrodes. The short circuit

current density, J_{sc}, calculated from the measured EQE spectrum is 19.17 mA/cm^2 for the transfer-printed perovskite solar cells and 19.29 mA/cm^2 for thermally evaporated perovskite solar cells. The J_{sc} obtained from the EQE spectrum are in good agreement with those obtained from the measured J-V characteristics of the devices. The similar EQE spectrum of the perovskite solar cells with transfer-printed and thermally evaporated Au electrodes demonstrate that the method of deposition of Au electrodes didn't influence the generated and collected photocurrent.

Table 5.1: Photovoltaic parameters of the perovskite solar cells with transfer-printed and thermally evaporated Au electrodes.

Sample	Voltage sweep direction	V_{oc} (V)	J_{sc} (mA/cm^2)	FF	PCE (%) Best	PCE (%) Average*
Transfer-printed	Forward	1.03	20.96	0.53	11.44	11.01±0.52
	Reverse	1.05	20.74	0.63	13.72	13.18±0.48
Thermally evaporated	Forward	0.99	20.32	0.53	10.66	10.26±0.77
	Reverse	1.02	20.26	0.63	13.02	12.18±0.63

*The average PCE is obtained from at least 24 cells

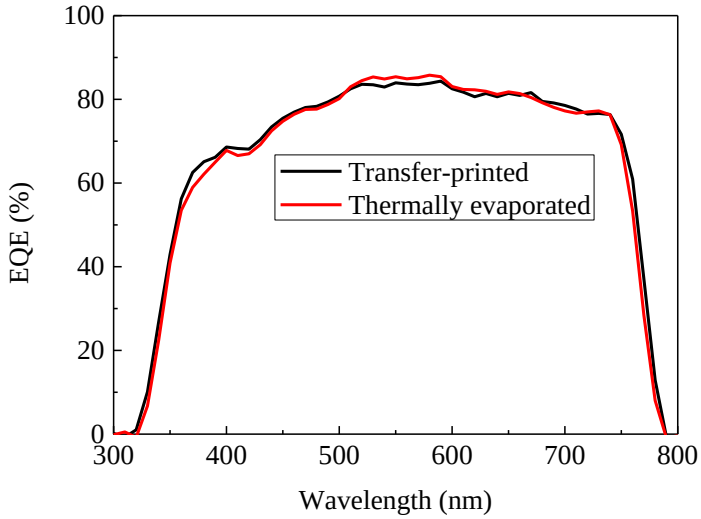

Figure 5.4: EQE spectrum of perovskite solar cells with transfer printed and thermally evaporated Au electrodes.

To evaluate the reproducibility of the transfer printing method, we fabricated at least 24 devices for each Au deposition method and the devices' performance was summarized in Figure 5.5. It is obvious that the perovskite solar cells by the transfer printing method have better performance with an average PCE of 13.18%, while the perovskite solar cells with the thermally evaporated Au have an average PCE of 12.18%. The PCE variation range of the perovskite solar cells with transfer-printed Au electrodes is within 1% indicating that the transfer-printing method for depositing Au electrodes is reproducible. These results suggest that good perovskite solar cells can be fabricated by simple transfer printing method without using vacuum process.

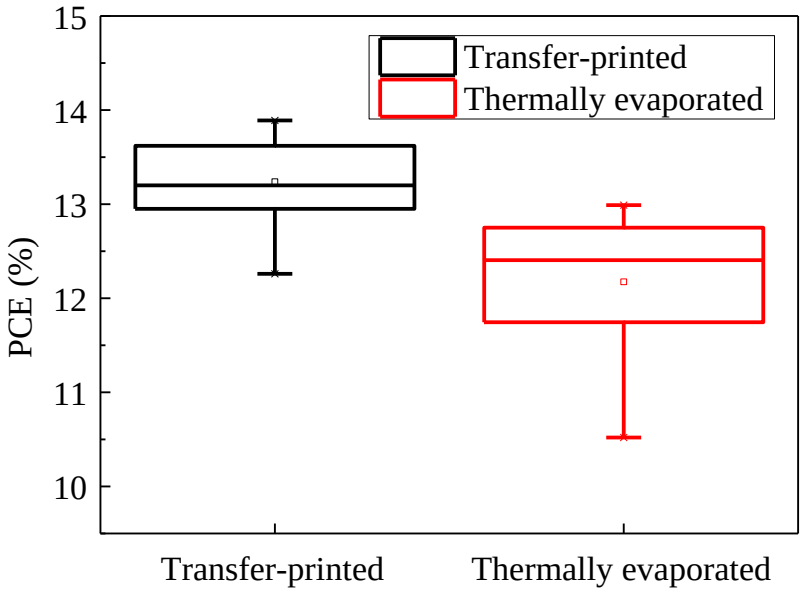

Figure 5.5: PCE variation range of perovskite solar cells with transfer-printed and thermally evaporated Au electrodes obtained from at least 24 devices.

To explore the universality of the transfer printing method, we used the transfer printing method to deposit the Au electrodes of the organic solar cells with a structure of ITO/ZnO/P3HT:$PC_{60}BM$/PEDOT:PSS/Au. Figure 5.6 (a) shows the J-V characteristics the organic solar cells with the transfer-printed and thermally evaporated Au electrodes fabricated in the same batch. The detailed photovoltaic parameters of the organic solar cells are shown in Table 5.2. The organic solar cells with transfer-printed Au electrodes have the highest PCE of 2.35% which is comparable with the highest PCE of the organic solar cells with the thermally evaporated Au electrodes, 2.49%. The average PCE of the organic solar cells was obtained from at least 6 cells. The organic solar cells with transfer-printed Au electrodes exhibit an average PCE of 2.21% which is slightly lower than that of the organic solar cells with thermally evaporated Au

electrodes, 2.31%. The J_{sc} of the organic solar cells was calibrated and in agreement with the EQE measurement as shown in Fig 5.6 (b). Similar to our observation in perovskite solar cells fabrication, the organic solar cells with transfer-printed Au electrodes also have a slightly higher V_{oc}, 0.60 V than the V_{oc} of organic solar cells with thermally evaporated electrodes, 0.59 V. Besides, the FF of the organic solar cells with transfer-printed Au electrodes is higher than that of the organic solar cells with thermally evaporated Au electrodes. These results indicate that the transfer-printing method can also be used for fabricating the P3HT based organic solar cells with good photovoltaic performance.

Table 5.2: Photovoltaic parameters of organic solar cells with transfer-printed and thermally evaporated Au electrodes.

Sample	V_{oc} (V)	J_{sc} (mA/cm^2)	FF	PCE (%) Average*	PCE (%) Best
Transfer-printed	0.60	7.24	0.54	2.21±0.08	2.35
Thermally evaporated	0.59	7.92	0.53	2.31±0.12	2.49

*The average PCE is obtained from at least 6 cells

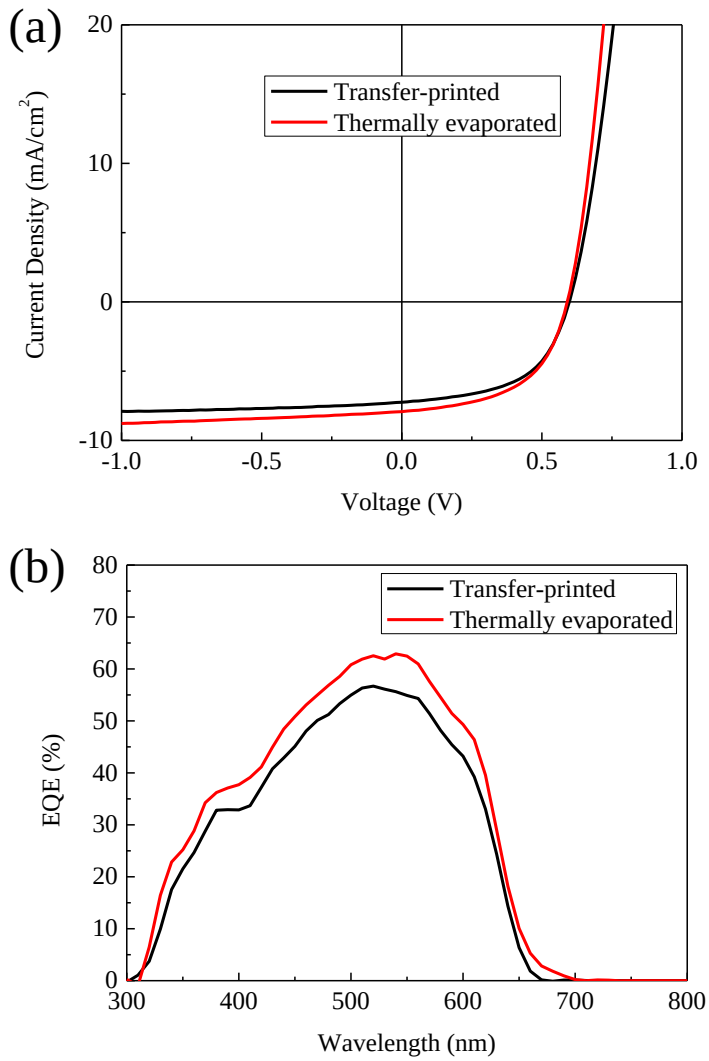

Figure 5.6: (a) J-V characteristics of organic solar cells with transfer-printed and thermally evaporated Au top electrodes. (b) EQE results of organic solar cells with transfer printed and thermally evaporated Au electrodes.

5.5 Study of Au Atoms in the Interfacial Layers of Perovskite Solar Cells and Organic Solar Cells

We have proposed that using the transfer printing method to deposit the top Au

electrodes can suppress the Au atoms diffusion into the Spiro-OMeTAD layer. As a result, the interface between the Spiro-OMeTAD layer and transfer-printed Au electrodes should have better charge carrier transport properties. To investigate the charge carrier transport between the Spiro-OMeTAD and Au electrode, we prepared the hole-only devices with a structure of ITO/PEDOT:PSS/Spiro-OMeTAD/Au. The Au electrodes of the structures were deposited by using transfer printing method and thermal evaporating method. A PEDOT:PSS layer was inserted between the ITO and Spiro-OMeTAD to block the electron injection from ITO. Figure 5.7 shows the measured J-V characteristics of the hole-only devices with the transfer printed Au electrode and thermally evaporated Au electrode, respectively. The space-charge-limited-current (SCLC) model was used to calculate the hole mobility in this hole-only device at low voltage As shown in Figure 5.7, the hole-only device with the transfer-printed Au electrode has higher hole mobility ($\mu_h = 2.05 \times 10^{-4} cm^2 V^{-1} s^{-1}$). The hole mobility of the hole-only device with the thermally evaporated Au electrode is one order lower ($\mu_h = 2.49 \times 10^{-5} cm^2 V^{-1} s^{-1}$). These results indicate that the interface between the Spiro-OMeTAD and transfer-printed Au electrode is better for facilitating hole transport. It has been reported that the thermally evaporated electrode metals could penetrate into the organic layer and introduce defects and shunt paths [284, 285]. So the increased hole-mobility in the hole-only device with transfer-printed Au electrodes should be because of less defects between the Spiro-OMeTAD and Au electrode interface [314]. The better performance of the perovskite solar cells with transfer-printed Au electrodes could be caused by the less defects and better charge carrier transport properties of the interface between the Spiro-OMeTAD and Au layers.

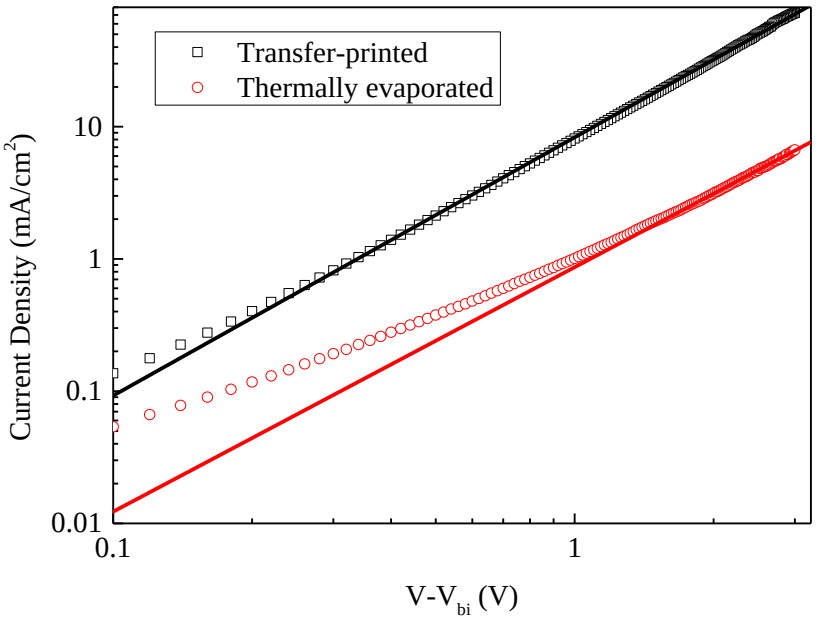

Figure 5.7: J-V characteristics of the hole-only devices based on Spiro-OMeTAD (FTO/PEDOT:PSS/Spiro-OMeTAD/Au) with transfer-printed and thermally evaporated Au electrodes in dark condition.

We also conducted the SCLC analysis to examine the charge carrier transport properties in the organic solar cells. The J-V characteristics of the hole-only devices with a structure of ITO/PEDOT:PSS/P3HT:$PC_{60}BM$/PEDOT:PSS/Au are shown in the Figure 5.8. The P3HT:$PC_{60}BM$ layer was sandwiched between two PEDOT:PSS layers. So the electrons injection into the device can be effectively blocked. Through SCLC analysis we found that the hole mobility of the hole-only device with transfer printed and thermally evaporated Au electrodes is $6.97 \times 10^{-4} cm^2 V^{-1} s^{-1}$ and $5.18 \times 10^{-4} cm^2 V^{-1} s^{-1}$ respectively. The hole mobility of the hole-only device with transfer-printed Au is slightly higher and can be considered comparable with the hole mobility of the hole-only device with thermally evaporated Au. The small difference between the mobility of the hole-only device with transfer printed and

thermally evaporated Au might be due to the uncertainty from the film's thickness measurement [315]. These results are consistent with the photovoltaic performance measurement results that the organic solar cells with transfer-printed and thermally evaporated Au electrodes have comparable photovoltaic performance.

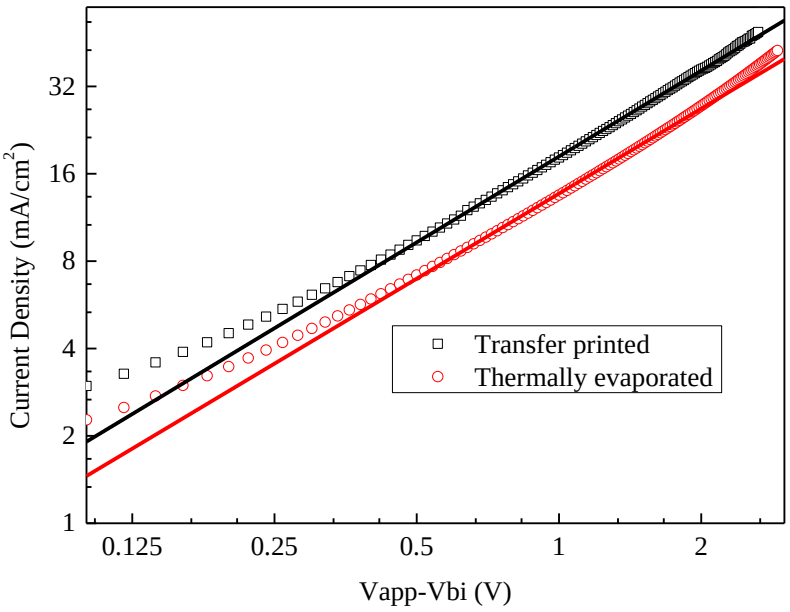

Figure 5.8: J-V characteristics of the hole-only devices based on P3HT (ITO/PEDOT:PSS/P3HT:PC_{60}BM/PEDOT:PSS/Au) with transfer-printed and thermally evaporated Au electrodes in dark condition.

To further investigate the Au atoms penetrated into the Spiro-OMeTAD layer of the structure, XPS measurement was conducted on the thermally evaporated Au of the Spiro-OMeTAD sample and the sample with the transfer-printed Au electrodes were prepared under the same conditions. To carry out the XPS measurement, the Au electrodes of the samples were peeled off by using Kapton tape to expose the Spiro-OMeTAD surface. Then, the residues of Au atoms in the Spiro-OMeTAD layer were detected by using XPS measurement. Figure 5.9

(a), (b) show the XPS spectra of the sample with the thermally evaporated Au and (c), (d) show the XPS spectra of the sample with the transfer printed Au electrode. The Au 4f spectra indicate that Au atoms exist in the two Spiro-OMeTAD samples after peeling off the deposited Au electrodes. These Au residues should be introduced by the Au atoms diffusion during the thermally evaporating or transfer printing process. Compare the Figure 5.9 (a) and (c), we can see that the sample prepared by thermal evaporation of Au has pronounced Au 4f peaks with higher intensity and the Au 4f 5/2 and 7/2 peaks can be clearly distinguished. On the other hand, the Au 4f peak intensity of the sample prepared by the transfer printing method is lower and the Au 4f 5/2 and 7/2 peaks are less distinguishable. As shown in the high-resolution Au XPS spectra (Figure 5.9 (a), (c)), the binding energy of Au 4f 5/2 and 7/2 photoelectrons for thermal evaporating method was shifted toward a lager value compared with that of transfer printing method. This shift to high binding energy should be caused by the less effective core hole screening of the metal clusters with smaller size in the sample with the thermally evaporated Au [316-318]. In the thermal evaporation process, Au atoms have higher kinetic energy thus penetrating into the Spiro-OMeTAD film deeper and dispersing quickly. So, these Au atoms have less chance to aggregate. The Au clusters formed in the Spiro-OMeTAD film have smaller size. While for the transfer printing Au sample, the Au atoms diffused into the Spiro-OMeTAD film aggregate at the surface of Spiro-OMeTAD to form Au cluster with larger size. Besides, we have noticed that there is a small peak at the binding energy of 91 eV in the Figure 5.9 (a), but this peak is not observed in Figure 5.9 (c). This peak could be attributed to Au 4f 5/2 in the formula of $[(C_4H_9)_4N][AuBr_4]$. The iodine migration from the perovskite layer to the interface between the Spiro-OMeTAD and Au electrodes in the perovskite solar cells has been

reported recently [319]. So, we suspect that the Au and Br compounds might be caused by bromine migrating to the interface between Spiro-OMeTAD and Au electrodes. Some of the Br atoms might react with the Au on the surface of the Spiro-OMeTAD. Due to the Au diffusion caused by the thermally evaporation process, some of the Au and Br compounds should locate inside the Spiro-OMeTAD layer and cannot be completely removed by the Kapton tape. So the residues of Au and Br compounds were detected in the XPS measurement. In the transfer printing process, less Au atoms diffused into the Spiro-OMeTAD layer. The Au atoms or the compounds of Au and Br should only exist at the surface of Spiro-OMeTAD. So the Au and Br compounds can be completely removed by the Kapton tape. As a result, there is no peak at the binding energy of 91 eV in Figure 5.9 (c). This finding can support that the transfer printing method introduced less diffused Au atoms into the Spiro-OMeTAD layer than the thermally evaporating method. To compare the amount of Au residues in the samples, O 1s spectra was measured and shown in Figure 5.9 (b) and (d) for calculation of atomic ratio of Au and O. The atomic ratio of Au and O is 0.11:99.89 for the Spiro-OMeTAD with thermally evaporated Au electrodes, while the atomic ratio of Au and O is 0.09:99.91 for the Spiro-OMeTAD with transfer-printed Au electrodes. Less Au atoms diffused into the Spiro-OMeTAD with the transfer printing method. The XPS measurement results indicate that the interfacial defects between Spiro-OMeTAD and transfer-printed Au electrodes induced by diffused Au atoms is suppressed. Diffused Au atoms inside the Spiro-OMeTAD layer with both the thermally evaporated and transfer-printed Au samples have been measured by using secondary ion mass spectroscopy measurement. As shown in Figure 5.10, significant signal of Au atoms was detected in the Spiro-OMeTAD layer of the sample with the thermally evaporated Au. For the sample with the

transfer-printed Au electrode, almost no Au signal was detected inside the Spiro-OMeTAD layer. The more Au atoms inside the Spiro-OMeTAD layer with thermally evaporated Au can act as defects and recombination center, thus leading to lower hole mobility of the hole-only devices and the slightly lower V_{oc}, J_{sc} and FF of the perovskite solar cells.

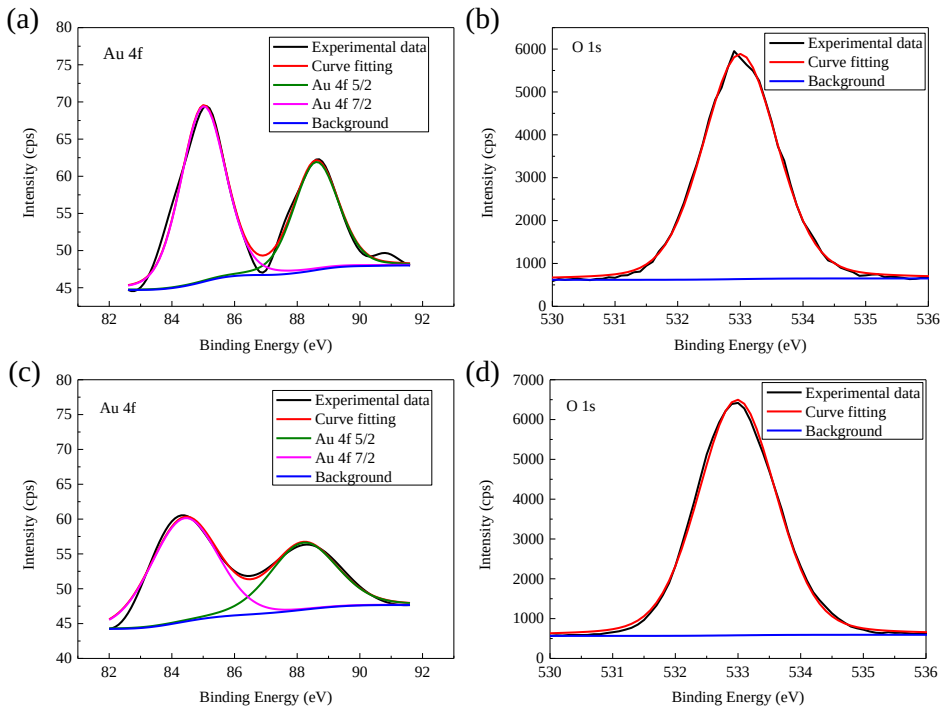

Figure 5.9: XPS spectra of Spiro-OMeTAD film with (a,b) thermally evaporated and (c,d) transfer-printed Au peeled off by Kapton tape.

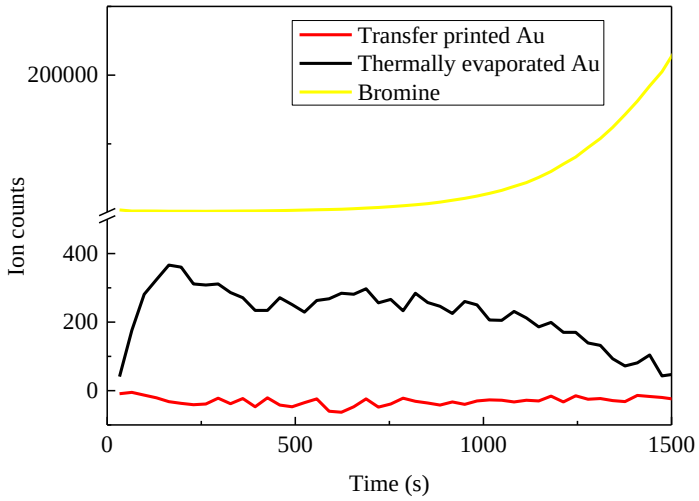

Figure 5.10: Secondary ion mass spectroscopy results: depth profiling of diffused Au atoms in Spiro-OMeTAD layer.

5.6 Stability Study of the Perovskite Solar Cells and Organic Solar Cells with the Transfer-printed Au Electrodes

According to the SCLC analysis and XPS measurement, thermal evaporating method introduced more diffused Au atoms into the Spiro-OMeTAD films than the transfer printing method. As mentioned before, thermally evaporated metal electrodes might penetrate into organic thin films and lead to poor device stability [286, 287]. So with less defects, the devices with transfer-printed electrodes might have better stability than the devices with thermally evaporated electrodes. To compare the stability of the perovskite solar cells with the Au electrode deposited using different methods, we stored the fabricated perovskite solar cells with the transfer-printed and thermally evaporated Au electrodes in a N_2 filled glovebox in dark condition without encapsulation for more than three months. The performance of the devices was measured during

the store period. Figure 5.11 shows the normalized PCE of the perovskite solar cells as a function of storing days. After storing for 97 days, the PCE of the perovskite solar cells with the transfer-printed Au electrode and thermally evaporated electrode decreased to 71% and 48% of their initial PCEs, respectively. Since the only difference between the two perovskite solar cells is the deposition method of the top Au electrodes, the slower degradation of the perovskite solar cells with the transfer-printed Au electrodes should result from less interfacial defects. The superior stability of the perovskite solar cells with transfer-printed Au electrodes indicates that the transfer printing method can be applied into fabrication of highly stable perovskite solar cells.

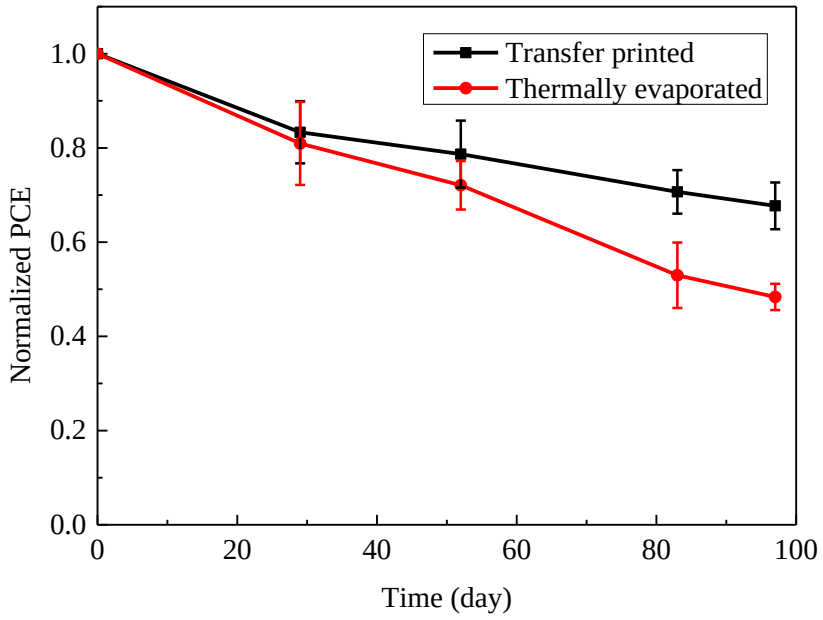

Figure 5.11: Normalized PCE of perovskite solar cells with transfer printed or thermally evaporated Au electrodes measured in a period of 97 days.

We also examined the stability of organic solar cells with transfer-printed Au electrode. The organic solar cells by transfer printing method also showed

excellent stability: after storing in N_2 filled glovebox in dark conditions without encapsulation for 103 days, the organic solar cells still remained 91% of the original PCE as shown in Fig 5.12 and Table 5.3. The J-V characteristics of the organic solar cells with transfer-printed Au top electrodes remained almost the same shape after storing for 103 days as shown in Figure 5.12 (a). From the EQE shown in Figure 5.12 (b), we observed that the EQE of organic solar cells retained almost the same. These results indicate that the transfer printing method can be applied not only in perovskite solar cells on Spiro-OMeTAD but also in organic solar cells on PEDOT:PSS. Both perovskite solar cells and organic solar cells fabricated by transfer printing method have good performance and stability demonstrating the universality of the transfer printing method.

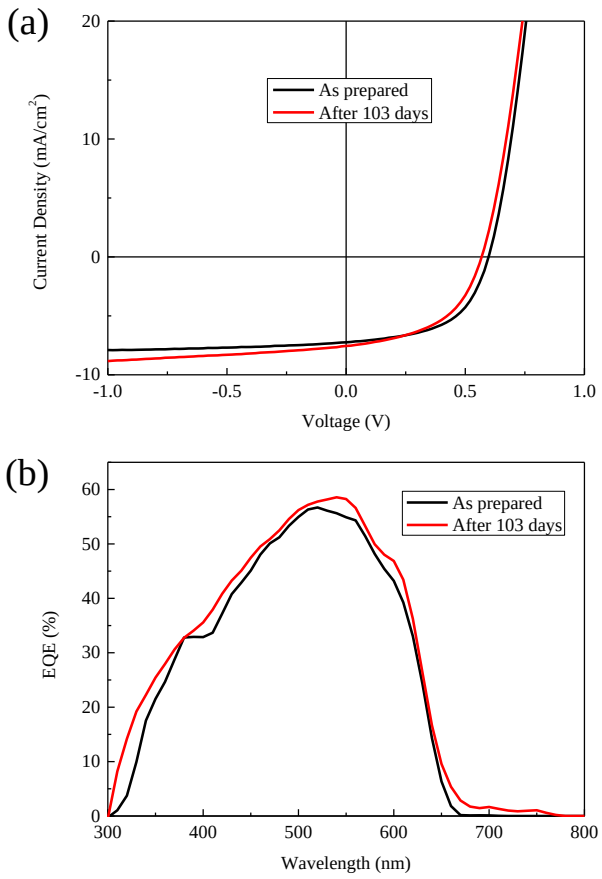

Figure 5.12: J-V characteristics (a) and EQE (b) of organic solar cells with transfer- printed Au top electrodes measured immediately after fabrication and 103 days stored in N_2 filled glovebox.

Table 5.3: Photovoltaics parameters of organic solar cells with transfer-printed Au electrodes measured after 103 days.

Sample	V_{oc} (V)	J_{sc} (mA/cm^2)	FF	PCE (%)
As-prepared	0.60	7.24	0.54	2.35
After 103 days	0.57	7.55	0.50	2.14

5.7 Conclusion

In summary, transfer-printed Au electrodes of the perovskite solar cells and

organic solar cells have been developed and investigated. perovskite solar cells with the transfer-printed Au electrodes exhibited a highest PCE of 13.72% which was higher than the highest PCE of the control devices with the thermally evaporated Au electrodes. From the SCLC analysis, we found that the hole mobility of the hole-only device with the transfer-printed Au electrodes is higher than that of the hole-only device with the thermally evaporated Au electrodes. According to XPS measurement, less Au atoms diffused into the Spiro-OMeTAD films with the transfer printing Au electrode process. As a result, the perovskite solar cells with the transfer-printed Au electrodes had better stability. It was measured that the transfer-printed Au electrodes PSCs retained 71% of the original PCE after storing the devices in glovebox in dark condition without encapsulation for 97 days. While the PCE of the perovskite solar cells with thermally evaporated Au electrodes decreased to only 48% of their original values. We also applied the transfer printing method into fabrication of organic solar cells based on P3HT and $PC_{60}BM$. The organic solar cells with transfer-printed Au electrodes have a comparable PCE (2.35%) with that of the organic solar cells with thermally evaporated Au electrodes (2.49%). The organic solar cells fabricated by transfer printing method also have excellent stability retaining 91% of the original PCE after storing for 103 days. With fabricating good performance perovskite solar cells and organic solar cells, transfer printing method is suitable for depositing metal electrodes on organic thin films in perovskite solar cells and organic solar cells. Our findings demonstrate that the electrode transfer printing method is a potential candidate for future manufacturing of perovskite solar cells and organic solar cells due to its high performance, simple processibility in different surfaces. Further work will focus on applying our technique with transfer electrode on flexible devices or the higher performance solar cells.

Chapter 5 Fully Printable Organic and Perovskite Solar Cells with Transfer-printed Flexible Electrodes

Chapter 6 Conclusion and Future Work

6.1 Conclusion

In this project, techniques for development of highly efficient and stable organic and perovskite solar cells through the interfacial material engineering of the device structures and novel fabrication techniques have been studied. Different low temperature processed polymer electron transporting and hole transporting interfacial materials have been applied to the organic solar cells and perovskite solar cells device structures to improve their performance and stability. We also investigated the fundamentals of the interfacial materials to propose guidelines for developing more high performance and stable interfacial materials in the future. A transfer printing technique for developing fully printable organic solar cells and perovskite solar cells has been developed and investigated.

In chapter three, a novel electron transporting layer (ETL) for fabrication of high performance organic solar cells with good stability and low costs is reported. The newly synthesized n-type conjugated polyelectrolyte, PFBD, was used as the ETL of the organic solar cells. The organic solar cells with the PFBD ETL achieved the highest PCE of 7.21% which is comparable with that of the organic solar cells with the conventionally used PFN ETL. The PCE of the organic solar cells with PFBD ETL keeps almost same after 26 days, which shows the improved stability. The so-called light-soaking effect was observed from the PFBD ETL organic solar cells, in which the device's PCE was observed increased with the solar illumination time. This was not observed in the organic solar cells with PFN ETL. This light-soaking effect of the organic

solar cells can be eliminated by using a pre-UV light treatment of the PFBD ETL layer during the device fabrication. With the pre-UV treatment, performance of the organic solar cells kept unchanged during the operation. It has been investigated that the polymer backbone of PFBD ETL plays an important role in influencing the organic solar cells' performance. Under UV illumination, the work function of ITO/PFBD was reduced from 5.2 eV to 4.6 eV, thus enabling more efficient charge carrier transfer from the LUMO level of $PC_{71}BM$ to ITO electrode. As a result, the UV illumination reduces series resistance of the PFBD ETL based organic solar cells. The influence of UV light was found to be on the polymer backbone of PFBD, the benzoxadiazole (BD) unites in particular. Under UV illumination, the BD units in the polymer backbone of PFBD breaks and the resulted PFBD ETL enables more efficient charge carrier transfer from the active layer to ITO electrode.

In chapter four, the new p-type polymers as the hole transporting layers (HTLs) for perovskite solar cells have been studied. Compared to commonly used other polymer or small molecular HTLs, the dopant-free polymer HTLs based perovskite solar cells we have developed show good performance with a high PCE and good stability. The highest PCE of the new polymer HTL perovskite solar cells reached 14.02%. The average PCE of more than 20 devices fabricated was calculated of 13.03%, demonstrating the reproducible of the new HTL perovskite solar cells. Excellent stability of the new polymer HTL based perovskite solar cells has been received. With the new polymer HTL, Jl-2-38, the perovskite solar cell's PCE was measured retained 80% of the original value after stored it in a N_2 filled glovebox for 113 days. The better performance of the perovskite solar cells with the Jl-2-38 HTL was attributed to the good charge carrier extraction ability of the Jl-2-38 HTL.

In chapter five, a transfer printing technique for depositing Au top electrodes of organic solar cells and perovskite solar cells has been developed and investigated. Compared with the traditional thermally evaporated Au electrode of the perovskite solar cell, better performance of the perovskite solar cell with the transfer-printed Au electrode has been received. The highest PCE of the transfer printed Au perovskite solar cells reached 13.72%. The perovskite solar cells with the transfer printed Au electrode are also more stable than the perovskite solar cells with the thermal evaporated Au electrode. The better performance of the perovskite solar cells with the transfer-printed Au electrode was investigated coming from less Au atoms diffused into the HTL layer of the device through the SCLC analysis and XPS measurement. This transfer printing technique can also be applied to organic solar cells. P3HT based organic solar cells by transfer printing technique demonstrated a highest PCE of 2.35% and excellent stability that 91% of the original PCE stilled remained after storing in N_2 filled glovebox for 103 days.

In chapter five, instead of improving the solar cells' performance by applying novel interfacial materials, we developed and demonstrated a novel low-cost transfer printing technique for deposition of top metal electrodes in organic solar cells and perovskite solar cells. Compared with the traditional thermally evaporating method, the transfer printing method can enable printable solar cells and reduce the diffused Au atoms into the Spiro-OMeTAD layer. A highest PCE of 13.72% of perovskite solar cells was achieved by using the transfer printing method. The performance of perovskite solar cells with transfer-printed Au electrodes is better than that of perovskite solar cells with thermally evaporated Au electrodes. The stability of perovskite solar cells by transfer printing method is also better that the PCE still retained 71% of the initial PCE

after storing in N_2 environment for 97 days without any encapsulation. The better performance and stability of perovskite solar cells by transfer printing method was demonstrated to come from less diffused Au atoms through SCLC analysis and XPS measurement. This transfer printing technique can also be applied to organic solar cells. P3HT-based organic solar cells by transfer printing technique demonstrated a highest PCE of 2.35% and excellent stability that 91% of the original PCE stilled remained after storing in N_2 filled glovebox for 103 days.

In summary, we have successfully improved the performance and stability of organic solar cells and perovskite solar cells through applying novel interfacial materials and electrode deposition techniques. Through this study, we have demonstrated that the polymer interfacial materials are promising candidates for achieving highly efficient, stable and cheap organic solar cells and perovskite solar cells. Besides, the traditional deposition techniques are replaced by a transfer printing technique which can reduce the metal penetration into the thin organic interfacial layers to improve the performance and stability of organic solar cells and perovskite solar cells. Despite some successes have been achieved, there is still some room for the interfacial materials and transfer printing techniques used in this study to be improved.

6.2 Recommendation for Future Research

The present research work can be further investigated and improved from the following aspects in the future.

6.2.1 Molecular Modification of the PFBD ETL

We have already demonstrated that the polymer ETL interfacial material, PFBD, for high performance organic solar cells. We found that the benzoxadiazole (BD) units of the polymer backbone might be broken down by UV irradiation to improve the light-soaking effects when use it in organic solar cells applications. To further improve the polymer PFBD in organic solar cells application, the backbone of PFBD must be modified. The poor UV stability of BD units can be solved by using other acceptor units or modifying the side chain of PFBD.

6.2.2 Incorporation of Metal Nanoparticles into Interfacial Materials

In the chapter 3, we have presented that the optimizated thickness of PFBD was only 2 nm, which is too thin to be produced in large areas. This very thin optimized thickness should be due to the low conductivity of PFBD. In order to increase the optimized layer thickness, the conductivity of PFBD should be increased, which can be solved by re-design the molecular structure. Another straightforward method is to incorporate metal nanoparticles into the PFBD ETL. Besides improve the ETL's conductivity, metal nanoparticles could induce surface plasmonic resonance to enhance the absorption of the photoactive layer [320, 321].

6.2.3 Study the Polymer HTLs' Chains Orientation on Perovskite Layer

It has been investigated that the crystallinity of the polymer HTLs greatly affects perovskite solar cells' performance of perovskite solar cells. But how the

orientation of polymer chains influences the performance is still not clear. The crystallinity of polymer is related to the polymer chains' orientation [259, 260]. It has been widely reported that the orientations of the polymer chains can influence the charge carrier transport properties [265], but reports on how the polymer chain orientation influences performance of perovskite solar cells are rare. Investigating the influence of polymer chain orientation on the perovskite solar cells' performance can provide researchers in chemistry or materials area with guidelines of synthesizing polymer HTLs with better performance.

6.2.4 To Transfer Print Solution-processed Materials for Top Electrodes

We have developed highly efficient and stable perovskite solar cells and organic solar cells using the transfer-printed Au electrodes. But the thermally evaporating process is still needed to deposit the Au electrodes on the PDMS first. To completely avoid the thermally evaporating process, we are trying to use solution-processed Au nanoparticles incorporated into conductive polymers, such as PEDOT:PSS, to replace the Au film [305, 322, 323]. The Au nanoparticles and conductive polymers can be deposited on PDMS by spin coating so the thermally evaporating process is completely avoided. But we cannot find suitable Au nanoparticle ink with high conductivity and capability of being low temperature processed for our transfer printing process so far. In the future, we will try to find or synthesize Au nanoparticle ink that has high conductivity and can be solution processed at low temperature. The advantage of this transfer printing technique is that the solvents of the Au nanoparticles and the underlying interfacial materials don't need to be orthogonal because the Au nanoparticles used in the transfer printing process are dry.

6.2.5 Fabricate Large-area Organic Solar Cells and Perovskite Solar Cells by Transfer Printing Method

The advantages of using transfer printing method for fabrication of large-area organic solar cells and perovskite solar cells are summarized as follows:

1. Using the traditional E-beam or thermally evaporating method to deposit the metal electrodes of perovskite solar cells or organic solar cells, the size of device is limited by the size of the chamber of evaporator. With increasing the fabricated device's size, the chamber of evaporator also needs to be increased. As a result, the time for pumping down will also be increased and the productivity will decrease.

2. In the process of depositing Au electrodes by E-beam or thermal evaporator, defects caused by diffusion Au atoms will be produced. With increasing the area of perovskite solar cells, the influence of these defects will accumulate. Besides, the variation of the thickness of Au electrodes on large-area perovskite solar cells deposited by E-beam or thermal evaporator is large. Using the transfer printing method will introduce fewer defects and the uniformity of Au electrodes is better.

To solve the above problems of using thermal evaporator to deposit electrodes, we will apply our transfer printing method into large-area fabrication of organic solar cells and perovskite solar cells. In the future, we will try to fabricate perovskite solar cells and organic solar cells with an active area of at least more than 5 cm^2. The Au nanoparticles and conductive polymers composite electrodes will be prepared by spin coating or blade coating on the PDMS substrates. Then the solution processed electrodes will be transfer printed on the device to be fabricated. A plastic rod can be used to roll over the PDMS to

uniformly laminate the PDMS sample on the device. In this way, large-area perovskite solar cells and organic solar cells can be fabricated without vacuum deposition of metal electrodes.

Author's publications

Journal Publications as 1st author

1. Xianqiang Li, Xiaohong Tang, Tao Ye, Dan Wu, Hong Wang, Xizu Wang, Jun Li, "A dopant-free polymer as hole-transporting material for highly efficient and stable perovskite solar cells", (submitted to ***ACS Applied Materials & Interfaces***).

2. **Xianqiang Li**, Xiaohong Tang, Tao Ye, Dan Wu, Hong Wang, Xizu Wang, "Fully printable organic and perovskite solar cells with transfer-printed flexible electrodes", ***ACS Applied Materials & Interfaces***, vol 9, pp. 18730−18738, 2017.

3. **Xianqiang Li**, Xiaohong Tang, Fei Wang, Vijila Chellappan, Tjiu Weng Weei, Shifeng Guo, Hong Wang, Dan Wu, Jun Li, "Investigations of a New High-Performance Low-Band-Gap Photovoltaic Polymer Semiconductor", ***IEEE Journal of Photovoltaics***, vol 6, pp. 696-704, 2016.

4. **Xianqiang Li**, Jie Liu, Xiaohong Tang, Shifeng Guo, Jun Li, Hong Wang, Bin Liu, Wei Lin Leong, "Improvement in polymer solar cell performance and eliminating light soaking effect via UV-light treatment on conjugated polyelectrolyte interlayer", ***Organic Electronics***, vol 25, pp. 105-111, 2015.

Conference Presentations as 1st author

5. **Xianqiang Li**, Tao Ye, Xizu Wang, Xiaohong Tang, "Highly Efficient IR Transparent Perovskite Solar Cells", Conference on Lasers and Electro-Optics (CLEO), San Jose, California, United States, 2017.

6. **Xianqiang Li**, Xiaohong Tang, Xizu Wang, Dan Wu, Jun Li, "Enhanced open circuit voltage and efficiency of the organic solar cells using a newly synthesized polymer donor", Hybrid and Organic Photovoltaics (HOPV), Swansea, United Kingdom, 2016.

7. **Xianqiang Li**, Jun Li, Hong Wang, Dan Wu, Xiaohong Tang, "The Effects of Molecular Weight of a New Hole Transporting Polymer on the Organic Solar Cells", International Conference on Materials for Advanced Technologies (ICMAT), Singapore, 2015.

Publications as co-author

8. Dan Wu, Xiaohong Tang, Kai Wang, **Xianqiang Li**, "An Analytic Approach for Optimal Geometrical Design of GaAs Nanowires for Maximal Light Harvesting in Photovoltaic Cells", ***Scientific Reports***, vol 7, pp. 46504, 2017.

9. Dan Wu, Xiaohong Tang, Kai Wang, **Xianqiang Li**, "Effective coupled optoelectrical design method for fully infiltrated semiconductor nanowires based hybrid solar cells", ***Optics Express***, vol 24, pp. A1336-A1348, 2016.

10. Dan Wu, Xiaohong Tang, Kai Wang, Aurelien Olivier, **Xianqiang Li**, "Parameters study on the growth of GaAs nanowires on indium tin oxide by

metal-organic chemical vapor deposition", ***Journal of Applied Physics***, vol 119, pp. 094305, 2016.

11. Dan Wu, Xiaohong Tang, Ho Sup Yoon, Kai Wang, Aurelien Olivier, **Xianqiang Li**, "MOCVD Growth of High-Quality and Density-Tunable GaAs Nanowires on ITO Catalyzed by Au Nanoparticles Deposited by Centrifugation", ***Nanorganic solar cellale research letters***, vol 10, pp. 1, 2015.

12. Dan Wu, Xiaohong Tang, **Xianqiang Li**, "Optimization of the Nanowire Size and Distribution of Compound Semiconductor Nanowire-Based Hybrid Solar Cells", ***IEEE Journal of Photovoltaics***, vol 5, pp. 1395-1401, 2015.

13. Dan Wu, Xiaohong Tang, Aurelien Olivier, **Xianqiang Li**, "Free-standing GaAs nanowires growth on ITO glass by MOCVD", ***Materials Research Express***, vol 2, pp. 045002, 2015.

Bibliography

[1] I. E. A. (IEA), "Key World Energy Statistics 2016," ed, 2016.

[2] E. Dlugokencky and P. Tans. (2016). Available: www.esrl.noaa.gov/gmd/ccgg/trends/

[3] R. K. Pachauri, M. R. Allen, V. Barros, J. Broome, W. Cramer, R. Christ, *et al.*, *Climate change 2014: synthesis Report. Contribution of working groups I, II and III to the fifth assessment report of the intergovernmental panel on climate change*: IPCC, 2014.

[4] J. E. Hansen, "Sir John Houghton: Global Warming: The Complete Briefing," *Journal of Atmospheric Chemistry,* vol. 30, pp. 409-412, 1998.

[5] J. T. Houghton, G. J. Jenkins, and J. Ephraums, "Climate change: the IPCC scientific assessment," *American Scientist;(United States),* vol. 80, 1990.

[6] A. Zervos, C. Lins, and J. Muth, *RE-thinking 2050: a 100% renewable energy vision for the European Union*: EREC, 2010.

[7] W. A. Hermann, "Quantifying global exergy resources," *Energy,* vol. 31, pp. 1685-1702, 9// 2006.

[8] REN21. Renewables 2016 global status report [Online]. Available: http://www.ren21.net/

[9] (2016). *World's Highest Conversion Efficiency of 26.33% Achieved in a Crystalline Sillicon Solar Cell*. Available: http://www.kaneka.co.jp/kaneka-e/images/topics/1473811995/1473811995_101.pdf

[10] M. A. Green, K. Emery, Y. Hishikawa, W. Warta, E. D. Dunlop, D. H.

Levi, *et al.*, "Solar cell efficiency tables (version 49)," *Progress in Photovoltaics: Research and Applications,* vol. 25, pp. 3-13, 2017.

[11] J. Kalowekamo and E. Baker, "Estimating the manufacturing cost of purely organic solar cells," *Solar Energy,* vol. 83, pp. 1224-1231, 2009.

[12] F. C. Krebs, M. Jørgensen, K. Norrman, O. Hagemann, J. Alstrup, T. D. Nielsen, *et al.*, "A Complete Process for Production of Flexible Large Area Polymer Solar Cells Entirely Using Screen Printing-First Public Demonstration," *Solar Energy Materials and Solar Cells,* vol. 93, pp. 422-441, 2009.

[13] G. Li, R. Zhu, and Y. Yang, "Polymer solar cells," *Nature Photonics,* vol. 6, pp. 153-161, 2012.

[14] J. H. Yim, S.-y. Joe, C. Pang, K. M. Lee, H. Jeong, J.-Y. Park, *et al.*, "Fully Solution-Processed Semitransparent Organic Solar Cells with a Silver Nanowire Cathode and a Conducting Polymer Anode," *ACS nano,* vol. 8, pp. 2857-2863, 2014.

[15] W. Gaynor, J.-Y. Lee, and P. Peumans, "Fully Solution-Processed Inverted Polymer Solar Cells with Laminated Nanowire Electrodes," *ACS nano,* vol. 4, pp. 30-34, 2009.

[16] M. Kaltenbrunner, M. S. White, E. D. Głowacki, T. Sekitani, T. Someya, N. S. Sariciftci, *et al.*, "Ultrathin and lightweight organic solar cells with high flexibility," *Nature communications,* vol. 3, p. 770, 2012.

[17] S. I. Na, S. S. Kim, J. Jo, and D. Y. Kim, "Efficient and Flexible ITO-Free Organic Solar Cells Using Highly Conductive Polymer Anodes," *Advanced Materials,* vol. 20, pp. 4061-4067, 2008.

[18] Z. Liu, J. Li, and F. Yan, "Package-Free Flexible Organic Solar Cells with Graphene top Electrodes," *Advanced Materials,* vol. 25, pp. 4296-4301, 2013.

Bibliography

[19] T. Kumari, S. M. Lee, S.-H. Kang, S. Chen, and C. Yang, "Ternary solar cells with a mixed face-on and edge-on orientation enable an unprecedented efficiency of 12.1%," *Energy & Environmental Science*, 2017.

[20] H. Hu, K. Jiang, G. Yang, J. Liu, Z. Li, H. Lin, *et al.*, "Terthiophene-Based D–A Polymer with an Asymmetric Arrangement of Alkyl Chains That Enables Efficient Polymer Solar Cells," *Journal of the American Chemical Society,* 2015/10/30 2015.

[21] S. Nho, G. Baek, S. Park, B. R. Lee, M. J. Cha, D. C. Lim, *et al.*, "Highly efficient inverted bulk-heterojunction solar cells with a gradiently-doped ZnO layer," *Energy & Environmental Science*, 2016.

[22] L. K. Jagadamma, M. Al-Senani, A. El-Labban, I. Gereige, N. Ndjawa, O. Guy, *et al.*, "Polymer Solar Cells with Efficiency>10% Enabled via a Facile Solution-Processed Al-Doped ZnO Electron Transporting Layer," *Advanced Energy Materials,* 2015.

[23] H. Zhou, Y. Zhang, C. K. Mai, S. D. Collins, G. C. Bazan, T. Q. Nguyen, *et al.*, "Polymer Homo-Tandem Solar Cells with Best Efficiency of 11.3%," *Advanced Materials,* vol. 27, pp. 1767-1773, 2015.

[24] C. C. Chen, W. H. Chang, K. Yoshimura, K. Ohya, J. You, J. Gao, *et al.*, "An Efficient Triple-Junction Polymer Solar Cell Having a Power Conversion Efficiency Exceeding 11%," *Advanced materials,* vol. 26, pp. 5670-5677, 2014.

[25] J. You, L. Dou, K. Yoshimura, T. Kato, K. Ohya, T. Moriarty, *et al.*, "A polymer tandem solar cell with 10.6% power conversion efficiency," *Nature communications,* vol. 4, p. 1446, 2013.

[26] J. You, C. C. Chen, Z. Hong, K. Yoshimura, K. Ohya, R. Xu, *et al.*, "10.2% Power Conversion Efficiency Polymer Tandem Solar Cells

Consisting of Two Identical Sub-Cells," *Advanced Materials,* vol. 25, pp. 3973-3978, 2013.

[27] Y. Liu, C.-C. Chen, Z. Hong, J. Gao, Y. M. Yang, H. Zhou, *et al.*, "Solution-processed small-molecule solar cells: breaking the 10% power conversion efficiency," *Scientific reports,* vol. 3, 2013.

[28] A. Kojima, K. Teshima, Y. Shirai, and T. Miyasaka, "Organometal halide perovskites as visible-light sensitizers for photovoltaic cells," *Journal of the American Chemical Society,* vol. 131, pp. 6050-6051, 2009.

[29] W. S. Yang, J. H. Noh, N. J. Jeon, Y. C. Kim, S. Ryu, J. Seo, *et al.*, "High-Performance Photovoltaic Perovskite Layers Fabricated Through Intramolecular Exchange," *Science,* vol. 348, pp. 1234-1237, 2015.

[30] D. Bi, W. Tress, M. I. Dar, P. Gao, J. Luo, C. Renevier, *et al.*, "Efficient Luminescent Solar Cells Based on Tailored Mixed-Cation Perovskites," *Science advances,* vol. 2, p. e1501170, 2016.

[31] T. J. Jacobsson, J.-P. Correa-Baena, M. Pazoki, M. Saliba, K. Schenk, M. Grätzel, *et al.*, "Exploration of the Compositional Space for Mixed Lead Halogen Perovskites for High Efficiency Solar Cells," *Energy & Environmental Science,* vol. 9, pp. 1706-1724, 2016.

[32] X. Li, D. Bi, C. Yi, J.-D. Décoppet, J. Luo, S. M. Zakeeruddin, *et al.*, "A Vacuum Flash-Assisted Solution Process for High-Efficiency Large-Area Perovskite Solar Cells," *Science,* p. aaf8060, 2016.

[33] M. Saliba, T. Matsui, J.-Y. Seo, K. Domanski, J.-P. Correa-Baena, M. K. Nazeeruddin, *et al.*, "Cesium-Containing Triple Cation Perovskite Solar Cells: Improved Stability, Reproducibility and High Efficiency," *Energy & Environmental Science,* vol. 9, pp. 1989-1997, 2016.

[34] K. T. Cho, S. Paek, G. Grancini, C. Roldan Carmona, P. Gao, Y. H. Lee,

et al., "Highly efficient perovskite solar cells with a compositional engineered perovskite/hole transporting material interface," *Energy & Environmental Science*, 2017.

[35] A. Goetzberger, J. Knobloch, and B. Voss, "Crystalline silicon solar cells," *editorial John Wiley & Sons Ltd*, vol. 1, 1998.

[36] P. Auger, "Sur les rayons β secondaires produits dans un gaz par des rayons X," *C.R.A.S.*, vol. 177, 1923.

[37] R. N. Hall, "Electron-Hole Recombination in Germanium," *Phys. Rev.*, vol. 87, 1952.

[38] S. M. Sze and K. K. Ng, *Physics of semiconductor devices*: John wiley & sons, 2006.

[39] C. W. Tang, "Multilayer organic photovoltaic elements," ed: Google Patents, 1979.

[40] M. Pope and C. E. Swenberg, *Electronic processes in organic crystals and polymers*: Oxford University Press on Demand, 1999.

[41] S. R. Forrest, "The path to ubiquitous and low-cost organic electronic appliances on plastic," *Nature*, vol. 428, pp. 911-918, 2004.

[42] G. Yu, J. Gao, J. C. Hummelen, F. Wudl, and A. J. Heeger, "Polymer photovoltiac cells: Enhanced efficiencies via a network of internal donor-acceptor heterojunctions," *Science*, vol. 270, p. 1789, 1995.

[43] J. Halls, C. Walsh, N. Greenham, and E. Marseglia, "Efficient photodiodes from interpenetrating polymer networks," *Nature*, vol. 376, p. 498, 1995.

[44] J. C. Hummelen, B. W. Knight, F. LePeq, F. Wudl, J. Yao, and C. L. Wilkins, "Preparation and characterization of fulleroid and methanofullerene derivatives," *The Journal of Organic Chemistry*, vol. 60, pp. 532-538, 1995.

Bibliography

[45] S. Mori, H. Oh-oka, H. Nakao, T. Gotanda, Y. Nakano, H. Jung, *et al.*, "Organic photovoltaic module development with inverted device structure," in *MRS Proceedings*, 2015.

[46] B. Kraabel, C. Lee, D. McBranch, D. Moses, N. Sariciftci, and A. Heeger, "Ultrafast photoinduced electron transfer in conducting polymer-buckminsterfullerene composites," *Chemical physics letters*, vol. 213, pp. 389-394, 1993.

[47] X. Yang and J. Loos, "Toward high-performance polymer solar cells: the importance of morphology control," *Macromolecules*, vol. 40, pp. 1353-1362, 2007.

[48] M. C. Scharber, D. Mühlbacher, M. Koppe, P. Denk, C. Waldauf, A. J. Heeger, *et al.*, "Design rules for donors in bulk-heterojunction solar cells-Towards 10% energy-conversion efficiency," *Advanced materials*, vol. 18, pp. 789-794, 2006.

[49] N. Blouin, A. Michaud, and M. Leclerc, "A low-bandgap poly (2, 7-carbazole) derivative for use in high-performance solar cells," *Advanced Materials*, vol. 19, pp. 2295-2300, 2007.

[50] Q. Zhou, Q. Hou, L. Zheng, X. Deng, G. Yu, and Y. Cao, "Fluorene-based low band-gap copolymers for high performance photovoltaic devices," *Applied Physics Letters*, vol. 84, pp. 1653-1655, 2004.

[51] A. Gadisa, W. Mammo, L. M. Andersson, S. Admassie, F. Zhang, M. R. Andersson, *et al.*, "A new donor-acceptor-donor polyfluorene copolymer with balanced electron and hole mobility," *Advanced Functional Materials*, vol. 17, pp. 3836-3842, 2007.

[52] L. Huo, J. Hou, S. Zhang, H. Y. Chen, and Y. Yang, "A Polybenzo [1, 2-b: 4, 5-b′] dithiophene Derivative with Deep HOMO Level and Its

Application in High-Performance Polymer Solar Cells," *Angewandte Chemie International Edition*, vol. 49, pp. 1500-1503, 2010.

[53] J.-J. Yun, H.-S. Jung, S.-H. Kim, E.-M. Han, V. Vaithianathan, and S. A. Jenekhe, "Chlorophyll-layer-inserted poly (3-hexyl-thiophene) solar cell having a high light-to-current conversion efficiency up to 1.48%," *Applied Physics Letters*, vol. 87, p. 123102, 2005.

[54] G. Li, V. Shrotriya, J. Huang, Y. Yao, T. Moriarty, K. Emery, *et al.*, "High-efficiency solution processable polymer photovoltaic cells by self-organization of polymer blends," *Nature materials*, vol. 4, pp. 864-868, 2005.

[55] Y.-J. Cheng, S.-H. Yang, and C.-S. Hsu, "Synthesis of conjugated polymers for organic solar cell applications," *Chem. Rev,* vol. 109, pp. 5868-5923, 2009.

[56] E. Havinga, W. Ten Hoeve, and H. Wynberg, "Alternate donor-acceptor small-band-gap semiconducting polymers; Polysquaraines and polycroconaines," *Synthetic Metals*, vol. 55, pp. 299-306, 1993.

[57] Q. T. Zhang and J. M. Tour, "Low optical bandgap polythiophenes by an alternating donor/acceptor repeat unit strategy," *Journal of the American Chemical Society*, vol. 119, pp. 5065-5066, 1997.

[58] D. Mühlbacher, M. Scharber, M. Morana, Z. Zhu, D. Waller, R. Gaudiana, *et al.*, "High photovoltaic performance of a low-bandgap polymer," *Advanced Materials*, vol. 18, pp. 2884-2889, 2006.

[59] J. Hou, H.-Y. Chen, S. Zhang, G. Li, and Y. Yang, "Synthesis, characterization, and photovoltaic properties of a low band gap polymer based on silole-containing polythiophenes and 2, 1, 3-benzothiadiazole," *Journal of the American Chemical Society*, vol. 130, pp. 16144-16145, 2008.

Bibliography

[60] H. Y. Chen, J. Hou, A. E. Hayden, H. Yang, K. Houk, and Y. Yang, "Silicon Atom Substitution Enhances Interchain Packing in a Thiophene-Based Polymer System," *Advanced materials,* vol. 22, pp. 371-375, 2010.

[61] D. Chen, F. Liu, C. Wang, A. Nakahara, and T. P. Russell, "Bulk heterojunction photovoltaic active layers via bilayer interdiffusion," *Nano letters,* vol. 11, pp. 2071-2078, 2011.

[62] R. Steim, F. R. Kogler, and C. J. Brabec, "Interface materials for organic solar cells," *Journal of Materials Chemistry,* vol. 20, pp. 2499-2512, 2010.

[63] Y. Lin, Q. He, F. Zhao, L. Huo, J. Mai, X. Lu, *et al.,* "A facile planar fused-ring electron acceptor for as-cast polymer solar cells with 8.71% efficiency," *J. Am. Chem. Soc,* vol. 138, pp. 2973-2976, 2016.

[64] N. Pellet, P. Gao, G. Gregori, T. Y. Yang, M. K. Nazeeruddin, J. Maier, *et al.,* "Mixed-organic-cation Perovskite photovoltaics for enhanced solar-light harvesting," *Angewandte Chemie International Edition,* vol. 53, pp. 3151-3157, 2014.

[65] J.-H. Im, C.-R. Lee, J.-W. Lee, S.-W. Park, and N.-G. Park, "6.5% efficient perovskite quantum-dot-sensitized solar cell," *Nanoscale,* vol. 3, pp. 4088-4093, 2011.

[66] M. M. Lee, J. Teuscher, T. Miyasaka, T. N. Murakami, and H. J. Snaith, "Efficient hybrid solar cells based on meso-superstructured organometal halide perovskites," *Science,* vol. 338, pp. 643-647, 2012.

[67] H.-S. Kim, C.-R. Lee, J.-H. Im, K.-B. Lee, T. Moehl, A. Marchioro, *et al.,* "Lead iodide perovskite sensitized all-solid-state submicron thin film mesoscopic solar cell with efficiency exceeding 9%," *Scientific reports,* vol. 2, p. 591, 2012.

Bibliography

[68] W. S. Yang, B.-W. Park, E. H. Jung, N. J. Jeon, Y. C. Kim, D. U. Lee, *et al.*, "Iodide management in formamidinium-lead-halide–based perovskite layers for efficient solar cells," *Science,* vol. 356, pp. 1376-1379, 2017.

[69] J. S. Manser, J. A. Christians, and P. V. Kamat, "Intriguing optoelectronic properties of metal halide perovskites," *Chemical Reviews,* vol. 116, pp. 12956-13008, 2016.

[70] L. Calió, S. Kazim, M. Grätzel, and S. Ahmad, "Hole-Transport Materials for Perovskite Solar Cells," *Angewandte Chemie International Edition,* 2016.

[71] G. E. Eperon, S. D. Stranks, C. Menelaou, M. B. Johnston, L. M. Herz, and H. J. Snaith, "Formamidinium lead trihalide: a broadly tunable perovskite for efficient planar heterojunction solar cells," *Energy & Environmental Science,* vol. 7, pp. 982-988, 2014.

[72] K. A. Bush, A. F. Palmstrom, J. Y. Zhengshan, M. Boccard, R. Cheacharoen, J. P. Mailoa, *et al.*, "23.6%-efficient monolithic perovskite/silicon tandem solar cells with improved stability," *Nature Energy,* vol. 2, p. 17009, 2017.

[73] T. J. Savenije, C. S. Ponseca Jr, L. Kunneman, M. Abdellah, K. Zheng, Y. Tian, *et al.*, "Thermally activated exciton dissociation and recombination control the carrier dynamics in organometal halide perovskite," *The journal of physical chemistry letters,* vol. 5, pp. 2189-2194, 2014.

[74] Q. Dong, Y. Fang, Y. Shao, P. Mulligan, J. Qiu, L. Cao, *et al.*, "Electron-hole diffusion lengths> 175 μm in solution-grown CH3NH3PbI3 single crystals," *Science,* vol. 347, pp. 967-970, 2015.

[75] K. Tanaka, T. Takahashi, T. Ban, T. Kondo, K. Uchida, and N. Miura,

"Comparative study on the excitons in lead-halide-based perovskite-type crystals CH3NH3PbBr3CH3NH3PbI3," *Solid state communications,* vol. 127, pp. 619-623, 2003.

[76] M. Hirasawa, T. Ishihara, T. Goto, K. Uchida, and N. Miura, "Magnetoabsorption of the lowest exciton in perovskite-type compound (CH3NH3) PbI3," *Physica B: Condensed Matter,* vol. 201, pp. 427-430, 1994.

[77] W. Zhang, M. Saliba, S. D. Stranks, Y. Sun, X. Shi, U. Wiesner, *et al.*, "Enhancement of perovskite-based solar cells employing core-shell metal nanoparticles," *Nano letters,* vol. 13, pp. 4505-4510, 2013.

[78] V. D'Innocenzo, G. Grancini, M. J. Alcocer, A. R. S. Kandada, S. D. Stranks, M. M. Lee, *et al.*, "Excitons versus free charges in organo-lead tri-halide perovskites," *Nature communications,* vol. 5, 2014.

[79] J. H. Heo, S. H. Im, J. H. Noh, T. N. Mandal, C.-S. Lim, J. A. Chang, *et al.*, "Efficient inorganic-organic hybrid heterojunction solar cells containing perovskite compound and polymeric hole conductors," *Nature photonics,* vol. 7, pp. 486-491, 2013.

[80] G. Xing, N. Mathews, S. Sun, S. S. Lim, Y. M. Lam, M. Grätzel, *et al.*, "Long-range balanced electron-and hole-transport lengths in organic-inorganic CH3NH3PbI3," *Science,* vol. 342, pp. 344-347, 2013.

[81] S. D. Stranks, G. E. Eperon, G. Grancini, C. Menelaou, M. J. Alcocer, T. Leijtens, *et al.*, "Electron-hole diffusion lengths exceeding 1 micrometer in an organometal trihalide perovskite absorber," *Science,* vol. 342, pp. 341-344, 2013.

[82] D. Yang, X. Zhou, R. Yang, Z. Yang, W. Yu, X. Wang, *et al.*, "Surface optimization to eliminate hysteresis for record efficiency planar perovskite solar cells," *Energy & Environmental Science,* vol. 9, pp.

3071-3078, 2016.

[83] W. Nie, H. Tsai, R. Asadpour, J.-C. Blancon, A. J. Neukirch, G. Gupta, *et al.*, "High-efficiency solution-processed perovskite solar cells with millimeter-scale grains," *Science*, vol. 347, pp. 522-525, 2015.

[84] H. Zhou, Q. Chen, G. Li, S. Luo, T.-b. Song, H.-S. Duan, *et al.*, "Interface engineering of highly efficient perovskite solar cells," *Science*, vol. 345, pp. 542-546, 2014.

[85] L. Meng, J. You, T.-F. Guo, and Y. Yang, "Recent Advances in the Inverted Planar Structure of Perovskite Solar Cells," *Accounts of chemical research*, 2015.

[86] Q. Lin, A. Armin, R. C. R. Nagiri, P. L. Burn, and P. Meredith, "Electro-optics of perovskite solar cells," *Nature Photonics*, vol. 9, pp. 106-112, 2015.

[87] Q. Chen, H. Zhou, Z. Hong, S. Luo, H.-S. Duan, H.-H. Wang, *et al.*, "Planar heterojunction perovskite solar cells via vapor-assisted solution process," *Journal of the American Chemical Society*, vol. 136, pp. 622-625, 2013.

[88] M. Liu, M. B. Johnston, and H. J. Snaith, "Efficient planar heterojunction perovskite solar cells by vapour deposition," *Nature*, vol. 501, pp. 395-398, 2013.

[89] J. Burschka, N. Pellet, S.-J. Moon, R. Humphry-Baker, P. Gao, M. K. Nazeeruddin, *et al.*, "Sequential deposition as a route to high-performance perovskite-sensitized solar cells," *Nature*, vol. 499, pp. 316-319, 2013.

[90] X. Zheng, B. Chen, C. Wu, and S. Priya, "Room temperature fabrication of CH3NH3PbBr3 by anti-solvent assisted crystallization approach for perovskite solar cells with fast response and small J–V hysteresis,"

Nano Energy, vol. 17, pp. 269-278, 10// 2015.

[91] N. J. Jeon, J. H. Noh, Y. C. Kim, W. S. Yang, S. Ryu, and S. I. Seok, "Solvent Engineering for High-Performance Inorganic-Organic Hybrid Perovskite Solar Cells," *Nature materials*, 2014.

[92] M. Xiao, F. Huang, W. Huang, Y. Dkhissi, Y. Zhu, J. Etheridge, *et al.*, "A fast deposition-crystallization procedure for highly efficient lead iodide perovskite thin-film solar cells," *Angewandte Chemie*, vol. 126, pp. 10056-10061, 2014.

[93] C. E. Small, S. Chen, J. Subbiah, C. M. Amb, S.-W. Tsang, T.-H. Lai, *et al.*, "High-efficiency inverted dithienogermole-thienopyrrolodione-based polymer solar cells," *Nature Photonics*, vol. 6, pp. 115-120, 2012.

[94] Y. Sun, J. H. Seo, C. J. Takacs, J. Seifter, and A. J. Heeger, "Inverted Polymer Solar Cells Integrated with a Low-Temperature-Annealed Sol-Gel-Derived ZnO Film as an Electron Transport Layer," *Advanced Materials*, vol. 23, pp. 1679-1683, 2011.

[95] C. Pang, V. Chellappan, J. H. Yim, M. J. Tan, G. T. W. Goh, S. Lee, *et al.*, "Enhanced Performance Using an SU-8 Dielectric Interlayer in a Bulk Heterojunction Organic Solar Cell," *ACS applied materials & interfaces*, vol. 7, pp. 5219-5225, 2015.

[96] J. Y. Kim, S. H. Kim, H. H. Lee, K. Lee, W. Ma, X. Gong, *et al.*, "New Architecture for high-efficiency polymer photovoltaic cells using solution-based titanium oxide as an optical spacer," *Advanced materials*, vol. 18, pp. 572-576, 2006.

[97] D. Liu and T. L. Kelly, "Perovskite Solar Cells with a Planar Heterojunction Structure Prepared Using Room-Temperature Solution Processing Techniques," *Nature photonics*, vol. 8, pp. 133-138, 2014.

Bibliography

[98] Z. Lin, C. Jiang, C. Zhu, and J. Zhang, "Development of inverted organic solar cells with TiO2 interface layer by using low-temperature atomic layer deposition," *ACS applied materials & interfaces,* vol. 5, pp. 713-718, 2013.

[99] B. A. MacLeod, P. Schulz, S. R. Cowan, A. Garcia, D. S. Ginley, A. Kahn, *et al.*, "Improved Performance in Bulk Heterojunction Organic Solar Cells with a Sol-Gel MgZnO Electron-Collecting Layer," *Advanced Energy Materials,* vol. 4, pp. 1400073-n/a, 2014.

[100] Z. Yin, Q. Zheng, S.-C. Chen, D. Cai, and Y. Ma, "Controllable ZnMgO Electron-Transporting Layers for Long-Term Stable Organic Solar Cells with 8.06% Efficiency after One-Year Storage," *Advanced Energy Materials,* pp. n/a-n/a, 2015.

[101] K. Mahmood, B. S. Swain, and H. S. Jung, "Controlling the surface nanostructure of ZnO and Al-doped ZnO thin films using electrostatic spraying for their application in 12% efficient perovskite solar cells," *Nanoscale,* vol. 6, pp. 9127-9138, 2014.

[102] X. Zhao, H. Shen, Y. Zhang, X. Li, X. Zhao, M. Tai, *et al.*, "Aluminum doped zinc oxide as highly stable electron collection layer for perovskite solar cells," *ACS applied materials & interfaces,* 2016.

[103] F. Giordano, A. Abate, J. P. C. Baena, M. Saliba, T. Matsui, S. H. Im, *et al.*, "Enhanced electronic properties in mesoporous TiO2 via lithium doping for high-efficiency perovskite solar cells," *Nature communications,* vol. 7, 2016.

[104] B. Roose, K. C. Gödel, S. Pathak, A. Sadhanala, J. P. C. Baena, B. D. Wilts, *et al.*, "Enhanced Efficiency and Stability of Perovskite Solar Cells Through Nd-Doping of Mesostructured TiO2," *Advanced Energy Materials,* pp. n/a-n/a, 2015.

Bibliography

[105] J. P. C. Baena, L. Steier, W. Tress, M. Saliba, S. Neutzner, T. Matsui, *et al.*, "Highly efficient planar perovskite solar cells through band alignment engineering," *Energy & Environmental Science*, vol. 8, pp. 2928-2934, 2015.

[106] K. Wang, Y. Shi, Q. Dong, Y. Li, S. Wang, X. Yu, *et al.*, "Low-Temperature and Solution-Processed Amorphous WO X as Electron-Selective Layer for Perovskite Solar Cells," *The Journal of Physical Chemistry Letters*, vol. 6, pp. 755-759, 2015.

[107] K. X. Steirer, P. F. Ndione, N. E. Widjonarko, M. T. Lloyd, J. Meyer, E. L. Ratcliff, *et al.*, "Enhanced efficiency in plastic solar cells via energy matched solution processed NiOx interlayers," *Advanced Energy Materials*, vol. 1, pp. 813-820, 2011.

[108] Z. Zhai, X. Huang, M. Xu, J. Yuan, J. Peng, and W. Ma, "Greatly Reduced Processing Temperature for a Solution-Processed NiOx Buffer Layer in Polymer Solar Cells," *Advanced Energy Materials*, vol. 3, pp. 1614-1622, 2013.

[109] J. You, L. Meng, T.-B. Song, T.-F. Guo, Y. M. Yang, W.-H. Chang, *et al.*, "Improved air stability of perovskite solar cells via solution-processed metal oxide transport layers," *Nature nanotechnology*, 2015.

[110] S. Murase and Y. Yang, "Solution processed MoO3 interfacial layer for organic photovoltaics prepared by a facile synthesis method," *Advanced Materials*, vol. 24, pp. 2459-2462, 2012.

[111] F. Xie, W. C. Choy, C. Wang, X. Li, S. Zhang, and J. Hou, "Low-Temperature Solution-Processed Hydrogen Molybdenum and Vanadium Bronzes for an Efficient Hole-Transport Layer in Organic Electronics," *Advanced Materials*, vol. 25, pp. 2051-2055, 2013.

[112] C. P. Chen, Y. D. Chen, and S. C. Chuang, "High-Performance and

Highly Durable Inverted Organic Photovoltaics Embedding Solution-Processable Vanadium Oxides as an Interfacial Hole-Transporting Layer," *Advanced Materials,* vol. 23, pp. 3859-3863, 2011.

[113] T. Stubhan, N. Li, N. A. Luechinger, S. C. Halim, G. J. Matt, and C. J. Brabec, "High fill factor polymer solar cells incorporating a low temperature solution processed WO3 hole extraction layer," *Advanced Energy Materials,* vol. 2, pp. 1433-1438, 2012.

[114] F. Wang, Q. Xu, Z. a. Tan, L. Li, S. Li, X. Hou, *et al.*, "Efficient polymer solar cells with a solution-processed and thermal annealing-free RuO 2 anode buffer layer," *Journal of Materials Chemistry A,* vol. 2, pp. 1318-1324, 2014.

[115] Z. a. Tan, L. Li, F. Wang, Q. Xu, S. Li, G. Sun, *et al.*, "Solution-Processed Rhenium Oxide: A Versatile Anode Buffer Layer for High Performance Polymer Solar Cells with Enhanced Light Harvest," *Advanced Energy Materials,* vol. 4, 2014.

[116] Q. Xu, F. Wang, Z. a. Tan, L. Li, S. Li, X. Hou, *et al.*, "High-Performance Polymer Solar Cells with Solution-Processed and Environmentally Friendly CuOx Anode Buffer Layer," *ACS applied materials & interfaces,* vol. 5, pp. 10658-10664, 2013.

[117] X. Tu, F. Wang, C. Li, Z. a. Tan, and Y. Li, "Solution-Processed and Low-Temperature Annealed CrOx as Anode Buffer Layer for Efficient Polymer Solar Cells," *The Journal of Physical Chemistry C,* vol. 118, pp. 9309-9317, 2014.

[118] K. Wang, H. Ren, C. Yi, C. Liu, H. Wang, L. Huang, *et al.*, "Solution-processed Fe3O4 magnetic nanoparticle thin film aligned by an external magnetostatic field as a hole extraction layer for polymer

solar cells," *ACS applied materials & interfaces,* vol. 5, pp. 10325-10330, 2013.

[119] X. Zhao, C. Xu, H. Wang, F. Chen, W. Zhang, Z. Zhao, *et al.*, "Application of Biuret, Dicyandiamide, or Urea as a Cathode Buffer Layer toward the Efficiency Enhancement of Polymer Solar Cells," *ACS Applied Materials & Interfaces,* vol. 6, pp. 4329-4337, 2014/03/26 2014.

[120] Q. Chen, B. J. Worfolk, T. C. Hauger, U. Al-Atar, K. D. Harris, and J. M. Buriak, "Finely Tailored Performance of Inverted Organic Photovoltaics through Layer-by-Layer Interfacial Engineering," *ACS Applied Materials & Interfaces,* vol. 3, pp. 3962-3970, 2011/10/26 2011.

[121] K. Sun, B. Zhao, V. Murugesan, A. Kumar, K. Zeng, J. Subbiah, *et al.*, "High-performance polymer solar cells with a conjugated zwitterion by solution processing or thermal deposition as the electron-collection interlayer," *Journal of Materials Chemistry,* vol. 22, pp. 24155-24165, 2012.

[122] H. Ye, X. Hu, Z. Jiang, D. Chen, X. Liu, H. Nie, *et al.*, "Pyridinium salt-based molecules as cathode interlayers for enhanced performance in polymer solar cells," *Journal of Materials Chemistry A,* vol. 1, pp. 3387-3394, 2013.

[123] D. Chen, H. Zhou, M. Liu, W.-M. Zhao, S.-J. Su, and Y. Cao, "Novel Cathode Interlayers Based on Neutral Alcohol-Soluble Small Molecules with a Triphenylamine Core Featuring Polar Phosphonate Side Chains for High-Performance Polymer Light-Emitting and Photovoltaic Devices," *Macromolecular Rapid Communications,* vol. 34, pp. 595-603, 2013.

[124] K. Sun, J. Chang, F. H. Isikgor, P. Li, and J. Ouyang, "Efficiency

enhancement of planar perovskite solar cells by adding zwitterion/LiF double interlayers for electron collection," *Nanoscale*, vol. 7, pp. 896-900, 2015.

[125] T. H. Reilly, A. W. Hains, H.-Y. Chen, and B. A. Gregg, "A Self-Doping, O2-Stable, n-Type Interfacial Layer for Organic Electronics," *Advanced Energy Materials*, vol. 2, pp. 455-460, 2012.

[126] Z.-G. Zhang, B. Qi, Z. Jin, D. Chi, Z. Qi, Y. Li, *et al.*, "Perylene diimides: a thickness-insensitive cathode interlayer for high performance polymer solar cells," *Energy & Environmental Science*, vol. 7, pp. 1966-1973, 2014.

[127] J. Min, Z. G. Zhang, Y. Hou, C. O. R. Quiroz, T. Przybilla, C. Bronnbauer, *et al.*, "Interface Engineering of Perovskite Hybrid Solar Cells with Solution-Processed Perylene–Diimide Heterojunctions toward High Performance," *Chemistry of Materials*, vol. 27, pp. 227-234, 2015.

[128] W. Zhang, Y. Wu, Q. Bao, F. Gao, and J. Fang, "Morphological Control for Highly Efficient Inverted Polymer Solar Cells Via the Backbone Design of Cathode Interlayer Materials," *Advanced Energy Materials*, 2014.

[129] Z. G. Zhang, H. Li, Z. Qi, Z. Jin, G. Liu, J. Hou, *et al.*, "Poly(ethylene glycol) modified [60]fullerene as electron buffer layer for high-performance polymer solar cells," *Applied Physics Letters*, vol. 102, pp. 143902-143902-5, 2013.

[130] Z. G. Zhang, H. Li, B. Qi, D. Chi, Z. Jin, Z. Qi, *et al.*, "Amine group functionalized fullerene derivatives as cathode buffer layers for high performance polymer solar cells," *Journal of Materials Chemistry A*, vol. 1, pp. 9624-9629, 2013.

Bibliography

[131] S. Li, M. Lei, M. Lv, S. E. Watkins, Z. A. Tan, J. Zhu, *et al.*, "[6,6]-Phenyl-C 61 -Butyric Acid Dimethylamino Ester as a Cathode Buffer Layer for High-Performance Polymer Solar Cells," *Advanced Energy Materials*, vol. 3, pp. 1569–1574, 2013.

[132] C. Duan, W. Cai, B. B. Y. Hsu, C. Zhong, K. Zhang, C. Liu, *et al.*, "Toward green solvent processable photovoltaic materials for polymer solar cells: the role of highly polar pendant groups in charge carrier transport and photovoltaic behavior," *Energy & Environmental Science*, vol. 6, pp. 3022-3034, 2013.

[133] C. Duan, C. Zhong, C. Liu, F. Huang, and Y. Cao, "Highly Efficient Inverted Polymer Solar Cells Based on an Alcohol Soluble Fullerene Derivative Interfacial Modification Material," *Chemistry of Materials*, vol. 24, pp. 1682–1689, 2012.

[134] C. Z. Li, C. Y. Chang, Y. Zang, H. X. Ju, C. C. Chueh, P. W. Liang, *et al.*, "Suppressed charge recombination in inverted organic photovoltaics via enhanced charge extraction by using a conductive fullerene electron transport layer," *Advanced Materials*, vol. 26, pp. 6262-7, 2014.

[135] Y. Y. Lai, P. I. Shih, Y. P. Li, C. E. Tsai, J. S. Wu, Y. J. Cheng, *et al.*, "Interface engineering to enhance the efficiency of conventional polymer solar cells by alcohol-/water-soluble C60 materials doped with alkali carbonates," *Acs Applied Materials & Interfaces*, vol. 5, p. 5122, 2013.

[136] K. Yao, M. Salvador, C. C. Chueh, X. K. Xin, Y. X. Xu, D. W. Dequilettes, *et al.*, "A General Route to Enhance Polymer Solar Cell Performance using Plasmonic Nanoprisms," *Advanced Energy Materials*, vol. 4, pp. 1289-1295, 2014.

[137] F. Zuo, S. T. Williams, P. W. Liang, C. C. Chueh, C. Y. Liao, and A. K.

Jen, "Binary-metal perovskites toward high-performance planar-heterojunction hybrid solar cells," *Advanced Materials*, vol. 26, pp. 6454-60, 2014.

[138] P. W. Liang, C. C. Chueh, X. K. Xin, F. Zuo, S. T. Williams, C. Y. Liao, *et al.*, "High-Performance Planar-Heterojunction Solar Cells Based on Ternary Halide Large-Band-Gap Perovskites," *Advanced Energy Materials*, vol. 5, 2015.

[139] P. W. Liang, C. Y. Liao, C. C. Chueh, F. Zuo, S. T. Williams, X. K. Xin, *et al.*, "Additive Enhanced Crystallization of Solution-Processed Perovskite for Highly Efficient Planar-Heterojunction Solar Cells," *Advanced Materials*, vol. 26, p. 3748, 2014.

[140] J. H. Kim, P. W. Liang, S. T. Williams, N. Cho, C. C. Chueh, M. S. Glaz, *et al.*, "High-Performance and Environmentally Stable Planar Heterojunction Perovskite Solar Cells Based on a Solution-Processed Copper-Doped Nickel Oxide Hole-Transporting Layer," *Advanced Materials*, vol. 27, pp. 695-701, 2015.

[141] C. C. Chueh, C. Y. Liao, F. Zuo, S. T. Williams, P. W. Liang, Y. Jen, *et al.*, "The roles of alkyl halide additives in enhancing perovskite solar cell performance," *Journal of Materials Chemistry A*, vol. 3, pp. 9058-9062, 2014.

[142] Z. A. Page, Y. Liu, V. V. Duzhko, T. P. Russell, and T. Emrick, "Fulleropyrrolidine interlayers: tailoring electrodes to raise organic solar cell efficiency," *Science*, vol. 346, pp. 441-4, 2014.

[143] Q. Mei, C. Li, X. Gong, H. Lu, E. Jin, C. Du, *et al.*, "Enhancing the performance of polymer photovoltaic cells by using an alcohol soluble fullerene derivative as the interfacial layer," *Acs Applied Materials & Interfaces*, vol. 5, p. 8076, 2013.

[144] X. Li, W. Zhang, Y. Wu, C. Min, and J. Fang, "High performance polymer solar cells with a polar fullerene derivative as the cathode buffer layer," *Journal of Materials Chemistry A*, vol. 1, pp. 12413-12416, 2013.

[145] J. Y. Jeng, Y. F. Chiang, M. H. Lee, S. R. Peng, T. F. Guo, P. Chen, *et al.*, "CH3NH3PbI3 Perovskite/Fullerene Planar-Heterojunction Hybrid Solar Cells," *Advanced Materials*, vol. 25, p. 3727, 2013.

[146] Y. J, H. Z, Y. YM, C. Q, C. M, S. TB, *et al.*, "Low-Temperature Solution-Processed Perovskite Solar Cells with High Efficiency and Flexibility," *Acs Nano*, vol. 8, pp. 1674-80, 2014.

[147] O. Malinkiewicz, A. Yella, H. L. Yong, G. M. Espallargas, M. Graetzel, M. K. Nazeeruddin, *et al.*, "Perovskite solar cells employing organic charge-transport layers," *Nature Photonics*, vol. 8, pp. 128-132, 2014.

[148] Z. Xiao, C. Bi, Y. Shao, Q. Dong, Q. Wang, Y. Yuan, *et al.*, "Efficient, high yield perovskite photovoltaic devices grown by interdiffusion of solution-processed precursor stacking layers," *Energy & Environmental Science*, vol. 7, pp. 2619-2623, 2014.

[149] Y. Zhou, C. Fuentes-Hernandez, J. Shim, J. Meyer, A. J. Giordano, H. Li, *et al.*, "A universal method to produce low-work function electrodes for organic electronics," *Science*, vol. 336, p. 327, 2012.

[150] S. Woo, W. Hyun Kim, H. Kim, Y. Yi, H.-K. Lyu, and Y. Kim, "8.9% Single-Stack Inverted Polymer Solar Cells with Electron-Rich Polymer Nanolayer-Modified Inorganic Electron-Collecting Buffer Layers," *Advanced Energy Materials*, vol. 4, pp. 1301692-n/a, 2014.

[151] H. Zhang, H. Azimi, Y. Hou, T. Ameri, T. Przybilla, E. Spiecker, *et al.*, "Improved High-Efficiency Perovskite Planar Heterojunction Solar Cells via Incorporation of a Polyelectrolyte Interlayer," *Chemistry of*

Materials, vol. 26, pp. 5190-5193, 2014/09/23 2014.

[152] Z. He, C. Zhong, S. Su, M. Xu, H. Wu, and Y. Cao, "Enhanced power-conversion efficiency in polymer solar cells using an inverted device structure," *Nature Photonics,* vol. 6, pp. 591-595, 2012.

[153] S.-H. Liao, Y.-L. Li, T.-H. Jen, Y.-S. Cheng, and S.-A. Chen, "Multiple Functionalities of Polyfluorene Grafted with Metal Ion-Intercalated Crown Ether as an Electron Transport Layer for Bulk-Heterojunction Polymer Solar Cells: Optical Interference, Hole Blocking, Interfacial Dipole, and Electron Conduction," *Journal of the American Chemical Society,* vol. 134, pp. 14271-14274, 2012/09/05 2012.

[154] S. Liu, K. Zhang, J. Lu, J. Zhang, H.-L. Yip, F. Huang, *et al.*, "High-Efficiency Polymer Solar Cells via the Incorporation of an Amino-Functionalized Conjugated Metallopolymer as a Cathode Interlayer," *Journal of the American Chemical Society,* vol. 135, pp. 15326-15329, 2013/10/16 2013.

[155] X. Guo, M. Zhang, W. Ma, L. Ye, S. Zhang, S. Liu, *et al.*, "Enhanced photovoltaic performance by modulating surface composition in bulk heterojunction polymer solar cells based on PBDTTT-C-T/PC71 BM," *Advanced Materials,* vol. 26, p. 4043, 2014.

[156] I. K. Hong, T. T. T. Bui, G. W. Kim, G. Kang, W. S. Shin, and T. Park, "A Benzodithiophene-Based Novel Electron Transport Layer for a Highly Efficient Polymer Solar Cell," *Acs Applied Materials & Interfaces,* vol. 6, p. 15875, 2014.

[157] M. Lv, S. Li, J. J. Jasieniak, J. Hou, J. Zhu, Z. a. Tan, *et al.*, "A Hyperbranched Conjugated Polymer as the Cathode Interlayer for High-Performance Polymer Solar Cells," *Advanced Materials,* vol. 25, pp. 6889-6894, 2013.

Bibliography

[158] Z. Tang, W. Tress, Q. Bao, M. J. Jafari, J. Bergqvist, T. Ederth, *et al.*, "Improving Cathodes with a Polymer Interlayer in Reversed Organic Solar Cells," *Advanced Energy Materials*, vol. 4, 2015.

[159] J. You, Y. M. Yang, Z. Hong, T.-B. Song, L. Meng, Y. Liu, *et al.*, "Moisture assisted perovskite film growth for high performance solar cells," *Applied Physics Letters*, vol. 105, p. 183902, 2014.

[160] C.-C. Chen, S.-H. Bae, W.-H. Chang, Z. Hong, G. Li, Q. Chen, *et al.*, "Perovskite/polymer monolithic hybrid tandem solar cells utilizing a low-temperature, full solution process," *Materials Horizons*, vol. 2, pp. 203-211, 2015.

[161] J. Sun, Y. Zhu, X. Xu, L. Lan, L. Zhang, P. Cai, *et al.*, "High Efficiency and High V oc Inverted Polymer Solar Cells Based on a Low-Lying HOMO Polycarbazole Donor and a Hydrophilic Polycarbazole Interlayer on ITO Cathode," *Journal of Physical Chemistry C*, vol. 116, pp. 14188–14198, 2012.

[162] Y. Zhu, X. Xu, L. Zhang, J. Chen, and Y. Cao, "High efficiency inverted polymeric bulk-heterojunction solar cells with hydrophilic conjugated polymers as cathode interlayer on ITO," *Solar Energy Materials & Solar Cells*, vol. 97, pp. 83-88, 2012.

[163] G. Xing, K. Zhang, F. Huang, G. C. Bazan, and Y. Cao, "Amino N-Oxide Functionalized Conjugated Polymers and their Amino-Functionalized Precursors: New Cathode Interlayers for High-Performance Optoelectronic Devices," *Advanced Functional Materials*, vol. 22, pp. 2846–2854, 2012.

[164] T. Yang, M. Wang, C. Duan, X. Hu, L. Huang, J. Peng, *et al.*, "Inverted polymer solar cells with 8.4% efficiency by conjugated polyelectrolyte," *Energy & Environmental Science*, vol. 5, pp. 8208-8214, 2012.

Bibliography

[165] C. Duan, K. Zhang, X. Guan, C. Zhong, H. Xie, F. Huang, *et al.*, "Conjugated zwitterionic polyelectrolyte-based interface modification materials for high performance polymer optoelectronic devices," *Chemical Science,* vol. 4, pp. 1298-1307, 2013.

[166] B. J. Worfolk, T. C. Hauger, K. D. Harris, D. A. Rider, J. A. M. Fordyce, S. Beaupré, *et al.*, "Work Function Control of Interfacial Buffer Layers for Efficient and Air-Stable Inverted Low-Bandgap Organic Photovoltaics," *Advanced Energy Materials,* vol. 2, pp. 361–368, 2012.

[167] J. Kesters, T. Ghoos, H. Penxten, J. Drijkoningen, T. Vangerven, D. M. Lyons, *et al.*, "Imidazolium log ubstituted Polythiophenes as Efficient Electron Transport Materials Improving Photovoltaic Performance," *Advanced Energy Materials,* vol. 3, pp. 1180-1185, 2013.

[168] L. Feng, Z. A. Page, V. V. Duzhko, T. P. Russell, and E. Todd, "Conjugated polymeric zwitterions as efficient interlayers in organic solar cells," *Advanced Materials,* vol. 25, p. 6868, 2013.

[169] E. Puodziukynaite, H. W. Wang, J. Lawrence, A. J. Wise, T. P. Russell, M. D. Barnes, *et al.*, "Azulene Methacrylate Polymers: Synthesis, Electronic Properties, and Solar Cell Fabrication," *Journal of the American Chemical Society,* vol. 136, p. 11043, 2014.

[170] J. R. Manders, S. W. Tsang, M. J. Hartel, T. H. Lai, S. Chen, C. M. Amb, *et al.*, "Solution-Processed Nickel Oxide Hole Transport Layers in High Efficiency Polymer Photovoltaic Cells," *Advanced Functional Materials,* vol. 23, pp. 2993-3001, 2013.

[171] J. Zhang, J. Wang, Y. Fu, B. Zhang, and Z. Xie, "Efficient and stable polymer solar cells with annealing-free solution-processible NiO nanoparticles as anode buffer layers," *Journal of Materials Chemistry C,* vol. 2, pp. 8295-8302, 2014.

Bibliography

[172] W. Chen, Y. Wu, Y. Yue, J. Liu, W. Zhang, X. Yang, *et al.*, "Efficient and stable large-area perovskite solar cells with inorganic charge extraction layers," *Science*, p. aad1015, 2015.

[173] Q. Wang, C. C. Chueh, T. Zhao, J. Cheng, M. Eslamian, W. C. Choy, *et al.*, "Effects of Self-Assembled Monolayer Modification of Nickel Oxide Nanoparticles Layer on the Performance and Application of Inverted Perovskite Solar Cells," *ChemSusChem*, 2017.

[174] C. K. Mai, H. Zhou, Y. Zhang, Z. B. Henson, T. Q. Nguyen, A. J. Heeger, *et al.*, "Facile Doping of Anionic Narrow-Band-Gap Conjugated Polyelectrolytes During Dialysis," *Angewandte Chemie International Edition*, vol. 52, pp. 12874-12878, 2013.

[175] H. Zhou, Y. Zhang, C. K. Mai, S. D. Collins, T. Q. Nguyen, G. C. Bazan, *et al.*, "Conductive Conjugated Polyelectrolyte as Hole-Transporting Layer for Organic Bulk Heterojunction Solar Cells," *Advanced Materials*, vol. 26, pp. 780-785, 2014.

[176] G. K. Mor, D. Jones, T. P. Le, Z. Shang, P. J. Weathers, M. K. B. Woltermann, *et al.*, "Contact Doping with Sub-Monolayers of Strong Polyelectrolytes for Organic Photovoltaics," *Advanced Energy Materials*, vol. 4, pp. 1294-1305, 2015.

[177] K.-G. Lim, H.-B. Kim, J. Jeong, H. Kim, J. Y. Kim, and T.-W. Lee, "Boosting the Power Conversion Efficiency of Perovskite Solar Cells Using Self-Organized Polymeric Hole Extraction Layers with High Work Function," *Advanced Materials*, vol. 26, pp. 6461-6466, 2014.

[178] U. Bach, D. Lupo, P. Comte, J. Moser, F. Weissörtel, J. Salbeck, *et al.*, "Solid-state dye-sensitized mesoporous TiO2 solar cells with high photon-to-electron conversion efficiencies," *Nature*, vol. 395, pp. 583-585, 1998.

[179] J. Krüger, R. Plass, L. Cevey, M. Piccirelli, M. Grätzel, and U. Bach, "High efficiency solid-state photovoltaic device due to inhibition of interface charge recombination," *Applied Physics Letters,* vol. 79, pp. 2085-2087, 2001.

[180] N. J. Jeon, H. G. Lee, Y. C. Kim, J. Seo, J. H. Noh, J. Lee, *et al.*, "o-Methoxy substituents in spiro-OMeTAD for efficient inorganic-organic hybrid perovskite solar cells," *Journal of the American Chemical Society,* vol. 136, pp. 7837-7840, 2014.

[181] B. Xu, E. Sheibani, P. Liu, J. Zhang, H. Tian, N. Vlachopoulos, *et al.*, "Carbazole-Based Hole-Transport Materials for Efficient Solid-State Dye-Sensitized Solar Cells and Perovskite Solar Cells," *Advanced Materials,* vol. 26, pp. 6629-34, 2014.

[182] S. D. Sung, M. S. Kang, I. T. Choi, H. M. Kim, H. Kim, M. Hong, *et al.*, "14.8% Perovskite Solar Cells Employing Carbazole Derivatives as Hole Transporting Materials," *Chemical Communications,* vol. 50, pp. 14161-3, 2014.

[183] P. Qin, S. Paek, M. I. Dar, N. Pellet, J. Ko, M. Grätzel, *et al.*, "Perovskite solar cells with 12.8% efficiency by using conjugated quinolizino acridine based hole transporting material," *Journal of the American Chemical Society,* vol. 136, p. 8516, 2014.

[184] J. Liu, Y. Wu, C. Qin, X. Yang, T. Yasuda, A. Islam, *et al.*, "A dopant-free hole-transporting material for efficient and stable perovskite solar cells," *Energy & Environmental Science,* vol. 7, pp. 2963-2967, 2014.

[185] M. Saliba, S. Orlandi, T. Matsui, S. Aghazada, M. Cavazzini, J.-P. Correa-Baena, *et al.*, "A molecularly engineered hole-transporting material for efficient perovskite solar cells," *Nature Energy,* vol. 1, p.

15017, 01/18/online 2016.

[186] K. Rakstys, A. Abate, M. I. Dar, P. Gao, V. Jankauskas, G. n. Jacopin, *et al.*, "Triazatruxene-based hole transporting materials for highly efficient perovskite solar cells," *Journal of the American Chemical Society,* vol. 137, pp. 16172-16178, 2015.

[187] S. Park, J. H. Heo, C. H. Cheon, H. Kim, S. H. Im, and H. J. Son, "A [2,2]paracyclophane triarylamine-based hole-transporting material for high performance perovskite solar cells," *Journal of Materials Chemistry A,* vol. 3, pp. 24215-24220, 2015.

[188] D. Liu, J. Yang, and T. L. Kelly, "Compact layer free perovskite solar cells with 13.5% efficiency," *Journal of the American Chemical Society,* vol. 136, pp. 17116-17122, 2014.

[189] W. Chen, X. Bao, Q. Zhu, D. Zhu, M. Qiu, M. Sun, *et al.*, "Simple planar perovskite solar cells with a dopant-free benzodithiophene conjugated polymer as hole transporting material," *Journal of Materials Chemistry C,* vol. 3, pp. 10070-10073, 2015.

[190] Y. Liu, Q. Chen, H. S. Duan, H. Zhou, Y. Yang, H. Chen, *et al.*, "Dopant-Free Organic Hole Transport Material for Efficient Planar Heterojunction Perovskite Solar Cells," *Journal of Materials Chemistry A,* vol. 3, pp. 11940-11947, 2015.

[191] W. H. Nguyen, C. D. Bailie, E. L. Unger, and M. D. Mcgehee, "Enhancing the Hole-Conductivity of Spiro-OMeTAD without Oxygen or Lithium Salts by Using Spiro(TFSI)2 in Perovskite and Dye-Sensitized Solar Cells," *Journal of the American Chemical Society,* vol. 136, p. 10996, 2014.

[192] C. N. Hoth, S. A. Choulis, P. Schilinsky, and C. J. Brabec, "High photovoltaic performance of inkjet printed polymer: fullerene blends,"

Advanced Materials, vol. 19, pp. 3973-3978, 2007.

[193] P. Schilinsky, C. Waldauf, and C. J. Brabec, "Performance Analysis of Printed Bulk Heterojunction Solar Cells," *Advanced Functional Materials,* vol. 16, pp. 1669-1672, 2006.

[194] P. Gaskell, G. Innes, and M. Savage, "An experimental investigation of meniscus roll coating," *Journal of Fluid Mechanics,* vol. 355, pp. 17-44, 1998.

[195] F. C. Krebs, J. Fyenbo, and M. Jørgensen, "Product integration of compact roll-to-roll processed polymer solar cell modules: methods and manufacture using flexographic printing, slot-die coating and rotary screen printing," *Journal of Materials Chemistry,* vol. 20, pp. 8994-9001, 2010.

[196] F. C. Krebs, "Fabrication and processing of polymer solar cells: a review of printing and coating techniques," *Solar energy materials and solar cells,* vol. 93, pp. 394-412, 2009.

[197] T. Aernouts, T. Aleksandrov, C. Girotto, J. Genoe, and J. Poortmans, "Polymer based organic solar cells using ink-jet printed active layers," *Applied Physics Letters,* vol. 92, p. 22, 2008.

[198] F. C. Krebs, "Polymer solar cell modules prepared using roll-to-roll methods: knife-over-edge coating, slot-die coating and screen printing," *Solar Energy Materials and Solar Cells,* vol. 93, pp. 465-475, 2009.

[199] Z. Ku, Y. Rong, M. Xu, T. Liu, and H. Han, "Full printable processed mesoscopic CH3NH3PbI3/TiO2 heterojunction solar cells with carbon counter electrode," *Scientific reports,* vol. 3, p. 3132, 2013.

[200] K. Cao, Z. Zuo, J. Cui, Y. Shen, T. Moehl, S. M. Zakeeruddin, *et al.*, "Efficient screen printed perovskite solar cells based on mesoscopic TiO2/Al2O3/NiO/carbon architecture," *Nano Energy,* vol. 17, pp.

171-179, 2015.

[201] J. H. Kim, S. T. Williams, N. Cho, C. C. Chueh, and A. K. Y. Jen, "Enhanced Environmental Stability of Planar Heterojunction Perovskite Solar Cells Based on Blade-Coating," *Advanced Energy Materials*, vol. 5, 2015.

[202] K. Hwang, Y. S. Jung, Y. J. Heo, F. H. Scholes, S. E. Watkins, J. Subbiah, *et al.*, "Toward Large Scale Roll-to-Roll Production of Fully Printed Perovskite Solar Cells," *Advanced materials*, vol. 27, pp. 1241-1247, 2015.

[203] Y. Liu, J. Zhao, Z. Li, C. Mu, W. Ma, H. Hu, *et al.*, "Aggregation and morphology control enables multiple cases of high-efficiency polymer solar cells," *Nature communications*, vol. 5, 2014.

[204] H. Kang, S. Kee, K. Yu, J. Lee, G. Kim, J. Kim, *et al.*, "Simplified Tandem Polymer Solar Cells with an Ideal Self-Organized Recombination Layer," *Advanced Materials*, vol. 27, pp. 1408-1413, 2015.

[205] L.-M. Chen, Z. Xu, Z. Hong, and Y. Yang, "Interface investigation and engineering-achieving high performance polymer photovoltaic devices," *Journal of Materials Chemistry*, vol. 20, pp. 2575-2598, 2010.

[206] C. J. Brabec, S. E. Shaheen, C. Winder, N. S. Sariciftci, and P. Denk, "Effect of LiF/metal electrodes on the performance of plastic solar cells," *Applied Physics Letters*, vol. 80, pp. 1288-1290, 2002.

[207] S. Jönsson, E. Carlegrim, F. Zhang, W. R. Salaneck, and M. Fahlman, "Photoelectron spectroscopy of the contact between the cathode and the active layers in plastic solar cells: the role of LiF," *Japanese journal of applied physics*, vol. 44, p. 3695, 2005.

[208] C. Lee, "Enhanced efficiency and durability of organic

electroluminescent devices by inserting a thin insulating layer at the Alq3/cathode interface," *Synthetic metals,* vol. 91, pp. 125-127, 1997.

[209] G. Jabbour, B. Kippelen, N. Armstrong, and N. Peyghambarian, "Aluminum based cathode structure for enhanced electron injection in electroluminescent organic devices," *Applied physics letters,* vol. 73, pp. 1185-1187, 1998.

[210] J. Gilot, I. Barbu, M. M. Wienk, and R. A. Janssen, "The use of ZnO as optical spacer in polymer solar cells: theoretical and experimental study," *Applied physics letters,* vol. 91, p. 113520, 2007.

[211] H. Choi, J. S. Park, E. Jeong, G. H. Kim, B. R. Lee, S. O. Kim, *et al.*, "Combination of Titanium Oxide and a Conjugated Polyelectrolyte for High-Performance Inverted-Type Organic Optoelectronic Devices," *Advanced Materials,* vol. 23, pp. 2759-2763, 2011.

[212] A. Duarte, K.-Y. Pu, B. Liu, and G. C. Bazan, "Recent Advances in Conjugated Polyelectrolytes for Emerging Optoelectronic Applications†," *Chemistry of Materials,* vol. 23, pp. 501-515, 2010.

[213] J. H. Seo, A. Gutacker, Y. Sun, H. Wu, F. Huang, Y. Cao, *et al.*, "Improved high-efficiency organic solar cells via incorporation of a conjugated polyelectrolyte interlayer," *Journal of the American Chemical Society,* vol. 133, pp. 8416-8419, 2011.

[214] C. He, C. Zhong, H. Wu, R. Yang, W. Yang, F. Huang, *et al.*, "Origin of the enhanced open-circuit voltage in polymer solar cells via interfacial modification using conjugated polyelectrolytes," *Journal of Materials Chemistry,* vol. 20, pp. 2617-2622, 2010.

[215] S.-I. Na, S.-H. Oh, S.-S. Kim, and D.-Y. Kim, "Efficient organic solar cells with polyfluorene derivatives as a cathode interfacial layer," *Organic Electronics,* vol. 10, pp. 496-500, 2009.

[216] R. Xia, D. S. Leem, T. Kirchartz, S. Spencer, C. Murphy, Z. He, *et al.*, "Investigation of a conjugated polyelectrolyte interlayer for inverted polymer: fullerene solar cells," *Advanced Energy Materials*, vol. 3, pp. 718-723, 2013.

[217] R. Kang, S.-H. Oh, and D.-Y. Kim, "Influence of the Ionic Functionalities of Polyfluorene Derivatives as a Cathode Interfacial Layer on Inverted Polymer Solar Cells," *ACS Applied Materials & Interfaces*, vol. 6, pp. 6227-6236, 2014/05/14 2014.

[218] B. H. Lee, I. H. Jung, H. Y. Woo, H. K. Shim, G. Kim, and K. Lee, "Multi-Charged Conjugated Polyelectrolytes as a Versatile Work Function Modifier for Organic Electronic Devices," *Advanced Functional Materials*, vol. 24, pp. 1100-1108, 2014.

[219] T. Stubhan, H. Oh, L. Pinna, J. Krantz, I. Litzov, and C. J. Brabec, "Inverted organic solar cells using a solution processed aluminum-doped zinc oxide buffer layer," *Organic Electronics*, vol. 12, pp. 1539-1543, 2011.

[220] N. Espinosa, R. Garc á-Valverde, A. Urbina, F. Lenzmann, M. Manceau, D. Angmo, *et al.*, "Life cycle assessment of ITO-free flexible polymer solar cells prepared by roll-to-roll coating and printing," *Solar Energy Materials and Solar Cells*, vol. 97, pp. 3-13, 2012.

[221] S. H. Oh, S. I. Na, J. Jo, B. Lim, D. Vak, and D. Y. Kim, "Water-Soluble Polyfluorenes as an Interfacial Layer Leading to Cathode-Independent High Performance of Organic Solar Cells," *Advanced Functional Materials*, vol. 20, pp. 1977-1983, 2010.

[222] Y. M. Chang, R. Zhu, E. Richard, C. C. Chen, G. Li, and Y. Yang, "Electrostatic Self-Assembly Conjugated Polyelectrolyte-Surfactant Complex as an Interlayer for High Performance Polymer Solar Cells,"

Advanced Functional Materials, vol. 22, pp. 3284-3289, 2012.

[223] Z. He, H. Wu, and Y. Cao, "Recent Advances in Polymer Solar Cells: Realization of High Device Performance by Incorporating Water/Alcohol-Soluble Conjugated Polymers as Electrode Buffer Layer," *Advanced Materials,* vol. 26, pp. 1006-1024, 2014.

[224] K. Zilberberg, A. Behrendt, M. Kraft, U. Scherf, and T. Riedl, "Ultrathin interlayers of a conjugated polyelectrolyte for low work-function cathodes in efficient inverted organic solar cells," *Organic Electronics,* vol. 14, pp. 951-957, Mar 2013.

[225] C.-Y. Nam, "Ambient Air Processing Causes Light Soaking Effects in Inverted Organic Solar Cells Employing Conjugated Polyelectrolyte Electron Transfer Layer," *The Journal of Physical Chemistry C,* vol. 118, pp. 27219-27225, 2014/11/26 2014.

[226] Y. Liang, Z. Xu, J. Xia, S. T. Tsai, Y. Wu, G. Li, *et al.,* "For the bright future-bulk heterojunction polymer solar cells with power conversion efficiency of 7.4%," *Advanced Materials,* vol. 22, pp. E135-E138, 2010.

[227] J. Liu, G. Feng, R. Liu, N. Tomczak, L. Ma, G. G. Gurzadyan, *et al.*, "Bright Quantum-Dot-Sized Single-Chain Conjugated Polyelectrolyte Nanoparticles: Synthesis, Characterization and Application for Specific Extracellular Labeling and Imaging," *Small,* vol. 10, pp. 3110-3118, 2014.

[228] A. Yadav, A. Agarwal, P. B. Agarwal, and P. Saini, "Ammonia Sensing by PANI-DBSA Based Gas Sensor Exploiting Kelvin Probe Technique," *Journal of Nanoparticles,* vol. 2015, 2015.

[229] J. W. Shim, H. Cheun, J. Meyer, C. Fuentes-Hernandez, A. Dindar, Y. Zhou, *et al.*, "Polyvinylpyrrolidone-modified indium tin oxide as an electron-collecting electrode for inverted polymer solar cells," *Applied*

Physics Letters, vol. 101, p. 073303, 2012.

[230] A. Garcia, R. C. B. Ii, P. Zalar, C. V. Hoven, J. Z. Brzezinski, and T. Q. Nguyen, "Controlling ion motion in polymer light-emitting diodes containing conjugated polyelectrolyte electron injection layers," *Journal of the American Chemical Society*, vol. 133, pp. 2492-8, 2011.

[231] C. Brabec, U. Scherf, and V. Dyakonov, *Organic photovoltaics: materials, device physics, and manufacturing technologies*: John Wiley & Sons, 2011.

[232] J.-H. Huang, F.-C. Chen, C.-L. Chen, A. T. Huang, Y.-S. Hsiao, C.-M. Teng, *et al.*, "Molecular-weight-dependent nanoscale morphology in silole-containing cyclopentadithiophene polymer and fullerene derivative blends," *Organic Electronics*, vol. 12, pp. 1755-1762, 2011.

[233] X. Li, X. Tang, F. Wang, V. Chellappan, T. W. Weei, S. Guo, *et al.*, "Investigations of a New High-Performance Low-Band-Gap Photovoltaic Polymer Semiconductor," *IEEE Journal of Photovoltaics*, vol. 6, pp. 696-704, 2016.

[234] J. H. Seo and T.-Q. Nguyen, "Electronic Properties of Conjugated Polyelectrolyte Thin Films," *Journal of the American Chemical Society*, vol. 130, pp. 10042-10043, 2008/08/01 2008.

[235] W. Chen, Y. Wu, Y. Yue, J. Liu, W. Zhang, X. Yang, *et al.*, "Efficient and stable large-area perovskite solar cells with inorganic charge extraction layers," *Science*, vol. 350, pp. 944-948, 2015.

[236] E. Edri, S. Kirmayer, A. Henning, S. Mukhopadhyay, K. Gartsman, Y. Rosenwaks, *et al.*, "Why lead methylammonium tri-iodide perovskite-based solar cells require a mesoporous electron transporting scaffold (but not necessarily a hole conductor)," *Nano letters*, vol. 14, pp. 1000-1004, 2014.

Bibliography

[237] W. Zhang, M. Saliba, D. T. Moore, S. K. Pathak, M. T. Hörantner, T. Stergiopoulos, *et al.*, "Ultrasmooth organic–inorganic perovskite thin-film formation and crystallization for efficient planar heterojunction solar cells," *Nature communications,* vol. 6, 2015.

[238] J. You, Z. Hong, Y. M. Yang, Q. Chen, M. Cai, T.-B. Song, *et al.*, "Low-Temperature Solution-Processed Perovskite Solar Cells with High Efficiency and Flexibility," 2014.

[239] W. Yan, Y. Li, Y. Li, S. Ye, Z. Liu, S. Wang, *et al.*, "High-performance hybrid perovskite solar cells with open circuit voltage dependence on hole-transporting materials," *Nano Energy,* vol. 16, pp. 428-437, 2015.

[240] Y. Shao, Z. Xiao, C. Bi, Y. Yuan, and J. Huang, "Origin and elimination of photocurrent hysteresis by fullerene passivation in CH3NH3PbI3 planar heterojunction solar cells," *Nature communications,* vol. 5, 2014.

[241] H. J. Snaith, A. Abate, J. M. Ball, G. E. Eperon, T. Leijtens, N. K. Noel, *et al.*, "Anomalous hysteresis in perovskite solar cells," *The journal of physical chemistry letters,* vol. 5, pp. 1511-1515, 2014.

[242] W. Tress, N. Marinova, T. Moehl, S. M. Zakeeruddin, M. K. Nazeeruddin, and M. Gratzel, "Understanding the rate-dependent J-V hysteresis, slow time component, and aging in CH3NH3PbI3 perovskite solar cells: the role of a compensated electric field," *Energy & Environmental Science,* vol. 8, pp. 995-1004, 2015.

[243] E. L. Unger, E. T. Hoke, C. D. Bailie, W. H. Nguyen, A. R. Bowring, T. Heumuller, *et al.*, "Hysteresis and transient behavior in current-voltage measurements of hybrid-perovskite absorber solar cells," *Energy & Environmental Science,* vol. 7, pp. 3690-3698, 2014.

[244] Z. Hawash, L. K. Ono, S. R. Raga, M. V. Lee, and Y. Qi, "Air-Exposure Induced Dopant Redistribution and Energy Level Shifts in Spin-Coated

Spiro-MeOTAD Films," *Chemistry of Materials,* vol. 27, pp. 562-569, 2015/01/27 2015.

[245] Y. K. Wang, Z. C. Yuan, G. Z. Shi, Y. X. Li, Q. Li, F. Hui, *et al.*, "Dopant-Free Spiro-Triphenylamine/Fluorene as Hole-Transporting Material for Perovskite Solar Cells with Enhanced Efficiency and Stability," *Advanced Functional Materials,* vol. 26, pp. 1375-1381, 2016.

[246] M. Franckevicius, A. Mishra, F. Kreuzer, J. Luo, S. M. Zakeeruddin, and M. Gratzel, "A dopant-free spirobi[cyclopenta[2,1-b:3,4-b[prime or minute]]dithiophene] based hole-transport material for efficient perovskite solar cells," *Materials Horizons,* vol. 2, pp. 613-618, 2015.

[247] S. Kazim, F. J. Ramos, P. Gao, M. K. Nazeeruddin, M. Gratzel, and S. Ahmad, "A dopant free linear acene derivative as a hole transport material for perovskite pigmented solar cells," *Energy & Environmental Science,* vol. 8, pp. 1816-1823, 2015.

[248] C. Huang, W. Fu, C.-Z. Li, Z. Zhang, W. Qiu, M. Shi, *et al.*, "Dopant-Free Hole-Transporting Material with a C 3 h Symmetrical Truxene Core for Highly Efficient Perovskite Solar Cells," *Journal of the American Chemical Society,* vol. 138, pp. 2528-2531, 2016.

[249] Y. Liu, Z. Hong, Q. Chen, H. Chen, W. H. Chang, Y. M. Yang, *et al.*, "Perovskite Solar Cells Employing Dopant-Free Organic Hole Transport Materials with Tunable Energy Levels," *Advanced Materials,* vol. 28, pp. 440-446, 2016.

[250] A. T. Murray, J. M. Frost, C. H. Hendon, C. D. Molloy, D. R. Carbery, and A. Walsh, "Modular design of SPIRO-OMeTAD analogues as hole transport materials in solar cells," *Chemical Communications,* vol. 51, pp. 8935-8938, 2015.

[251] F. J. Ramos, K. Rakstys, S. Kazim, M. Gratzel, M. K. Nazeeruddin, and S. Ahmad, "Rational design of triazatruxene-based hole conductors for perovskite solar cells," *RSC Advances*, vol. 5, pp. 53426-53432, 2015.

[252] L. Cabau, I. Garcia-Benito, A. Molina-Ontoria, N. F. Montcada, N. Martin, A. Vidal-Ferran, *et al.*, "Diarylamino-substituted tetraarylethene (TAE) as an efficient and robust hole transport material for 11% methyl ammonium lead iodide perovskite solar cells," *Chemical Communications*, vol. 51, pp. 13980-13982, 2015.

[253] Y. Song, S. Lv, X. Liu, X. Li, S. Wang, H. Wei, *et al.*, "Energy level tuning of TPB-based hole-transporting materials for highly efficient perovskite solar cells," *Chemical Communications*, vol. 50, pp. 15239-15242, 2014.

[254] S. Lv, Y. Song, J. Xiao, L. Zhu, J. Shi, H. Wei, *et al.*, "Simple Triphenylamine-Based Hole-Transporting Materials for Perovskite Solar Cells," *Electrochimica Acta*, vol. 182, pp. 733-741, 11/10/ 2015.

[255] A. Dubey, N. Adhikari, S. Venkatesan, S. Gu, D. Khatiwada, Q. Wang, *et al.*, "Solution processed pristine PDPP3T polymer as hole transport layer for efficient perovskite solar cells with slower degradation," *Solar Energy Materials and Solar Cells*, vol. 145, Part 3, pp. 193-199, 2// 2016.

[256] J. Luo, J.-H. Im, M. T. Mayer, M. Schreier, M. K. Nazeeruddin, N.-G. Park, *et al.*, "Water photolysis at 12.3% efficiency via perovskite photovoltaics and Earth-abundant catalysts," *Science*, vol. 345, pp. 1593-1596, 2014.

[257] Y. Xiao, G. Han, Y. Chang, H. Zhou, M. Li, and Y. Li, "An all-solid-state perovskite-sensitized solar cell based on the dual function polyaniline as the sensitizer and p-type hole-transporting material,"

Journal of Power Sources, vol. 267, pp. 1-8, 12/1/ 2014.

[258] J. W. Lee, S. Park, M. J. Ko, H. J. Son, and N. G. Park, "Enhancement of the Photovoltaic Performance of CH3NH3PbI3 Perovskite Solar Cells through a Dichlorobenzene-Functionalized Hole-Transporting Material," *ChemPhysChem,* vol. 15, pp. 2595-2603, 2014.

[259] K. Zhao, Q. Wang, B. Xu, W. Zhao, X. Liu, B. Yang, *et al.*, "Efficient fullerene-based and fullerene-free polymer solar cells using two wide band gap thiophene-thiazolothiazole-based photovoltaic materials," *Journal of Materials Chemistry A,* vol. 4, pp. 9511-9518, 2016.

[260] Z. Zhao, H. Liu, Y. Zhao, C. Cheng, J. Zhao, Q. Tang, *et al.*, "Anisotropic Charge-Carrier Transport in High-Mobility Donor-Acceptor Conjugated Polymer Semiconductor Films," *Chemistry–An Asian Journal,* vol. 11, pp. 2725-2729, 2016.

[261] M. Saito, I. Osaka, Y. Suzuki, K. Takimiya, T. Okabe, S. Ikeda, *et al.*, "Highly Efficient and Stable Solar Cells Based on Thiazolothiazole and Naphthobisthiadiazole Copolymers," *Scientific reports,* vol. 5, 2015.

[262] S. Subramaniyan, H. Xin, F. S. Kim, N. M. Murari, B. A. Courtright, and S. A. Jenekhe, "Thiazolothiazole Donor-Acceptor Conjugated Polymer Semiconductors for Photovoltaic Applications," *Macromolecules,* vol. 47, pp. 4199-4209, 2014.

[263] I. Osaka, M. Saito, T. Koganezawa, and K. Takimiya, "Thiophene-thiazolothiazole copolymers: significant impact of side chain composition on backbone orientation and solar cell performances," *Advanced Materials,* vol. 26, pp. 331-338, 2014.

[264] Y. Liu, H. Dong, S. Jiang, G. Zhao, Q. Shi, J. Tan, *et al.*, "High Performance Nanocrystals of a Donor-Acceptor Conjugated Polymer," *Chemistry of Materials,* vol. 25, pp. 2649-2655, 2013.

Bibliography

[265] S. Subramaniyan, F. S. Kim, G. Ren, H. Li, and S. A. Jenekhe, "High mobility thiazole-diketopyrrolopyrrole copolymer semiconductors for high performance field-effect transistors and photovoltaic devices," *Macromolecules,* vol. 45, pp. 9029-9037, 2012.

[266] I. Osaka, M. Saito, H. Mori, T. Koganezawa, and K. Takimiya, "Drastic Change of Molecular Orientation in a Thiazolothiazole Copolymer by Molecular-Weight Control and Blending with PC61BM Leads to High Efficiencies in Solar Cells," *Advanced Materials,* vol. 24, pp. 425-430, 2012.

[267] Q. Shi, H. Fan, Y. Liu, J. Chen, Z. Shuai, W. Hu, *et al.*, "Thiazolothiazole-containing polythiophenes with low HOMO level and high hole mobility for polymer solar cells," *Journal of Polymer Science Part A: Polymer Chemistry,* vol. 49, pp. 4875-4885, 2011.

[268] S. K. Lee, J. M. Cho, Y. Goo, W. S. Shin, J.-C. Lee, W.-H. Lee, *et al.*, "Synthesis and characterization of a thiazolo [5, 4-d] thiazole-based copolymer for high performance polymer solar cells," *Chemical Communications,* vol. 47, pp. 1791-1793, 2011.

[269] I. Osaka, R. Zhang, J. Liu, D.-M. Smilgies, T. Kowalewski, and R. D. McCullough, "Highly stable semiconducting polymers based on thiazolothiazole," *Chemistry of Materials,* vol. 22, pp. 4191-4196, 2010.

[270] Z. Zhu, Y. Bai, H. K. H. Lee, C. Mu, T. Zhang, L. Zhang, *et al.*, "Polyfluorene Derivatives are high-performance organic hole-transporting materials for Inorganic-organic hybrid perovskite solar cells," *Advanced Functional Materials,* vol. 24, pp. 7357-7365, 2014.

[271] B. Wu, K. Fu, N. Yantara, G. Xing, S. Sun, T. C. Sum, *et al.*, "Charge Accumulation and Hysteresis in Perovskite-Based Solar Cells: An Electro-Optical Analysis," *Advanced Energy Materials,* vol. 5, 2015.

[272] M. Li, Z. K. Wang, Y. G. Yang, Y. Hu, S. L. Feng, J. M. Wang, *et al.*, "Copper Salts Doped Spiro-OMeTAD for High-Performance Perovskite Solar Cells," *Advanced Energy Materials*, vol. 6, 2016.

[273] Y. B. Cheng, Y. Han, S. Meyer, Y. Dkhissi, K. Weber, J. Pringle, *et al.*, "Degradation observations of encapsulated planar CH3NH3PbI3 perovskite solar cells at high temperatures and humidity," *Journal of Materials Chemistry A*, vol. 3, pp. 8139-8147, 2015.

[274] R. S. Sanchez and E. Mas-Marza, "Light-induced effects on Spiro-OMeTAD films and hybrid lead halide perovskite solar cells," *Solar Energy Materials & Solar Cells*, vol. 158, pp. 189-194, 2016.

[275] F. Zhang, X. Zhao, C. Yi, D. Bi, X. Bi, P. Wei, *et al.*, "Dopant-free star-shaped hole-transport materials for efficient and stable perovskite solar cells," *Dyes & Pigments*, vol. 136, pp. 273-277, 2017.

[276] N. H. Tiep, Z. Ku, and H. J. Fan, "Recent Advances in Improving the Stability of Perovskite Solar Cells," *Advanced Energy Materials*, vol. 6, pp. 1501420-n/a, 2016.

[277] T. A. Berhe, W.-N. Su, C.-H. Chen, C.-J. Pan, J.-H. Cheng, H.-M. Chen, *et al.*, "Organometal halide perovskite solar cells: degradation and stability," *Energy & Environmental Science*, 2015.

[278] M. Yang, Y. Zhou, Y. Zeng, C.-S. Jiang, N. P. Padture, and K. Zhu, "Square-Centimeter Solution-Processed Planar CH3NH3PbI3 Perovskite Solar Cells with Efficiency Exceeding 15%," *Advanced Materials*, vol. 27, pp. 6363-6370, 2015.

[279] N. J. Jeon, J. H. Noh, W. S. Yang, Y. C. Kim, S. Ryu, J. Seo, *et al.*, "Compositional Engineering of Perovskite Materials for High-Performance Solar Cells," *Nature*, vol. 517, pp. 476-480, 2015.

[280] J. H. Heo, H. J. Han, D. Kim, T. K. Ahn, and S. H. Im, "Hysteresis-Less

Inverted CH3NH3PbI3 Planar Perovskite Hybrid Solar Cells with 18.1% Power Conversion Efficiency," *Energy & Environmental Science,* vol. 8, pp. 1602-1608, 2015.

[281] N. J. Jeon, J. H. Noh, Y. C. Kim, W. S. Yang, S. Ryu, and S. I. Seok, "Solvent Engineering for High-Performance Inorganic-Organic Hybrid Perovskite Solar Cells," *Nat Mater,* vol. 13, pp. 897-903, 09//print 2014.

[282] C. Y. Jiang, X. W. Sun, D. W. Zhao, A. K. K. Kyaw, and Y. N. Li, "Low Work Function Metal Modified ITO as Cathode for Inverted Polymer Solar Cells," *Solar Energy Materials and Solar Cells,* vol. 94, pp. 1618-1621, 10// 2010.

[283] P. Peumans, A. Yakimov, and S. R. Forrest, "Small Molecular Weight Organic Thin-Film Photodetectors and Solar Cells," *Journal of Applied Physics,* vol. 93, pp. 3693-3723, 2003.

[284] S. Dongaonkar, J. D. Servaites, G. M. Ford, S. Loser, J. Moore, R. M. Gelfand, *et al.*, "Universality of Non-Ohmic Shunt Leakage in Thin-Film Solar Cells," *Journal of Applied Physics,* vol. 108, p. 124509, 2010.

[285] J. Wagner, M. Gruber, A. Wilke, Y. Tanaka, K. Topczak, A. Steindamm, *et al.*, "Identification of Different Origins for S-Shaped Current Voltage Characteristics in Planar Heterojunction Organic Solar Cells," *Journal of Applied Physics,* vol. 111, p. 054509, 2012.

[286] M. O. Reese, M. S. White, G. Rumbles, D. S. Ginley, and S. E. Shaheen, "Optimal Negative Electrodes for Poly(3-hexylthiophene):[6, 6]-phenyl C61-butyric Acid Methyl Ester Bulk Heterojunction Photovoltaic Devices," *Applied Physics Letters,* vol. 92, p. 053307, 2008.

[287] G. Amarandei, I. Clancy, C. O'Dwyer, A. Arshak, and D. Corcoran, "Stability of Ultrathin Nanocomposite Polymer Films Controlled by the

Embedding of Gold Nanoparticles," *ACS applied materials & interfaces,* vol. 6, pp. 20758-20767, 2014.

[288] X. Wang, C. Xinxin Zhao, G. Xu, Z.-K. Chen, and F. Zhu, "Degradation Mechanisms in Organic Solar Cells: Localized Moisture Encroachment and Cathode Reaction," *Solar Energy Materials and Solar Cells,* vol. 104, pp. 1-6, 9// 2012.

[289] X. Z. Wang, Z. T. Xie, X. J. Wang, Y. C. Zhou, W. H. Zhang, X. M. Ding, *et al.*, "Blocking of Interfacial Diffusion at Ag/Alq3 by LiF," *Applied Surface Science,* vol. 253, pp. 3930-3932, 2/15/ 2007.

[290] S. Mack, M. Meitl, A. Baca, Z.-T. Zhu, and J. Rogers, "Mechanically Flexible Thin-Film Transistors that Use Ultrathin Ribbons of Silicon Derived from Bulk Wafers," *Applied physics letters,* vol. 88, p. 213101, 2006.

[291] M. A. Meitl, Z.-T. Zhu, V. Kumar, K. J. Lee, X. Feng, Y. Y. Huang, *et al.*, "Transfer Printing by Kinetic Control of Adhesion to an Elastomeric Stamp," *Nature materials,* vol. 5, pp. 33-38, 2006.

[292] X. Liang, Z. Fu, and S. Y. Chou, "Graphene Transistors Fabricated via Transfer-Printing in Device Active-Areas on Large Wafer," *Nano Lett,* vol. 7, pp. 3840-3844, 2007.

[293] S.-H. Hur, D.-Y. Khang, C. Kocabas, and J. A. Rogers, "Nanotransfer Printing by Use of Noncovalent Surface Forces: Applications to Thin-Film Transistors that Use Single-Walled Carbon Nanotube Networks and Semiconducting Polymers," *Applied Physics Letters,* vol. 85, pp. 5730-5732, 2004.

[294] A. Carlson, A. M. Bowen, Y. Huang, R. G. Nuzzo, and J. A. Rogers, "Transfer Printing Techniques for Materials Assembly and Micro/nanodevice Fabrication," *Advanced Materials,* vol. 24, pp.

5284-5318, 2012.

[295] D. Aldakov, D. Tondelier, S. Palacin, and Y. Bonnassieux, "Ethanol-Mediated Metal Transfer Printing on Organic Films," *ACS applied materials & interfaces*, vol. 3, pp. 740-745, 2011.

[296] J.-H. Ahn, H.-S. Kim, K. J. Lee, Z. Zhu, E. Menard, R. G. Nuzzo, *et al.*, "High-Speed Mechanically Flexible Single-Crystal Silicon Thin-Film Transistors on Plastic Substrates," *IEEE Electron Device Letters*, vol. 27, pp. 460-462, 2006.

[297] K. J. Lee, M. A. Meitl, J.-H. Ahn, J. A. Rogers, R. G. Nuzzo, V. Kumar, *et al.*, "Bendable GaN High Electron Mobility Transistors on Plastic Substrates," *Journal of Applied Physics*, vol. 100, p. 124507, 2006.

[298] E. Menard, R. G. Nuzzo, and J. A. Rogers, "Bendable Single Crystal Silicon Thin Film Transistors Formed by Printing on Plastic Substrates," *Applied Physics Letters*, vol. 86, p. 093507, 2005.

[299] S.-I. Park, Y. Xiong, R.-H. Kim, P. Elvikis, M. Meitl, D.-H. Kim, *et al.*, "Printed Assemblies of Inorganic Light-Emitting Diodes for Deformable and Semitransparent Displays," *science*, vol. 325, pp. 977-981, 2009.

[300] J.-h. Choi, K.-H. Kim, S.-J. Choi, and H. H. Lee, "Whole Device Printing for Full Colour Displays with Organic Light Emitting Diodes," *Nanotechnology*, vol. 17, p. 2246, 2006.

[301] J. Yoon, A. J. Baca, S.-I. Park, P. Elvikis, J. B. Geddes, L. Li, *et al.*, "Ultrathin Silicon Solar Microcells for Semitransparent, Mechanically Flexible and Microconcentrator Module Designs," *Nature materials*, vol. 7, pp. 907-915, 2008.

[302] A. J. Baca, K. J. Yu, J. Xiao, S. Wang, J. Yoon, J. H. Ryu, *et al.*, "Compact Monocrystalline Silicon Solar Modules with High Voltage Outputs and Mechanically Flexible Designs," *Energy & Environmental*

Science, vol. 3, pp. 208-211, 2010.

[303] L. Chen, P. Degenaar, and D. D. Bradley, "Polymer Transfer Printing: Application to Layer Coating, Pattern Definition, and Diode Dark Current Blocking," *Advanced Materials*, vol. 20, pp. 1679-1683, 2008.

[304] L. Yin, Z. Zhao, F. Jiang, Z. Li, S. Xiong, and Y. Zhou, "PEDOT:PSS Top Electrode Prepared by Transfer Lamination Using Plastic Wrap as the Transfer Medium for Organic Solar Cells," *Organic Electronics*, vol. 15, pp. 2593-2598, 2014.

[305] F. Jiang, T. Liu, S. Zeng, Q. Zhao, X. Min, Z. Li, *et al.*, "Metal Electrode-Free Perovskite Solar Cells with Transfer-Laminated Conducting Polymer Electrode," *Optics express*, vol. 23, pp. A83-A91, 2015.

[306] X. Wang, T. Ishwara, W. Gong, M. Campoy-Quiles, J. Nelson, and D. D. Bradley, "High-Performance Metal-Free Solar Cells Using Stamp Transfer Printed Vapor Phase Polymerized Poly (3, 4-Ethylenedioxythiophene) Top Anodes," *Advanced Functional Materials*, vol. 22, pp. 1454-1460, 2012.

[307] Y. Zhou, T. M. Khan, J.-C. Liu, C. Fuentes-Hernandez, J. W. Shim, E. Najafabadi, *et al.*, "Efficient Recyclable Organic Solar Cells on Cellulose Nanocrystal Substrates with a Conducting Polymer Top Electrode Deposited by Film-Transfer Lamination," *Organic Electronics*, vol. 15, pp. 661-666, 2014.

[308] P. You, Z. Liu, Q. Tai, S. Liu, and F. Yan, "Efficient Semitransparent Perovskite Solar Cells with Graphene Electrodes," *Advanced Materials*, vol. 27, pp. 3632-3638, 2015.

[309] F. Zhang, W. Shi, J. Luo, N. Pellet, C. Yi, X. Li, *et al.*, "Isomer-Pure Bis-PCBM-Assisted Crystal Engineering of Perovskite Solar Cells

Showing Excellent Efficiency and Stability," *Advanced Materials,* vol. 29, p. 1606806, 2017.

[310] H. J. Park, M.-G. Kang, S. H. Ahn, and L. J. Guo, "A Facile Route to Polymer Solar Cells with Optimum Morphology Readily Applicable to a Roll-to-Roll Process without Sacrificing High Device Performances," *Advanced Materials,* vol. 22, pp. E247-E253, 2010.

[311] D. Yang, L. Zhou, L. Chen, B. Zhao, J. Zhang, and C. Li, "Chemically Modified Graphene Oxides as a Hole Transport Layer in Organic Solar Cells," *Chemical Communications,* vol. 48, pp. 8078-8080, 2012.

[312] T. Hu, F. Li, K. Yuan, and Y. Chen, "Efficiency and Air-Stability Improvement of Flexible Inverted Polymer Solar Cells Using ZnO/poly (Ethylene Glycol) Hybrids as Cathode Buffer Layers," *ACS applied materials & interfaces,* vol. 5, pp. 5763-5770, 2013.

[313] K. I. Jayawardena, R. Rhodes, K. K. Gandhi, M. R. Prabhath, G. D. M. Dabera, M. J. Beliatis, *et al.*, "Solution Processed Reduced Graphene Oxide/metal Oxide Hybrid Electron Transport Layers for Highly Efficient Polymer Solar Cells," *Journal of Materials Chemistry A,* vol. 1, pp. 9922-9927, 2013.

[314] H. Zhou, Y. Zhang, J. Seifter, S. D. Collins, C. Luo, G. C. Bazan, *et al.*, "High-Efficiency Polymer Solar Cells Enhanced by Solvent Treatment," *Advanced Materials,* vol. 25, pp. 1646-1652, 2013.

[315] J. C. Blakesley, F. A. Castro, W. Kylberg, G. F. Dibb, C. Arantes, R. Valaski, *et al.*, "Towards Reliable Charge-Mobility Benchmark Measurements for Organic Semiconductors," *Organic Electronics,* vol. 15, pp. 1263-1272, 2014.

[316] C. R. Henry, "Surface Studies of Supported Model Catalysts," *Surface Science Reports,* vol. 31, pp. 231-325, // 1998.

Bibliography

[317] C. Kuhrt and M. Harsdorff, "Photoemission and Electron Microscopy of Small Supported Palladium Clusters," *Surface science,* vol. 245, pp. 173-179, 1991.

[318] V. Papaefthimiou, A. Siokou, and S. Kennou, "A Study of the Interface Formation between Gold and a Thin Conjugated Oligomer Film," *Surface Science,* vol. 532–535, pp. 255-260, 6/10/ 2003.

[319] S. Cacovich, L. Cina, F. Matteocci, G. Divitini, P. A. Midgley, A. Di Carlo, *et al.*, "Gold and Iodine Diffusion in Large Area Perovskite Solar Cells under Illumination," *Nanoscale,* vol. 9, pp. 4700-4706, 2017.

[320] J.-D. Chen, C. Cui, Y.-Q. Li, L. Zhou, Q.-D. Ou, C. Li, *et al.*, "Single-Junction Polymer Solar Cells Exceeding 10% Power Conversion Efficiency," *Advanced Materials,* vol. 27, pp. 1035-1041, 2015.

[321] S.-W. Baek, G. Park, J. Noh, C. Cho, C.-H. Lee, M.-K. Seo, *et al.*, "Au@Ag Core–Shell Nanocubes for Efficient Plasmonic Light Scattering Effect in Low Bandgap Organic Solar Cells," *ACS Nano,* vol. 8, pp. 3302-3312, 2014/04/22 2014.

[322] S. Hong, J. Yeo, G. Kim, D. Kim, H. Lee, J. Kwon, *et al.*, "Nonvacuum, Maskless Fabrication of a Flexible Metal Grid Transparent Conductor by Low-Temperature Selective Laser Sintering of Nanoparticle Ink," *ACS Nano,* vol. 7, pp. 5024-5031, 2013/06/25 2013.

[323] D. Gupta, M. M. Wienk, and R. A. Janssen, "Efficient Polymer Solar Cells on Opaque Substrates with a Laminated PEDOT:PSS Top Electrode," *Advanced Energy Materials,* vol. 3, pp. 782-787, 2013.